UNIVERSITY
OF MICHIGAN
JAN 29 1954
PHYSICS
LIBRARY

REGISTERED No. M. 3121

PROCEEDINGS

OF THE

INDIAN ACADEMY OF SCIENCES

VOL. XXXVIII] *SECTION A* [No. 5

NOVEMBER 1953

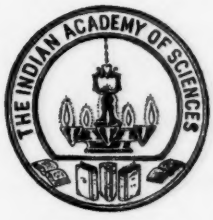

Price Rs. 2 or 3 Sh. *Annual Subscription Rs. 18*

PRINTED AT THE BANGALORE PRESS, BANGALORE CITY, BY C. VASUDEVA RAO,
SUPERINTENDENT AND PUBLISHED BY THE INDIAN ACADEMY OF
SCIENCES, BANGALORE.

THE STRUCTURE AND OPTICAL BEHAVIOUR OF IRIDESCENT OPAL

By Sir C. V. Raman and A. Jayaraman

(*Memoir No. 42 of the Raman Research Institute, Bangalore-6*)

(Received November 11, 1953)

1. Introduction

The remarkable and very beautiful effects exhibited by iridescent opal have long been known and have made it one of the most admired of gems. In the finest specimens, the play of colour takes the form of localised internal reflections exhibiting hues of extraordinary brilliance and saturation which vary from place to place over the area of the gem and change in a surprising manner with the angle of incidence of the light. Not the least part of the beauty of a fine opal is the orange-red colour of the transmitted light which may be seen reflected back by the rear surface of the gem and then appears all the more vivid by reason of its contrast with the greens and blues so frequently seen in the iridescence. Spectroscopic examination reveals that the internal reflections and the corresponding extinctions in the transmitted light are highly monochromatic. From this, it is evident that they are consequent on the presence within the material of regularly stratified layers in great number. Indeed, the existence of such stratifications is not just a hypothesis. When a gem-opal is examined through a microscope which has arrangements for illuminating the object from above the stage and viewing it by the internally reflected light, the lamellar structure of the material becomes immediately evident. In not a few cases, geometric patterns of a very striking character are observed (see Figs. 1 to 4 in Plate XXVI).

A reasonable hypothesis which would fit the observed character of the stratifications as well as the optical effects to which they give rise is that iridescent opal consists of alternate layers of two crystalline modifications of silica of slightly different refractive index. In a recent paper[1] in these *Proceedings*, we presented evidence which supports this hypothesis derived from a study of the X-ray diffraction patterns of hyalite which is a material having a composition similar to that of gem-opal and exhibiting optical phenomena of a similar nature. Further studies have since been carried out by us in which X-ray cameras of higher resolving powers were used and the resulting photographs were precisely measured. They have enabled us

to reach the definite conclusion that the *two modifications of silica present in hyalite are respectively low-tridymite and high-cristobalite.* X-ray studies have also been made by us with common opal which occurs in massive form with a waxy lustre. These have led to a similar conclusion regarding the nature of the latter material.

The X-ray patterns of gem-opal are diffuse, thereby making it less easy than in the case of the crypto-crystalline materials hyalite and common opal to identify the nature of the atomic groupings which appear in the alternating layers of its lamellar structure. Nevertheless, a careful examination of the patterns leaves little room for doubt that, as in the case of the iridescent hyalite, we are concerned with two modifications of silica present side by side in it, one of them having a structure resembling that of low-tridymite and that the other that of high-cristobalite. Comparative studies of the optical behaviour of hyalite and of gem-opal made by us confirm this finding and establish this as the origin of the iridescence exhibited by these materials.

2. THE CRYPTO-CRYSTALLINE FORMS OF SILICA

As is well known, agate and chalcedony are massive forms of silica which X-ray studies show to consist of crystallites of quartz. The latter are frequently grouped together in specific orientations, thereby giving rise to the characteristic banding of the material, as has been shown by us in a recent paper.[2] *Prima-facie*, one may expect that two other crypto-crystalline forms of silica should also be forthcoming in nature consisting respectively of low-tridymite and low-cristobalite. The latter expectation, at least, is found to be fully justified. Some years ago, a white and compact porcelain-like material was collected by one of us on the open terrain not far from Indore in Central India. It was usually found associated with agate, but occasionally also appeared as separate masses. The density of the material has been determined and lies between 2·32 and 2·35, thus excluding the possibility of its being chalcedony. The density approximates closely to the known value for low-cristobalite, and examination by X-ray diffraction methods confirms this identification. On heating the substance to about 300° C., it transforms completely to high-cristobalite, and on cooling reverts again to low-cristobalite. These findings are illustrated in Figs. 12 (*a*) and (*b*) in Plate XXIX which show respectively the X-ray patterns of the material at the low and at the high temperature. The pattern was first recorded at the high temperature and later at the room temperature. Measurement of the photographs confirms the identification of the material with cristobalite.

It is clear from the X-ray patterns that the cristobalite is present in the material in random orientations and in a highly divided form, the particle size indicated being about 1 μ in diameter. This is confirmed by optical observations. A slice about half a millimeter thick cut from the material and polished on both sides regularly transmits light of a deep red colour which is unpolarised. From these observations again, one infers that the crystallites are of small dimensions and are randomly orientated. The most significant result that emerges is that high-cristobalite is unstable at ordinary temperature even when in a fine state of subdivision and reverts immediately to low-cristobalite.

3. The Structure of Common Opal

Another material examined by us in detail is common opal with a waxy lustre, two large lumps of which were purchased from a mineral dealer in New York. The material is translucent in thick layers, but in smaller thicknesses of the order of a millimeter transmits light freely. The density of the material is 2·02 and its refractive index 1·440. On heating to about 800° C., it becomes opaque and white and also loses about 10% of its weight, presumably due to the loss of adsorbed water. An X-ray diffraction pattern was recorded in the usual manner, using a fine rod prepared from the material with a cylindrical camera of 3 cm. radius. This is reproduced in Fig. 13 (*b*) in Plate XXX. Figs. 13 (*a*) and (*c*) in the same Plate are X-ray diffraction patterns respectively of high-cristobalite and low-tridymite, recorded under identical conditions. The low-tridymite was taken off a burnt-out silica brick and then finely powdered; the high-cristobalite is the same material as that described in the preceding section.

A careful comparison of the three patterns reproduced in Plate XXX is highly instructive. Particularly noteworthy is the fact that the principal ring of common opal is of considerable width, this being approximately the same as the total width covered by the triplet of lines appearing in the pattern of low-tridymite, while on the other hand, the principal ring of high-cristobalite is single, sharp and well defined. But in other respects, the patterns of common opal and of high-cristobalite exhibit a close similarity. But even so, there are recognisable differences. While the rings of high-cristobalite are all sharp and fairly intense, those of common opal are definitely weaker and also rather diffuse though to varying extents. The pattern of the opal also exhibits a much more intense small-angle scattering than that of high-cristobalite. A continuum of varying intensity is also present in the pattern of the opal which is absent in the case of high-cristobalite. On careful scrutiny, a close correspondence is revealed between the intensity

of the continuum in the pattern of common opal and the integrated intensity of the groups of lines appearing in the corresponding parts of the low-tridymite pattern.

All the facts set forth above indicate that common opal is a material in which high-cristobalite and low-tridymite co-exist in intimate juxtaposition.

4. THE STRUCTURE OF HYALITE

In our earlier paper which appeared in these *Proceedings* for August 1953, the X-ray diffraction patterns of four specimens of hyalite were reproduced. The pattern of specimen No. I which was recorded with a 3 cm. radius camera is reproduced again as Fig. 14 (*b*) in Plate XXXI. For comparison with it, the patterns of high-cristobalite and low-tridymite recorded under identical conditions are once again reproduced in Plate XXXI as Figs. 14 (*a*) and 14 (*c*) respectively. Apart from the circumstance that only one side of the pattern of the hyalite has been recorded, it will be seen that it closely resembles the pattern of common opal appearing in Fig. 13 (*b*) in Plate XXX, except that the outer rings are generally rather sharper and more intense in the case of the hyalite. Hence, the remarks made above regarding common opal apply *mutatis mutandis* to the case of hyalite.

To make the position clearer, the pattern of hyalite No. IV which had a very sharp edge has been recorded once again with X-ray cameras of higher resolving power. A picture taken with a camera of 5·73 cm. radius and an exposure of seven hours is reproduced as Fig. 9 in Plate XXVIII. Three prints of a pattern of the same specimen recorded with a camera of 19 cm. diameter and an exposure of twelve hours are reproduced as Fig. 10 in the same Plate. It is very clearly seen in both pictures that the principal ring in the pattern is a triplet, with a strong central component. Both the positions and relative intensities of the components of the triplet are explicable if the pattern is recognised to be a superposition of those of high-cristobalite and low-tridymite. This will be evident from Table I where the respective *d*-values of the more prominent lines have been tabulated. The table also makes it clear that the suggestion made in our earlier paper that the X-ray pattern of hyalite is a superposition of the patterns of high- and low-cristobalite is untenable.

5. THE STRUCTURE OF GEM-OPAL

The density of gem-opal ranges between 2·1 and 2·2, and its refractive index between 1·45 and 1·46. The density and the refractive index of hyalite are respectively 2·0 and 1·44 respectively, these lower values being related to those for gem-opal at least approximately in the manner demanded

TABLE I. *d-values in Angstroms with intensities*

Low-cristobalite	High-cristobalite	Hyalite	Low-tridymite
..	..	4·32 (moderate)	4·32 (intense)
..	4·13 (intense)	4·12 (intense)	4·10 (strong)
4·04 (intense)	..	..	..
..	..	3·9 (weak)	3·82 (strong)
3·12 (moderate)	..	..	..
..	..	..	2·97 (moderate)
2·85 (moderate)	..	..	..
2·48 (strong)	2·52 (strong)	2·51 (strong)	2·49 (moderate)

by the Gladstone-Dale formula. The principal difference between gem-opal and hyalite is that while the latter, as we have seen, gives a well-defined X-ray diffraction pattern, the pattern of the former is diffuse and resembles that of vitreous silica, though there are recognisable differences. Figs. 11 (*a*), (*b*), (*c*), (*d*) and (*e*) in Plate XXIX are X-ray diffraction-patterns recorded with a camera of 5·73 cm. diameter and the filtered radiation from a molybdenum target of the materials indicated respectively against each figure. Figs. 11 (*a*) and (*e*) are of two different specimens of gem-opal, while the other figures refer respectively to silica gel, vitreous silica and the natural silica glass from the Sand Sea in the Libyan Desert collected by Dr. L. J. Spencer. At a first glance, all the patterns seem to be similar, but a more careful scrutiny reveals significant differences. Remarkably enough, the difference is greatest as between gem-opal and vitreous silica. In the patterns of opal the two outer rings are seen clearly separated from each other and from the next inner ring, whereas with the vitreous silica, the two outer rings have nearly coalesced, and the next inner ring has joined up with the bright central area. The differences between the opal and the silica gel on the one hand, and between opal and the Libyan glass on the other, are of a less striking character. It should be remarked that in the case of all four materials, there are two outer bands of low intensity which can be scarcely glimpsed in the reproductions. The *d*-values calculated for the principal ring and for the five outer bands for the case of gem-opal are respectively 4·1 Å, 2·05 Å, 1·45 Å, 1·20 Å, 0·97 Å and 0·80 Å.

The use of the short-wave molybdenum radiation and a camera of small radius results in obscuring much of the visible detail in the inner parts of

the pattern. The latter are much clearer when recorded with the filtered radiation from a copper target. Two pictures, namely those of gem-opal and of silica glass, taken with CuK_α radiation and a flat camera with a film to specimen distance of 4 cm. are reproduced as Figs. 8 (*a*) and 8 (*b*) respectively in Plate XXVIII. The density of gem-opal being rather less than that of vitreous silica which is 2·22, one might have thought that the principal ring of opal should have a smaller angular diameter and give a larger *d*-value than that of silica glass. The actual position is the reverse, as can be seen on a careful comparison of the two figures. It will also be noticed that the first diffraction ring of gem-opal is definitely sharper and of greater intensity relatively to the region inside it than for silica glass.

Using the CuK_α radiation and an X-ray camera of 3 cm. radius with adequate exposures, the complete pattern of gem-opal can be satisfactorily recorded and shows features of great interest. Unfortunately, however, owing to the weakness of the outer bands relatively to the principal halo, it is difficult to copy it in a satisfactory manner for reproduction. Hence we have to content ourselves here with a description of the observed features. One can clearly see in the photographs besides the principal ring and a strong continuum stretching out from it, a distinct concentration of intensity along a ring with a *d*-value of 2·50 Å, besides the other bands with smaller *d*-values which are the same as those recorded with molybdenum radiation. The pattern in fact is essentially similar to that of hyalite reproduced as Fig. 14 (*b*) in Plate XXXI, provided that one supposes that the rings appearing in the latter had broadened out sufficiently to become a set of diffuse bands. The continuum seen in the hyalite pattern between its first and second rings is a conspicuous feature also in the pattern of the gem-opal as recorded with the CuK_α radiation.

Thus, the X-ray data point clearly to the conclusion that the structure of gem-opal is essentially the same as that of hyalite, except that the crystallites are now much smaller, thereby tending to make the material simulate a vitreous solid.

The essential similarity between hyalite and gem-opal indicated by the X-ray data is supported by other facts of observation. One of the most striking features observed with gem-opal is the appearance of visible stratifications in it. These are very conveniently observed with the aid of an 'Ultropak' microscope. In this arrangement, a conical beam of light is directed from above the stage on to the surface of the specimen and the latter is viewed by the light reflected from its interior and returned to the objective of the microscope. A great variety of geometric patterns are

observed, a few particularly striking examples of which are reproduced as Figs. 1, 2, 3 and 4 in Plate XXVI. Figs. 1 and 4 refer to exactly the same portion of a particular specimen but under slightly different conditions of illumination. Fig. 2 refers to another area on the same opal. Fig. 3 is a particular area on the finest gem-opal in the collection of this Institute. It will be seen from these pictures that the stratifications run in several directions simultaneously and in fact the entire material is honeycombed by them. The material is divided up into layers parallel to one, two or even three sets of parallel planes crossing each other. It is to be noted that hyalite also shows visible evidence of internal stratifications. One may refer for example, to the picture of our specimen II under transverse illumination reproduced as Fig. 5 in Plate IX of the earlier paper in which triangular patches shining by reflected light are clearly to be seen. The essential similarity of the structures of opal and hyalite is thus made clear.

6. Observations with Monochromatic Light

In examining the optical behaviour of regularly stratified media, the use of monochromatic light is very helpful. We shall proceed to recount some observations made with opals, respectively in the light of a sodium vapour lamp and of a mercury arc.

The finest opal in the collection of this Institute is a square tablet which in diffuse daylight exhibits bright green, blue or violet flashes of internal reflection. In the light of a sodium vapour lamp, however, this brilliance disappears and the gem is seen transformed to an insignificant and unsatisfactory object exhibiting numerous defects, including especially a cloudiness over part of its area on one face in which no iridescence is visible even in diffuse daylight. Every one of the opals in the collection of the Institute which exhibits a green or blue iridescence resembles in the light of a sodium lamp a piece of common but rather turbid glass. Such disappearance of the iridescence is intelligible in the light of optical theory, for a regularly stratified medium ceases to reflect at any incidence if the wave-length λ of the light is greater than $2\mu t$, where μ is the mean index and t is the spacing of the stratifications.

The opals which show up so badly in the light of the sodium lamp present a very different appearance in the light of a mercury arc. The difference between the mercury arc and diffuse daylight is however conspicuous in the colour exhibited by the internal reflections, as also in the colour of the transmitted light. The former shows less variety than in daylight, while, on the other hand, the transmitted colours are more lively, being less diluted by the light of longer wave-lengths present in daylight.

In our earlier paper,[1] we described and illustrated the optical effects exhibited by hyalite which were individually different in our three specimens I, II and III. The first showed a diffusion halo around the direction of the transmitted light, the second a set of radially directed diffraction spectra, while our specimen III behaved much like an opal and showed a great number of individual monochromatic reflections backwards towards the source of light, many of which are of a red colour. Examined in the light of a sodium lamp, hyalite No. III showed many sparkling reflections from its interior which disappeared and reappeared in other positions as the specimen was turned round.

It is clear from the facts that the optical effects exhibited by transparent hyalite and by iridescent opal form a continuous sequence in which there are three stages. In the first stage, the stratifications are too widely spaced to result in internal reflections, but give rise to diffraction haloes or diffraction spectra in forward directions. In the second stage, the stratifications are too closely spaced to give diffraction effects in forward directions, but result in reflections backwards towards the source. Finally, we have a third stage when the stratifications are too closely spaced to give any effects at all, unless the wave-length of the light is sufficiently small. In the cryptocrystalline hyalites, we would naturally expect the first stage to be commonest, and the second stage less common. In the gem-opals, on the other hand, where the material is approaching the vitreous condition, the stratifications may be expected to be much finer and the third stage therefore attained, unless the wave-length of the light is chosen sufficiently small. We do indeed have opals which exhibit a bright yellow or red iridescence. But those with a green, blue or violet iridescence are commoner, indicating that the more closely-spaced stratifications are favoured.

7. THE REFLECTION PATTERNS OF OPAL

In studying the optical behaviour of opal rather more closely, we may adopt one of two different methods. In the first method, we view the opal directly or through a microscope, illuminating it from one direction and viewing it in another, and vary these directions. The second method is the same as that described in our earlier paper. We illuminate the opal by a intense narrow pencil and the light reflected backwards is received on a white screen held not too far away from the specimen, a small aperture in the screen permitting the illuminating pencil to pass through and fall on the opal. The complete pattern of reflected, diffracted or scattered light returned by the opal is then visible on the screen.

Observations made in the manner described disclose a great variety of effects in different cases. With some specimens, we observe a bright spot or a group of bright spots constituting a reflection-pattern properly so-called. There are also cases in which no pattern appears but only a diffuse area of light on the observing screen, its colour being the same as that of the observed opalescence of the specimen. Opals giving brilliant localised reflections give, in general, complex patterns composed of bright spots, bright coloured streaks of light and brilliant diffraction spectra crossing each other in different directions, the whole pattern altering rapidly as the opal is moved with respect to the illuminating pencil of light. Even those opals which are not of much value as gems, exhibiting colour only in tiny specks or spots on a non-iridescent background, give interesting patterns of various kinds.

It would take us too far from the main purpose of the paper to describe or discuss the reflection patterns of opal in greater detail. We may, however, make a brief reference to the behaviour of a particularly interesting specimen in our collection. This is a so-called "black-opal" in other words, a layer of opal on a background of opaque ferruginous material. When it is illuminated by a narrow pencil of sunlight, the pattern seen on the viewing screen is a single bright streak of light covering a wide range of angles and exhibiting the usual sequence of colours seen in a diffraction spectrum. The distribution of intensity in the spectrum is however anamolous, a concentration of intensity appearing at one place and a dark gap elsewhere, the position of the former altering with the inclination of the reflecting surface to the incident pencil of light. Examination of the specimen under the microscope reveals the presence of parallel striations over its area. These presumably represent the stratifications of the opal meeting the surface of the specimen obliquely. That in these circumstances a diffraction spectrum appears and not a simple reflection is scarcely surprising.

8. The Spectroscopic Facts and Their Significance

Figs. 5 and 6 in Plate XXVII reproduce some spectroscopic records of the reflection of light by some specimens of gem-opal, a beam of white light being allowed to fall at nearly normal incidence on a restricted area of the specimen and after reflection being received on the slit of the instrument. Particularly remarkable is the spectrum reproduced in Fig. 5 (*d*). It shows a single monochromatic reflection in the red, the spectral width of which is only about 20 Å. Figs. 6 (*a*), (*b*), (*c*), (*d*), (*e*) and (*f*) are a series of reflection spectra recorded with a single specimen of opal immersed in a cell containing liquid paraffin, the angle of incidence of the light being varied by steps from nearly normal incidence to about 50°. The exposures

with which the spectra were recorded were not the same in all cases, and hence it is not possible to attach any quantitative significance to the spectral width as seen in the reproductions. In a general way, however, it is evident that there has been no noteworthy increase in the spectral width of the reflection in spite of the wave-length at which it appears having been shifted from 5820 Å to 4930 Å with the increasing angle of incidence.

Figs. 7 (*a*), (*b*) and (*c*) in Plate XXVII are the extinction spectra of three different gem-opals in the collection of the Institute. They were recorded by the simple device of holding the specimen against the slit of the recording spectrograph and allowing the light from a filament lamp 50 cm. away to enter the slit after passing through the specimen. The photographs exhibit the extinctions produced by the entire thickness of the opal which was about 3 millimeters in each case. They represent the joint effect of the sets of stratifications present at different depths and possibly also differently inclined to the path of the light-rays through the opal. The spectrograms exhibit a great variation in the effects recorded at different points along the slit of the instrument. Well-defined extinctions usually about 100 Å wide appear in the blue-green region, accompanying which are seen streaks of transmitted light extending towards the violet end of the spectrum. In other regions, there appears a general cut-off of the shorter wave-lengths and a free transmission of the longer wave-lengths. These facts will be readily understood in the light of the remarks made earlier in this paper.

The theory of the reflection of light by a regularly stratified medium has been elaborately discussed in these *Proceedings* by G. N. Ramachandran.[3] As has been shown by him, the degree of monochromatism of the reflections by such a medium cannot be indefinitely increased by increasing the number of its stratifications, their spectral width having a minimum limiting value which depends only on the reflecting power of an individual stratification. If such reflecting power be large, the monochromatism would necessarily be very imperfect; *per contra*, if high monochromatism is actually observed, it indicates that the reflecting power of an individual lamination is small. These conclusions have an important application to the case of opal. They indicate that the difference in refractive indices of the alternate layers of the stratifications in opal is quite small. Further, such variation is strictly periodic and of the same magnitude throughout an individual set of stratifications.

9. THE NATURE OF THE STRATIFICATIONS

The considerations set forth above suffice by themselves to exclude the explanations of the iridescence of opal which appear in the earlier literature of the subject. It is likewise not possible to entertain the idea that

the presence of adsorbed water in opals is responsible for their iridescence, as it would then be necessary to assume that the adsorbed water is so distributed as to give rise to a regular periodic variation in refractive index of small magnitude, an assumption for which there is no *prima facie* justification. We have made some observations on the effect of heating opals to temperatures sufficiently high to drive out all adsorbed water. This drastic treatment usually results in a disintegration of the opal, but the iridescence as such remains unaffected. We are thus forced to recognise that the iridescence of opal is a consequence of the inherent structure of the silica in the material.

The densities of low-tridymite and of high-cristobalite are not very different and their refractive indices would therefore differ just sufficiently little to account for the observed behaviour of opal if they exist as separate layers side by side. The same difference could equally account for the observed cloudiness of opal in many cases if the distribution of the two materials were irregular in such cases.

As is well known, high-cristobalite is a form of silica which is stable over a wide range of temperatures, but which reverts to low-cristobalite below 300° C. The presence of high-cristobalite admixed with low-tridymite in opal may be reasonably accounted for by assuming that its association with low-tridymite, which is itself a stable form at ordinary temperature, confers on it the requisite stability. Since the two materials have the same chemical composition and nearly the same density, and since their structures have the silicon-oxygen tetrahedra as a common factor, there is no inherent difficulty in making such an assumption. Since the two structures are not identical, the materials would naturally tend to segregate and form layers so disposed with respect to each other as to present the maximum possible degree of continuity in the chains of valence bonds between the silicon and oxygen atoms extending through the material. Since the structure of low-tridymite is psuedo-hexagonal while that of high-cristobalite is cubic, geometric patterns in which the two structures alternate may be expected to arise, as is indeed actually observed in opal.

Summary

The X-ray investigation of the structure of the cryptocrystalline hyalites reported in an earlier paper has now been revised using cameras of higher resolving power. Precise measurements of the resulting photographs reveal that low-tridymite and high-cristobalite are present associated with each other in this material. Investigation of the structure of common opal exhibiting

a waxy lustre leads to similar results. From a detailed examination of the diffuse X-ray patterns given by gem-opals as well as a comparative study of the iridescent hyalites and opals, it is concluded that in both of these materials, the presence of alternating layers of high-cristobalite and low-tridymite is responsible for the iridescence.

REFERENCES

1. C. V. Raman and A. Jayaraman .. *Proc. Ind. Acad. Sci.*, 1953, **38A**, 101.
2. ———— .. *Ibid.*, 1953, **38A**, 199.
3. G. N. Ramachandran .. *Ibid.*, 1942, **16A**, 336.

FIG. 1 FIG. 2

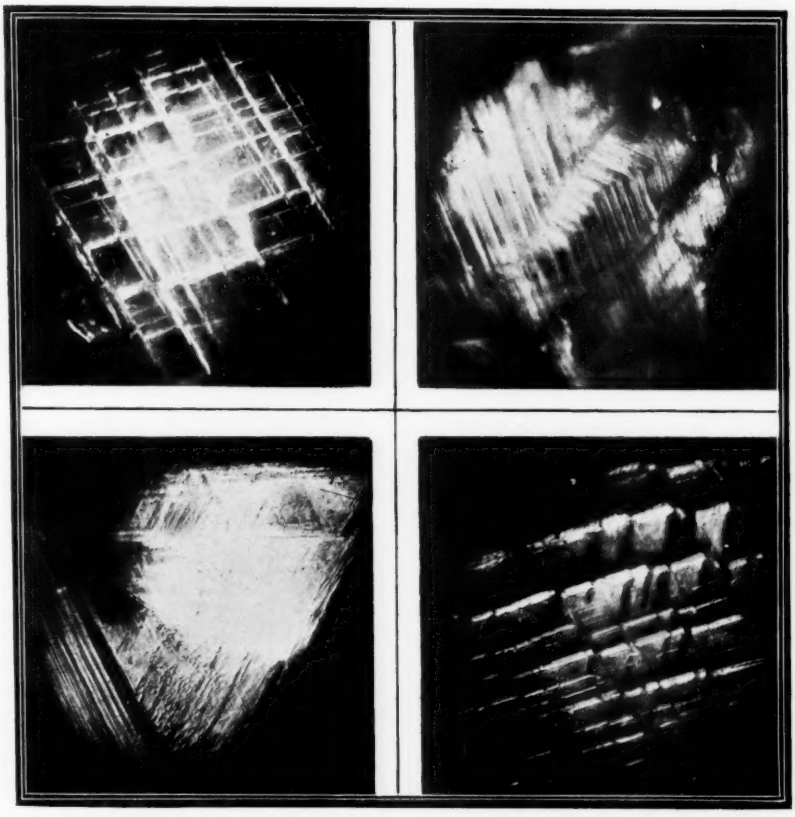

FIG. 3 FIG. 4

Lamellar Structures in Precious Opal

FIG. 5

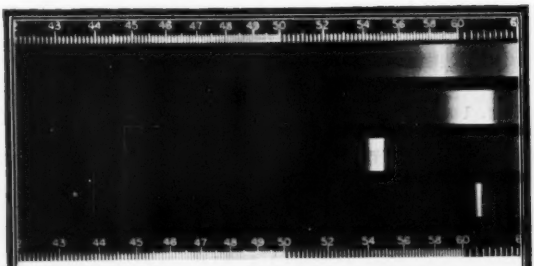

FIG. 6

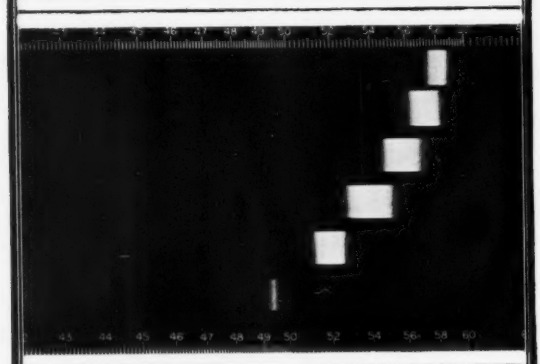

FIG. 7

Reflection and Extinction Spectra of Precious Opal

(*a*) Precious Opal (*b*) Silica Glass

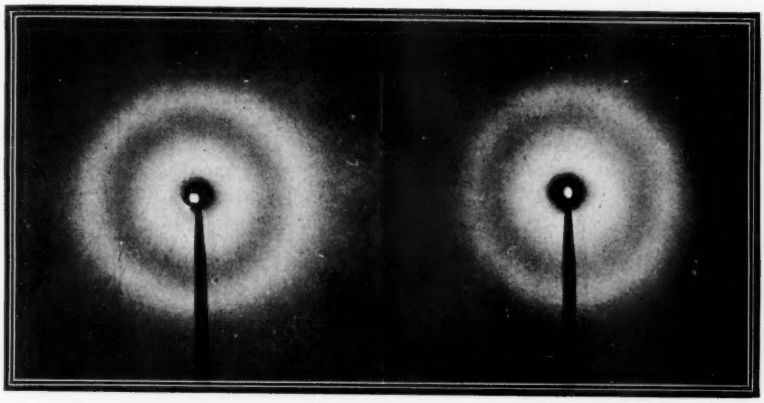

FIG. 8

Hyalite IV

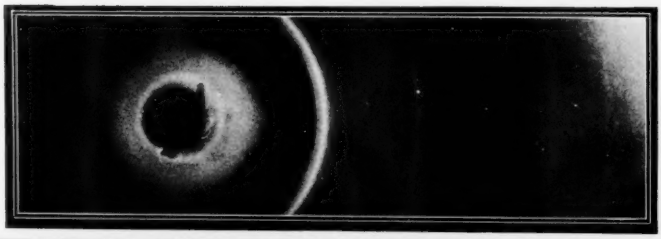

FIG. 9

Do

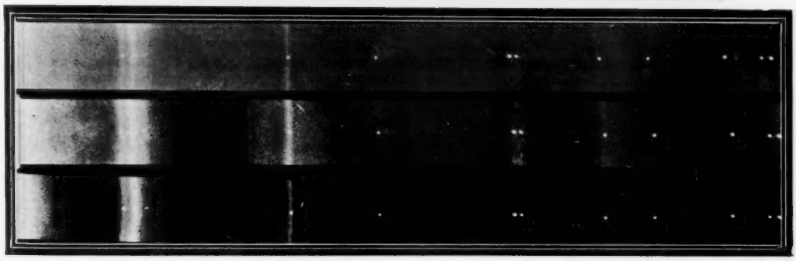

FIG. 10

X-Ray Diffraction Patterns

FIG. 11

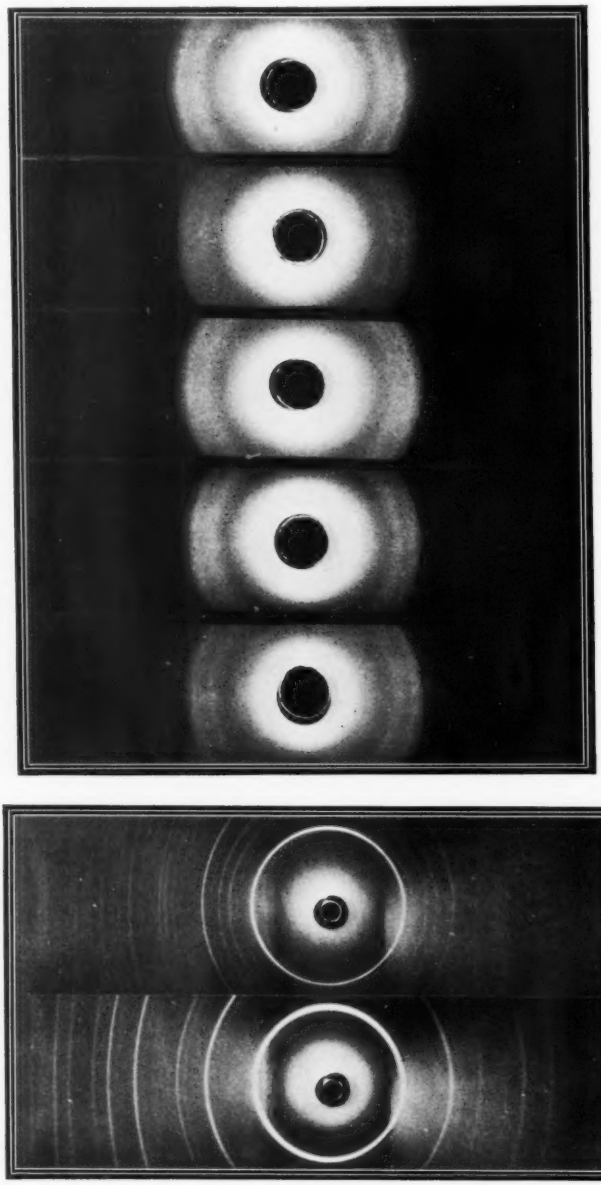

FIG. 12. X-Ray Diffraction Patterns

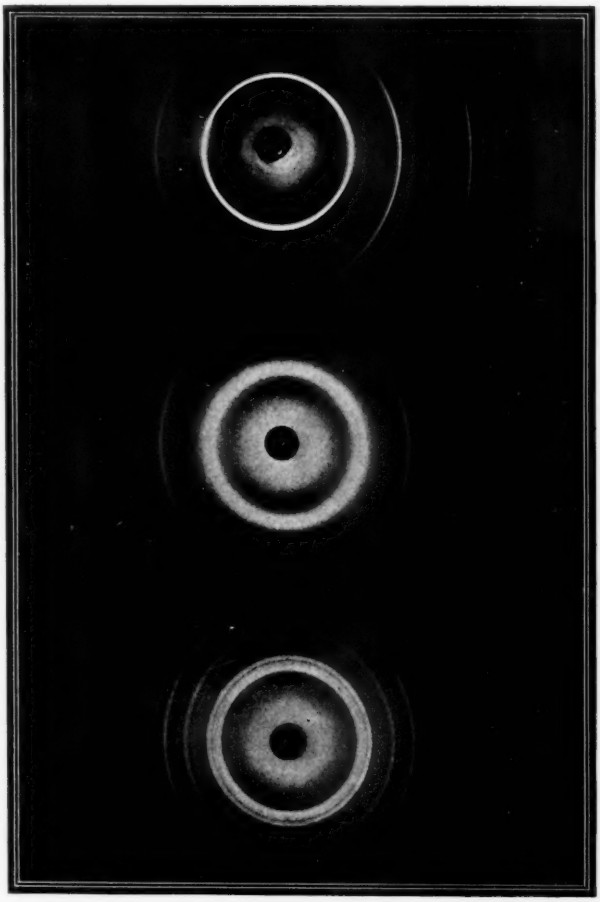

FIG. 13. X-Ray Diffraction Patterns

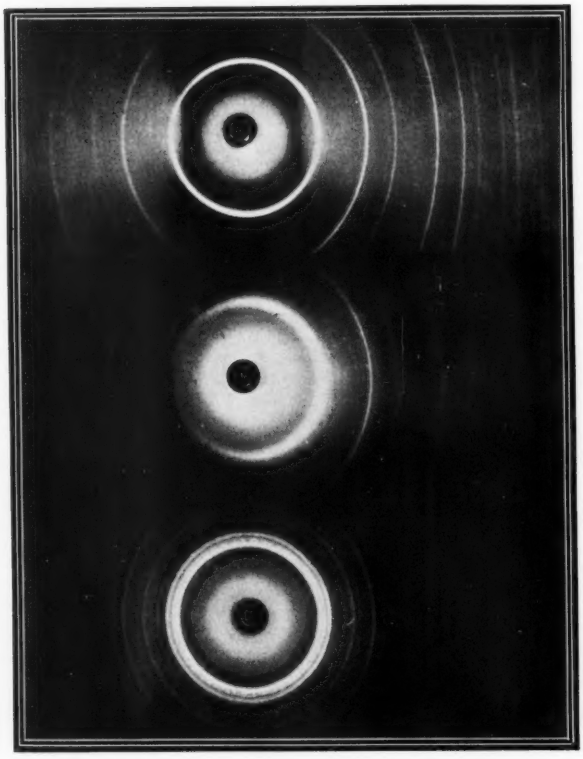

FIG. 14. X-Ray Diffraction Patterns

ANTHRAQUINONE AND ANTHRONE SERIES

Part XII. The Benzanthrone Condensation on 2-Chloroanthraquinone

By P. N. Pandit, B. D. Tilak, F.A.Sc. and
K. Venkataraman, F.A.Sc.
(*Department of Chemical Technology, University of Bombay*)

Received June 3, 1953

The benzanthrone condensation on substituted anthraquinones sometimes gives a mixture of substituted benzanthrones, and sometimes takes a single course. Thus α-chloroanthraquinone gives all the three possible chlorobenzanthrones,[1] while α- and β-hydroxyanthraquinone give 6- and 4-hydroxybenzanthrone respectively[2]; but the formation of the other possible isomers is not excluded since the products of reaction have not been submitted to chromatographic analysis. Alizarin gives 5:6-dihydroxybenzanthrone (isobenzalizarin).[2, 1] Neither anthraquinone-1-carboxylic acid nor the corresponding anthrone condenses with glycerol and sulphuric acid,[3] but the amide of anthraquinone-1-carboxylic acid leads to benzanthrone-8- and 11-carboxylic acids.[3] By the condensation of diphenylmethane-2:4′-dicarboxylic acid with glycerol and sulphuric acid benzanthrone-9-carboxylic acid has been obtained.[3] The benzanthrone condensation on anthraquinone-2-carboxylic acid gives mainly the 10-acid, together with a small quantity of the 9-acid.[3] From these results Copp and Simonsen[3] concluded that "condensations with glycerol occur in the unsubstituted anthraquinone ring as would perhaps be expected on general theoretical grounds". The deactivating effect of the carboxyl group results in the unsubstituted ring being involved in the reaction, while hydroxyl and chlorine do not preclude the benzanthrone cyclization taking place in the substituted ring. 4:9-Dichlorobenzanthrone is obtained as the sole product of the benzanthrone condensation on 2:6-dichloroanthraquinone.[4]

Scholl and Seer[5] attempted to identify the "chlorobenzanthrone" (A), m.p. 129–29·5°, obtained by the action of glycerol and sulphuric acid on 2-chloroanthraquinone in the presence of aniline sulphate.[6] They prepared 9-chlorobenzanthrone (I; m.p. 186–87°) and 10-chlorobenzanthrone (m.p. 187–88°) respectively from *m*-chlorophenyl α-naphthyl ketone and *p*-chlorophenyl α-naphthyl ketone. A mixture of 9- and 10-chlorobenzaanthrones sintered at 140° and melted at 150°, and they therefore concluded

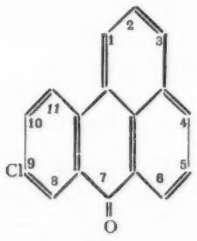

(I)

that the product (A) from 2-chloroanthraquinone must be 4- or 5-chlorobenzanthrone. On oxidizing compound (A) a β-chloro-anthraquinone-1-carboxylic acid (m.p. 297-99°) was obtained, which they considered to be 2- or 3-chloroanthraquinone-1-carboxylic acid.

The mixture of chlorobenzanthrones produced by the action of glycerol and sulphuric acid on 2-chloroanthraquinone in the presence of copper bronze has now been examined. From this crude mixture a homogeneous chlorobenzanthrone (B), m.p. 194·5–195°, was isolated by fractional crystallization from xylene. Chromic acid oxidation of this chlorobenzanthrone in acetic acid gave a β-chloroanthraquinone-1-carboxylic acid, m.p. 280–81°. Steam distillation of the xylene mother-liquor gave a yellow residue (C) which crystallized in needles from alcohol and melted at 128–30°. Oxidation of (C) with chromic acid gave a chloroanthraquinone-1-carboxylic acid, m.p. 295–300°. This compound (C) would therefore appear to be identical with the chlorobenzanthrone (A) isolated by Scholl and Seer[5] and assumed to be 4- or 5-chlorobenzanthrone.

The m.p.s of the known chlorobenzanthrones, which can be derived from β-chloroanthraquinone, and their corresponding oxidation products (β-chloroanthraquinone-1-carboxylic acids) are tabulated below:

Position of Cl in chlorobenzanthrone	m.p.	Position of Cl in chloroanthraquinone-1-carboxylic acid	m.p.
4	194–95°[1]	2	176–77°[7]
	204–05°[4]		
5	Not known	3	286–87°[8] (dec.)
9	186–87°[5, 9]	6	306–07°[9]
10	187–88°[5, 9]	7	262–64°[9]

Although the m.p. of compound (B) agrees with that of 4-chlorobenzanthrone, the m.p.s of the oxidation products (280–81°; 176–77°) do not agree. Both the chlorobenzanthrone (A) and its oxidation product do not agree in their m.p.s with any of the known chlorobenzanthrones and β-chloroanthraquinone-1-carboxylic acids. The only unknown chlorobenzanthrone being 5-chlorobenzanthrone, its oxidation product (3-chloroanthraquinone-1-carboxylic acid) was prepared from 1-amino-3-chloroanthraquinone[10] by conversion to 1-cyano-3-chloroanthraquinone and hydrolysis of the nitrile. The acid melted at 274–75° (ref. 8 cites m.p. 286–87°). With the oxidation product (m.p. 280–81°) of chlorobenzanthrone (B; m.p. 194·5–195°), the m.p. of 3-chloroanthraquinone-1-carboxylic acid was depressed to 240–50°, indicating that chlorobenzanthrone (B) was not the unknown 5-chlorobenzanthrone. The other three β-chlorobenzanthrones were therefore prepared for a direct comparison with (A) and (B). 9-Chlorobenzanthrone (I) was prepared from 9-aminobenzanthrone obtained by the dehalogenation of 3-bromo-9-aminobenzanthrone.[11] 10-Chlorobenzanthrone was prepared from *p*-chlorophenyl α-naphthyl ketone[5, 9] and 4-chlorobenzanthrone from 4-aminobenzanthrone.[2] 4-Chlorobenzanthrone, prepared by the Sandmeyer reaction on 4-aminobenzanthrone, had m.p. 194–95° (Luttringhaus and Neresheimer[4] quote 204–05°). A mixture of 9-chlorobenzanthrone or 10-chlorobenzanthrone with the chlorobenzanthrone (B) gave a depressed m.p.; but with (B) and 4-chlorobenzanthrone the m.p. remained unaltered. The benzanthrone condensation on 2-chloroanthraquinone therefore takes place partly in the substituted anthraquinone nucleus; and further, the m.p. cited in the literature[7] for 2-chloroanthraquinone-1-carboxylic acid is erroneous.

While the most readily isolable product of the condensation of glycerol with 2-chloroanthraquinone has now been shown to be 4-chlorobenzanthrone, the constitution of (C), m.p. 128–30°, which was probably identical with Scholl and Seer's chlorobenzanthrone (A), remained to be proved. Its low m.p. indicated that it was not a homogeneous compound, since it was unlikely that a chlorine atom in the β-position of the anthrone residue would lower the m.p. (170°) of benzanthrone. When a benzene solution of (C) was chromatographed on alumina, no clear separation into bands resulted; but when the main yellow band was eluted and the first portion of the yellow percolate concentrated, yellow needles, m.p. 185–86°, were obtained. There was no depression in m.p. on admixture with 9-chlorobenzanthrone. It was therefore obvious that the substance (C) was a mixture of chlorobenzanthrones. Other constituents of the mixture were difficult to isolate; but a second fraction of the percolate gave yellow needles, m.p. 175–85°,

raised to 180–85° by admixture with 10-chlorobenzanthrone, m.p. 187–88°. Mixtures of 9-chlorobenzanthrone and 10-chlorobenzanthrone in different proportions melted over a wide range, the lowest being 135–40°. Since the crude mixture first obtained from the glycerol condensation on 2-chloroanthraquinone analysed correctly for chlorobenzanthrone and melted at about 120°, and subsequent crystallization from alcohol raised the m.p. to 122–30°, it seems probable that Scholl and Seer's chlorobenzanthrone was a mixture of three chlorobenzanthrones: 4-, 9- and 10-.

EXPERIMENTAL

Benzanthrone condensation on 2-chloroanthraquinone

2-Chloroanthraquinone (25 g.) was dissolved in conc. sulphuric acid (380 c.c.) and the solution diluted with water (65 c.c.). A mixture of copper bronze (13 g.) and glycerol (13 g.) was added under stirring at 135° in 30 mins. Stirring was continued at the same temperature until all the chloroanthraquinone had been converted, as indicated by the absence of a red colour when a sample was made alkaline and treated with hydrosulphite (about 30 mins.). The reaction mixture was cooled to 70° and poured into warm water (21 g.). The precipitate was collected, washed with hot water and dried (27 g.). Extraction with boiling xylene (500 c.c.) and concentration of the filtrate to 150 c.c. after treatment with Norit, gave yellow needles (9 g.) with a range of m.p. (135–70°). Two crystallizations from acetic acid gave shining yellow needles, m.p. 194·5–95° (Found: C, 76·8; H, 3·1; Cl, 13·2. $C_{17}H_9ClO$ requires C, 77·2; H, 3·4; Cl, 13·4%). The mixed m.p. with authentic 4-chlorobenzanthrone,[1] m.p. 194·5–95° (Luttringhaus and Neresheimer,[4] m.p. 204–05°; Waldman *et al.*[1] m.p. 194·5°), prepared from 4-aminobenzanthrone,[2] was unchanged.

From the xylene mother-liquor on steam distillation a yellow product (15 g.), m.p. 120–25°, was obtained. Crystallization from alcohol (77 c.c.) gave yellow needles, m.p. 128–30° (Found: C, 76·8; H, 3·4; Cl, 13·0. $C_{17}H_9ClO$ requires C, 77·2; H, 3·4; Cl, 13·4%). This substance (1 g.) was dissolved in benzene (20 c.c.) and chromatographed on a column of alumina. Development was effected with the same solvent, and most of the substance formed a homogeneous yellow band. Less than half of the eluent from this yellow band, when collected separately and concentrated, gave yellow needles, m.p. 185°, unchanged on admixture with 9-chlorobenzanthrone (see later). The topmost portion of this yellow band, on extraction with alcohol and benzene and subsequent crystallization, gave yellow needles, m.p. 175–80°, depressed by admixture with either 4-chloro- or 9-chloro-benzanthrone; but with 10-chlorobenzanthrone,[5,9] m.p. 188–89°, the m.p. observed was 180–85°.

2-Chloroanthraquinone-1-carboxylic acid

To a boiling solution of 4-chlorobenzanthrone (1 g.) in glacial acetic acid (45 c.c.) chromic acid (4 g.) was added continuously in the course of 3 hours. Refluxing was continued for 3 hours and, on cooling, the reaction mixture was poured into water (200 c.c.). On adding sulphuric acid (2 c.c.), boiling for 15 minutes and cooling, a flocculent yellow precipitate separated. This was collected, washed with water and dried (0·4 g.). The carboxylic acid was purified by dissolving in dilute ammonia and precipitating. Two crystallizations from dilute acetic acid gave shining light yellow plates, softening at 279°, m.p. 280–81° (Literature,[7] m.p. 176–77°) (Found: C, 62·7; H, 2·3; Cl, 12·2. $C_{15}H_7ClO_4$ requires C, 62·8; H, 2·4; Cl, 12·4%).

9-Chlorobenzanthrone (I)

9-Aminobenzanthrone[11] (1 g.) was dissolved in conc. sulphuric acid (10 c.c.) and sodium nitrite (0·6 g.) was added to the solution, cooled to 0°, in the course of half an hour. The mixture was left in an ice-bath for 10 hours with shaking from time to time. On pouring into ice-water (200 c.c.) the yellow diazonium sulphate, which separated, was filtered and washed with a little ice-water. A suspension of this diazonium salt in conc. hydrochloric acid (10 c.c.) was added at 35° to a solution of cuprous chloride (1 g.) in 12% hydrochloric acid (30 c.c.) under stirring. The temperature was raised to 60° in the course of 1 hour and maintained at this temperature for 1 hour longer. The yellow product that separated was filtered, washed successively with water, 2% aqueous sodium hydroxide and water, and dried (1·2 g.; m.p. 175–80°). Two crystallizations from dilute acetic acid gave yellow needles, m.p. 186–87° (Scholl and Seer[5] cite m.p. 186–87°).

3-Chloro-1-cyanoanthraquinone (VIII)

To a solution of 1-amino-3-chloroanthraquinone[10] (3·6 g.) in conc. sulphuric acid (18 c.c.), cooled to 0°, was added a solution of sodium nitrite (1·1 g.) in conc. sulphuric acid (11 c.c.). The reaction mixture was kept in an ice-bath for 24 hours. On adding to ice (100 g.) the yellow diazonium sulphate separated. It was filtered, washed with a little ice-water, and treated with ice-water (80 c.c.), cuprous cyanide solution (40 c.c.), prepared from copper sulphate crystals (6·5 g.) and potassium cyanide (7·3 g.). A greyish substance separated with frothing. The reaction was continued on a boiling water-bath for 3 hours. The reaction product was collected, washed with boiling 8% potassium cyanide solution and then with boiling water, and dried (2·05 g.). Two crystallizations from benzonitrile gave shining grey needles, m.p. 275–76° (Found: N, 5·3; Cl, 13·5. $C_{15}H_6ClNO_2$ requires N, 5·2; Cl, 13·3%).

3-Chloroanthraquinone-1-carboxylic acid (IX)

3-Chloro-1-cyanoanthraquinone (VIII; 0·6 g.) was dissolved in conc. sulphuric acid (6 c.c.) and diluted with water (3 c.c.). The precipitate redissolved on warming and, after heating at 190° for 15 mins., the brownish product was collected on a sintered glass funnel, washed with dilute sulphuric acid and then with water, and dried. The carboxylic acid was purified by reprecipitating from ammonia solution and then crystallizing from dilute acetic acid, when light yellow needles, m.p. 274–75°, were obtained (Found: C, 62·6; H, 2·7; Cl, 12·2. $C_{15}H_7ClO_4$ requires C, 62·8; H, 2·8; Cl, 12·4%).

SUMMARY

From the product of the benzanthrone condensation on 2-chloroanthraquinone 4-chlorobenzanthrone, identical with the substance obtained by the Sandmeyer reaction on 4-aminobenzanthrone, has been isolated. Chromatographic analysis of a benzene solution of the residue on alumina gave 9-chlorobenzanthrone. The residue after separation of 9-chlorobenzanthrone contains the 10-isomer. 2-Chloroanthraquinone-1-carboxylic acid, prepared by chromic acid oxidation of 4-chlorobenzanthrone, has m.p. 280–81°, and not 176–77°, as stated in the literature. For comparison with the anthraquinone carboxylic acids obtained by oxidation of chlorobenzanthrones, 3-chloroanthraquinone-1-carboxylic acid has been prepared from 1-amino-3-chloroanthraquinone *via* 3-chloro-1-cyanoanthraquinone. There is no evidence of the formation of the unknown 5-chlorobenzanthrone in the product of the benzanthrone condensation on 2-chloroanthraquinone.

ACKNOWLEDGMENT

We are indebted to the Council of Scientific and Industrial Research for a Fellowship awarded to one of us (P. N. P.) and to Dr. T. S. Gore for the microanalyses recorded in the paper.

REFERENCES

1. Maki and Kikuti .. *Ber.*, 1938, **71**, 2031;
   Waldmann *et al.* .. *Chem. Ber.*, 1950, **83**, 171.
2. A. G. Perkin and Spencer .. *J. Chem. Soc.*, 1922, **121**, 474.
3. Copp and Simonsen .. *Ibid.*, 1942, 209.
4. Luttringhaus and Neresheimer .. *Ann.*, 1929, **473**, 259.
5. Scholl and Seer .. *Ber.*, 1922, **55**, 114.
6. .. D.R.P. 205, 294; Frdl, **9**, 820.
7. Dasgupta .. *Dissertation*, Berlin, 1913;
   Grandmougin .. *Chim. Ind.*, **9**, 46; F.P. 659, 962; Frdl. **16**, 1205.
8. Keimatsu, Hirano and Tanabe .. *J. Pharm. Soc.*, Japan, 1929, **49**, 85.
9. Cahn, Jones and Simonsen .. *J. Chem. Soc.*, 1933, 444.
10. B. S. Joshi .. *Ph.D. Thesis*, Bombay University.
11. Pandit, Tilak and Venkataraman .. *Proc. Ind. Acad. Sci.*, 1950, **32A**, 39.

ANTHRAQUINONE AND ANTHRONE SERIES

Part XIII. Synthesis of 5-Substituted Benzanthrones

By S. S. Malhotra, B. D. Tilak, F.A.Sc.
and K. Venkataraman, F.A.Sc.
(*Department of Chemical Technology, University of Bombay*)

Received June 3, 1953

The only 5-monosubstituted benzanthrone derivative to which a reference can be found in the literature is 5-nitrobenzanthrone, prepared by Boyes, Grieve and Rule[1] by a tedious route. Methyl 8-bromo-3-nitro-1-naphthoate was condensed with methyl *o*-iodobenzoate to form methyl 3-nitro-8-(*o*-carbomethoxyphenyl)-1-naphthoate; cyclization with sulphuric acid gave 5-nitrobenzanthrone-11-carboxylic acid, which was finally decarboxylated to 5-nitrobenzanthrone. Boriani[2] has mentioned a benzanthrone sulphonic acid obtained by sulphonation of benzanthrone and he considered that the sulphonic group probably entered the 5-position. The monosulphonation of benzanthrone has been studied by Pritchard and Simonsen[3] and Ioffe and Pavlova,[4] who have shown that the main product is the 9-sulphonic acid, the 3-sulphonic acid being formed to a very small extent. According to a German patent[5] 5-hydroxybenzanthrone is produced when 2-hydroxyanthranol, prepared from 2-hydroxyanthraquinone by reduction with zinc dust and ammonia, is heated with sulphuric acid and glycerine; the product, however, was later shown by Perkin[6, 7] to be 4-hydroxybenzanthrone. Two disubstituted benzanthrones in which one substituent is in the 5-position have been described. Waldmann *et al.*[8] synthesized 4:5-dihydroxybenzanthrone from 2:3-dihydroxyanthraquinone (hystazarin); the 5:6-isomer was prepared by the Scholl cyclization of 2:3-dihydroxy-1-benzoylnaphthalene and also by the action of glycerol and sulphuric acid on alizarin.

5-Nitrobenzanthrone (I) has now been synthesized by taking advantage of the powerful directing influence of the acetamido group. Nitration of 4-acetamidobenzanthrone with fuming nitric acid in glacial acetic acid gave 4-acetamido-5-nitrobenzanthrone (II). Deacetylation of (II) with alcoholic sulphuric acid proceeded in quantitative yield, and the constitution of the product as 4-amino-5-nitrobenzanthrone was established by reduction with methanolic sodium sulphide to a diamine which condensed with phenanthraquinone to a quinoxaline. The adjacent orientation of the

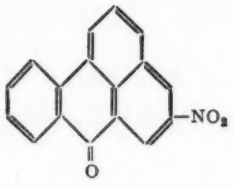

(I)

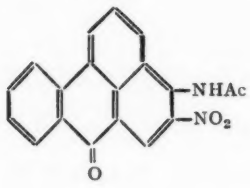

(II)

amino groups was also shown by the ready formation of the corresponding phenylimidazole (III) when the diamine was treated with benzoyl chloride.

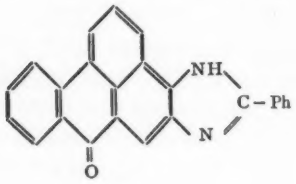

(III)

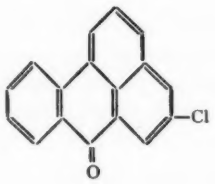

(IV)

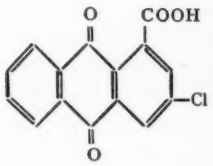

(V)

On diazotizing 4-amino-5-nitrobenzanthrone with sulphuric acid and sodium nitrite and refluxing the diazonium sulphate with alcohol, deamination took place to give 5-nitrobenzanthrone (I). Reduction of (I) with methanolic sodium sulphide gave 5-aminobenzanthrone from which 5-chlorobenzanthrone (IV) was prepared by the Sandmeyer reaction. Oxidation of this chlorobenzanthrone with chromic anhydride in acetic acid led to 3-chloroanthraquinone-1-carboxylic acid (V), identical with an authentic sample synthesized by an unambiguous route.[9] Oxidation of 5-nitrobenzanthrone gave 3-nitroanthraquinone-1-carboxylic acid.

EXPERIMENTAL

4-*Acetamido*-5-*nitrobenzanthrone*

4-Hydroxybenzanthrone was prepared by the action of potassium hydroxide and potassium chlorate on benzanthrone in the presence of anthraquinone according to the procedure described by Bradley and Jadhav.[10] Ammonolysis of 4-hydroxybenzanthrone according to Perkin and Spencer[7] gave 4-aminobenzanthrone, which was crystallized from chlorobenzene. Acetylation of 4-aminobenzanthrone was effected by heating the finely powdered substance (20 g.) with acetic anhydride (60 c.c.) on a low flame for 2 mins.; a yellow crystalline compound separated, which was washed with ether and dried (22 g.). The m.p. (264–65°) agreed with the m.p. cited for the monoacetyl derivative by Perkin.[7]

4-Acetamidobenzanthrone (20 g.) was heated on a water-bath with glacial acetic acid (1100 c.c.) under stirring. A solution of fuming nitric acid (d. 1·49; 12 c.c.) in glacial acetic acid (30 c.c.) was quickly added and stirring continued for 20 mins., when yellow needles (18·3 g.) separated. This substance was filtered off while the mixture was hot, and washed with hot acetic acid. On crystallization from nitrobenzene, 4-acetamido-5-nitrobenzanthrone was obtained as yellow needles, m.p. 312° (Found: C, 68·8; H. 3·6; N, 8·6. $C_{19}H_{12}N_2O_4$ requires C, 68·7; H, 3·6; N, 8·4%).

4-*Amino*-5-*nitrobenzanthrone*

A solution of 4-acetamido-5-nitrobenzanthrone (15 g.) in conc. sulphuric acid (150 c.c.) and 95% alcohol (750 c.c.) was refluxed for 4 hours and diluted with water. The precipitate was collected, washed free from acid and dried (13 g.). On crystallization from nitrobenzene 4-amino-5-nitrobenzanthrone was obtained as golden yellow silky needles, m.p. 347–48° (Found: C, 70·2; H, 3·4; N, 9·5. $C_{17}H_{10}N_2O_3$ requires C, 70·3; H, 3·5; N, 9·7%).

4: 5-*Diaminobenzanthrone*

Finely powdered 4-amino-5-nitrobenzanthrone (5 g.) was refluxed under stirring with 10% alcoholic sodium sulphide (110 c.c.) for 6 hours. A deep red crystalline mass separated and was filtered, washed with hot water and dried (4·2 g.). Two crystallizations from *o*-dichlorobenzene gave deep red shining needles which decomposed without melting at 257–58° (Found: C, 78·6; H, 4·5; N, 10·7. $C_{17}H_{12}N_2O$ requires C, 78·4; H, 4·6; N, 10·8%).

4: 5-*Diacetamidobenzanthrone*

To a clear solution of 4: 5-diaminobenzanthrone (0·2 g.) in hot glacial acetic acid (7 c.c.) acetic anhydride (0·8 c.c.) was added and the solution refluxed for 30 mins. On cooling minute yellow needles separated (0·2 g.). Crystallization from nitrobenzene gave microscopic yellow needles, m.p. 332–33° (*dec.*) (Found: C, 73·8; H, 4·6; N, 8·7. $C_{21}H_{16}N_2O_3$ requires C, 73·3; H, 4·6; N, 8·3%).

Condensation of 4: 5-*diaminobenzanthrone with phenanthraquinone*

A solution of 4: 5-diaminobenzanthrone (2·5 g.) and phenanthraquinone (2 g.) in alcohol (350 c.c.) was refluxed for 30 mins. The quinoxaline (3·8 g.) crystallized from nitrobenzene in yellow needles, m.p. 403–4° (Found: C, 85·9; H, 3·7; N, 6·5. $C_{31}H_{16}N_2O$ requires C, 86·1; H, 3·7; N, 6·5%).

Conversion of 4: 5-*diaminobenzanthrone into imidazole* (*III*)

Method (*a*).—The diamine (0·2 g.) was refluxed with benzoyl chloride (3 c.c.) for 15 minutes. A change in colour from red to yellow occurred.

The mixture was cooled, dropped into crushed ice and kept overnight. The yellow precipitate was filtered, washed with dilute ammonia, and dried (0·26 g.). Crystallization from nitrobenzene (30 c.c.) gave golden yellow needles, m.p. 417° (Found: C, 82·7; H, 4·5; N, 8·5. $C_{24}H_{14}N_2O$ requires C, 83·2; H, 4·1; N, 8·1%).

Method (*b*).—The diamine (0·2 g.) was dissolved in dry distilled dimethylaniline (4 c.c.) at the boil and the solution was cooled to about 80°. Benzoyl chloride (0·3 c.c.) was added, when a golden yellow crystalline precipitate separated immediately. On cooling, ether (40 c.c.) was added and the precipitate filtered, washed with ether and dried (0·25 g.). Crystallization from nitrobenzene gave golden yellow needles, m.p. 417°, identical with the substance obtained by method (*a*).

5-Nitrobenzanthrone

4-Amino-5-nitrobenzanthrone (10 g.) was dissolved in conc. sulphuric acid (200 c.c.) and cooled in ice and salt. Sodium nitrite (4 g.) was gradually added under vigorous stirring during one hour. Crushed ice (350 g.) was added from time to time, so that the temperature was not allowed to rise above 20°. After stirring for one hour longer the reaction mixture was poured into 95% alcohol (400 c.c.). Vigorous evolution of nitrogen took place and the colour changed from bluish violet to yellowish brown. On refluxing for 2 hours and cooling, the precipitate was collected, washed free from acid and dried (8 g.). Crystallization from 500 parts of glacial acetic acid or 50 parts of acetic anhydride or 10 parts of nitrobenzene gave light brown needles, m.p. 281° (Boyes, *et al.*, cite m.p. 287°) (Found: C, 74·4; H, 3·4; N, 5·2. $C_{17}H_9NO_3$ requires C, 74·2; H, 3·5; N, 5·1%).

3-Nitroanthraquinone-1-carboxylic acid

To a boiling suspension of 5-nitrobenzanthrone (1 g.) in acetic acid (40 c.c.), chromium trioxide (2·5 g.) in 50% acetic acid (10 c.c.) was added during 3 hours. Refluxing was further continued for 3 hours. The mixture was then poured into water (200 c.c.) and left overnight. The precipitate was filtered, washed, dissolved in hot dilute ammonia, and filtered. The ammoniacal solution was acidified with hydrochloric acid, and the precipitate collected, washed and dried (0·36 g.). Crystallization from acetic acid gave pale pink plates, m.p. 270° (Found: C, 60·7; H, 2·5; N, 4·9. $C_{15}H_7NO_6$ requires C, 60·6; H, 2·7; N, 4·7%).

5-Aminobenzanthrone

5-Nitrobenzanthrone (5 g.) was suspended in methanol (200 c.c.) and treated with fused sodium sulphide (10 g.) in water (10 c.c.). After stirring

under reflux for 6 hours, methanol was distilled off, the bright red residue washed with water and dried (4 g.). On crystallization from chlorobenzene bright red shining needles were obtained, m.p. 235° (Found: C, 83·5; H, 4·6; N, 6·0. $C_{17}H_{11}NO$ requires C, 83·2; H, 4·8; N, 5·7%).

5-Acetamidobenzanthrone

5-Aminobenzanthrone (0·2 g.) was dissolved in boiling glacial acetic acid (7 c.c.). The clear solution was cooled to 90° and acetic anhydride (0·5 c.c.) added, when a yellow crystalline precipitate immediately separated. The mixture was heated on a boiling water-bath for ten minutes and the product filtered and dried (0·22 g.). Crystallization from nitrobenzene gave yellow needles, m.p. 313° (Found: N, 5·1; $C_{19}H_{13}NO_2$ requires N, 4·9%).

5-Benzamidobenzanthrone

5-Aminobenzanthrone (0·2 g.) was refluxed with benzoyl chloride (2 c.c.) for 15 minutes and the mixture was dropped with stirring into crushed ice. The precipitate was collected, washed with ammonia and dried (0·26 g.). Crystallization from chlorobenzene gave small yellow needles, m.p. 266° (Found: N, 4·2. $C_{24}H_{15}NO_2$ requires N, 4·0%).

5-Chlorobenzanthrone

A solution of 5-aminobenzanthrone (1·5 g.) in conc. sulphuric acid (6 c.c.) was added gradually to a stirred solution of sodium nitrite (0·7 g.) in conc. sulphuric acid (5 c.c.) during half an hour, the temperature being kept below 10°. After one hour the mixture was poured over crushed ice. The yellow precipitate was collected, washed with a little water, and made into a paste with conc. hydrochloric acid (10 c.c.) and added to a well-stirred solution of freshly prepared cuprous chloride (1·5 g.) in 18% hydrochloric acid (25 c.c.). The mixture was stirred at room temperature till the evolution of nitrogen ceased (2 hours). The yellow precipitate was collected, washed free from acid, and purified by dissolving in boiling glacial acetic acid (30 c.c.), filtering and adding a few drops of water. Clusters of microscopic needles separated, m.p. 198–99°. Crystallization from benzene gave shining yellow needles, m.p. 205–6° (Found C, 77·6; H, 3·4; Cl, 13·1. $C_{17}H_9ClO$ requires C, 77·2; H, 3·4; Cl, 13·4%).

3-Chloroanthraquinone-1-carboxylic acid

A solution of 5-chlorobenzanthrone (0·5 g.) in boiling acetic acid (10 c.c.) was slowly treated during 3 hours with a solution of chromium trioxide (1·2 g.) in 50% acetic acid (3 c.c.). After refluxing for 3 hours and pouring

into water (100 c.c.), the precipitate was collected, washed, dissolved in dilute aqueous ammonia and reprecipitated with acid. The light yellow crystalline mass (0·23 g.) crystallized from dilute acetic acid in light yellow needles, m.p. 274°, unchanged on admixture with an authentic sample of 3-chloroanthraquinone-1-carboxylic acid prepared from 1-amino-3-chloroanthraquinone.

SUMMARY

5-Nitrobenzanthrone has been synthesized by nitration of 4-acetamidobenzanthrone, hydrolysis to 4-amino-5-nitrobenzanthrone and subsequent deamination. The adjacent orientation of the amino and nitro groups was shown by reduction to a diamine, which formed a quinoxaline with phenanthraquinone and an imidazole with benzoyl chloride. Reduction of 5-nitrobenzanthrone gave 5-aminobenzanthrone which was converted to 5-chlorobenzanthrone. Oxidation of 5-chlorobenzanthrone gave 3-chloroanthraquinone-1-carboxylic acid, identical with the acid prepared from 1-amino-3-chloroanthraquinone.

ACKNOWLEDGMENT

We are greatly indebted to the Council of Scientific and Industrial Research for a Fellowship awarded to one of us (S. S. M.) and to Dr. T. S. Gore for the microanalyses.

REFERENCES

1. Boyes, Grieve and Rule .. *J. Chem. Soc.*, 1938, 1841.
2. Boriani .. *Chem. Zentr.*, 1941, **2**, 1647.
3. Pritchard and Simonson .. *J. Chem. Soc.*, 1938, 2047.
4. Ioffe and Pavlova .. *J. Gen. Chem. U.S.S.R.*, 1944, **14**, 144.
5. B.A.S.F. .. D.R.P. 1,87,495; *Chem. Zentr.*, 1907, **2**, 1367.
6. A. G. Perkin .. *J. Chem. Soc.*, 1920, **117**, 697.
7. ——— and Spencer .. *Ibid.*, 1922, **121**, 474.
8. Waldmann, Postuwka and Maly *Ber.*, 1950, **83**, 171.
9. See preceding paper.
10. Bradley and Jadhav .. *J. Chem. Soc.*, 1937, 1792.

AN ELECTRO-STATIC BETA-RAY SPECTROMETER, USING A SPHERICAL CONDENSER

By M. C. Joshi and B. V. Thosar
(*Tata Institute of Fundamental Research, Bombay-1*)

Received August 3, 1953
(Communicated by Dr. H. J. Bhabha, F.R.S., F.A.SC.)

Introduction

The theory of a focussing device for electrons using the inverse first power radial electrostatic field within a cylindrical condenser was developed by Hughes and Rojansky (1929), who showed that a narrow diverging beam from a point source is refocussed at a point with angular separation of 127° from the source. A beta-ray spectrometer based on the principle was used by Backus (1945) and later in a modified form, using the second focus at 256°, by Thosar (1949). The latter also discussed the use of the inverse second power radial field between two concentric hemispherical shells and suggested a possible design for a beta-ray spectrometer of high luminosity, based on this principle, the theory of which was given earlier by Purcell (1938). Browne *et al.* (1951) have recently used a spherical electrostatic analyzer for measurement of nuclear reaction energies.

While the cylindrical condenser type of spectrometer is essentially a two-dimensional device, the spherical condenser type is a three-dimensional one and is, therefore, capable of giving very much larger transmission. A spectrometer using a spherical condenser has been constructed in this laboratory for work in the lower range of electron energies and this paper describes the instrument and its performance as tested by artificially accelerated electron beams.

Theory of the Instrument

Considering two concentric spherical shells of radii r_1 and r_2 respectively, differing in potential by P, the radial field at any point within the electrode space given by radius vestor r, is X, where

$$X = P \cdot \frac{r_1 r_2}{r_2 - r_1} \cdot \frac{1}{r^2}.$$

Following a line of treatment similar to that of Hughes and Rojansky for the cylindrical condenser, the following results can be readily obtained for this type of inverse, second power, radial field.

(*a*) An electron starting from a point on the medium sphere of mean radius r_0 and projected into the field perpendicular to the lines of force, will continue to move along the circular orbit of radius r_0 when its energy E in electron volts and potential difference P in volts on the electrodes satisfy the following relation.

$$E = k \cdot P$$

where the instrumental constant $k = \frac{1}{2r_0} \cdot \frac{r_1 \cdot r_2}{(r_2 - r_1)}$.

This is true of any central section of the electrodes and means that electrons of the right energy from a point source situated midway between the electrodes will travel along circular orbits over the medium sphere and will all meet at the opposite end of the diameter, the point of focus.

(*b*) It can be shown that in any given central section, the twin orbits of electrons of the right energy but making the small angle of divergence $\pm \alpha$ with the median circular orbit will also be refocussed, to a first approximation, at the focal point *i.e.*, at the pole opposite to the source. Actually there is a second order aberration of the focal position for these divergent orbits, where the departure from perfect focussing is $2\alpha^2 r_0$.

(*c*) The resolving power is obtained by calculating the spread of energy dE of the electrons that will be admitted through the width of this focal aberration, *i.e.*, $2r_0\alpha^2$. This gives the resolving power $\frac{dE}{E} = \alpha^2$.

In obtaining the above results, the relativity change of mass with velocity is neglected.

(*d*) The transmission of the instrument will be determined by the angle of divergence 2α, over which, in any central section, the electron beam is admitted through the slit system and the angle θ, giving the useful section of the sphere. In practice, it is not possible to use the complete hemisphere for collection of particles and some 25° section at each edge has to be left out, to reduce distortion due to the edges. Also the angle of divergence α has to be small, to keep the focal aberration at a small value.

CONSTRUCTION OF THE INSTRUMENT

Fig. 1 is a vertical section of the vacuum chamber with electrodes in position. The cylindrical vessel T is made of brass, $\frac{1}{4}''$ thick, and has internal diameter 15″ and height 11″. The upper lid, made convex for better mechanical strength, is removable and fits into the main chamber by means of a rubber gasket. An ionization gauze head can be inserted through an

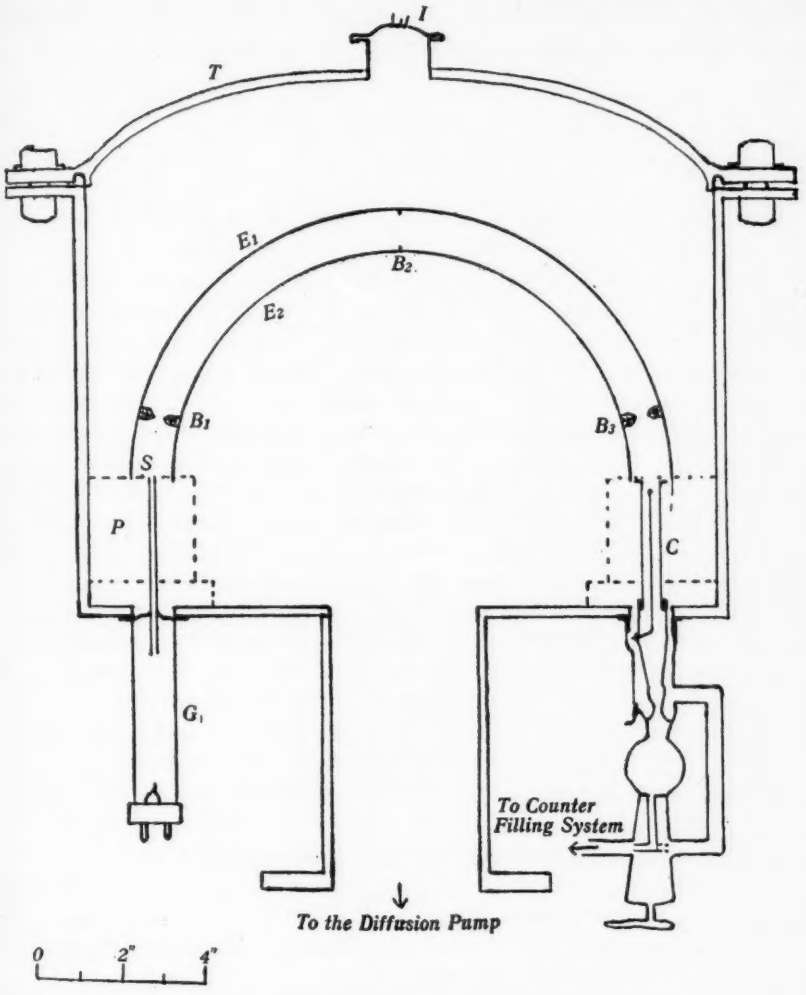

FIG. 1. Vertical Section of the Spectrometer

opening at the top of the lid, for measurement of pressure. Evacuation is by means of a forepump and a three-stage oil diffusion pump. The exit tube leading to the top of the diffusion pump is fitted at the centre of the bottom plate of the chamber. Pressures of the order of 10^{-5} mm. are obtained and this is adequate as the length of orbit from source to focus is about 19″. De-humidification and good vacuum conditions are, however, a special need

for this device as high voltages over narrow clearances have to be maintained and spurious electrical discharges must be prevented.

The electrodes E_1, E_2 are two hemi-spherical shells, made out of brass, 1/32″ thick. The inner radius of the outer sphere is 6 + 7/16″ and that of the outer surface of the inner sphere is 5 + 9/16″. The mean electrode distance is $\frac{7}{8}$″, which is estimated to be true to within 1/16″. Care was taken to have those surfaces well polished and free from sharp points to prevent electrical discharge at high voltages. The base P, on which the two electrodes are mounted consists of six perspex blocks, 2″ thick, equally spaced and cemented onto a perspex ring, which just fits inside the vacuum chamber and rests on the bottom plate. Concentricity of the two spheres is ensured, in the first place, by two accurately spaced circular grooves on the blocks into which the electrodes fit. Also the three slits B_1, B_2 and B_3, made out of perspex were so machined that their outer surfaces, in contact with the electrodes have the required curved shape to give a close fit between the electrodes. These perspex baffles, therefore, also serve as spacers between the electrodes. The central slit B_2 is midway between source and the focus, and is in the plane of symmetry. The two slits B_1 and B_3 unlike B_2 are at an angular distance of 15° from the source and the focus respectively. Considerable care had to be taken in the designing and making of these two slits as each of them occupies the electrode space in three dimensions, in an asymmetrical position. The widths of the slits was arranged, for experiments later described, to be such that the semi-angle of divergence α of the electron beam admitted into any central section of the electrode space was 3° 36′. The aperture in each slit extends over 130° in the middle, which defines the section of the spherical electrode space actually used for focussing, 25° on either side near the edges of the electrodes being left out to prevent distortion due to edge effects. Two alkathene rods fitted into the bottom plate of the vacuum chamber, carry the leads, which supply high voltage to the two electrodes. These leads, not shown in Fig. 1 may, however, be easily seen in the photographic reproduction of the instrument.

For the purpose of testing the performance of the instrument with beams of accelerated electrons to known variable energies, a simple design of an electron-gun was used. As the detecting device used was a G.M. Counter which is very much more sensitive compared to any device measuring electron-current, good collimation of the beam was aimed at, at the expense of intensity of the beam. A glass-tube with a tungstan filament sealed into it at the lower end was fixed to the bottom-plate of the tank such that the position of the source within the electrodes was vertically above a

sharp point on the filament. A vertical brass-tube, passing through a hole in the bottom-plate, projected into the glass-tube and its end directly facing the filament was covered with a fine wire-mesh. The other end of the tube was covered with a circular disc, with a central aperture of diameter 3/16″ and projected just inside the electrode space, occupying the position of the source. The electrones were accelerated by applying measured negative potential to the filament, the brass tube opposite being connected to the vacuum tank and, therefore, earthed. It was found that no heating of the filament was needed, quite high counting rates being attainable at room temperature, mainly due to field emission from the point on the filament.

Voltage supply to the electrodes is drawn from a voltage doubler circuit, using a 50 k.v. X-Ray transformer and two K.R. 3 rectifier tubes mounted on highly insulated secondary terminals of two filament transformers. There is a 50 Meg ohm resistance chain across the output as delivered by the smoothing condensers and a sensitive milliammeter, reading 1·2 m.a. at full scale, in series with this chain, reads the voltage developed. The voltage is varied by means of a variac auto-transformer, controlling the input to the H.T. transformer and this can be done in steps of 600 volts as read by the meter. A well insulated sensitive micro-ammeter and a 20 Meg ohm resistance is included in each of the two leads supplying the output voltage $\pm$ V/2 to the electrodes. Any leakage current in these meters is an indication of poor vacuum or other faults of insulation, while short-lived flicks in any of the meters serve to indicate spurious electrical discharges within the chamber. It is necessary to ensure that during any run of an experiment with this apparatus, there is a steadily negligible current in each of these micro-ammeters.

In theory, it is only the potential difference between the electrodes that determines the energy of the electrons focussed, but, in practice, it is an advantage to have the two electrodes above and below ground in potential by equal amounts. This makes the source and the counter, midway between the two electrodes, to be at ground potential, which is convenient. Also the difficulties of insulation are comparatively reduced in this arrangement.

A conventional H.T. supply with one rectifier tube and a smoothing condenser was used to give negative potential to the electron gun filament. The arrangement for measurement of voltage was similar to the one described above.

The end window counter C is a brass tube 2″ long and $\frac{1}{2}$″ diameter with a mica window of 1 mg./cm^2 thickness and a closely perforated brass disc on top as a support; 6 to 7 cm. pressure of argon and alcohol filling

mixture was used. As can be seen from Fig. 1, the counter can be evacuated first through the main vacuum chamber by turning the three-way tap below the tube supporting the counter. It can then be turned so as to connect the counter to the filling system. The difference of pressure on the two sides of the counter need not, therefore, exceed 7 cm.

PERFORMANCE OF THE INSTRUMENT

(1) The instrument was tested for its focussing properties in the range of electron energies 20 to 40 KeV. A known negative potential E was applied to the gun filament and the voltage $\pm$ V/2 on the two electrodes was slowly increased, keeping the counting rate under observation. The electrode voltage for which the counting rate is at a maximum was carefully noted. About six values of different electron energies were used and a plot was made of electron energy E in KeV against the electrode potential V in K. Volts. Fig. 2 gives the plot, showing that the points lie on a straight

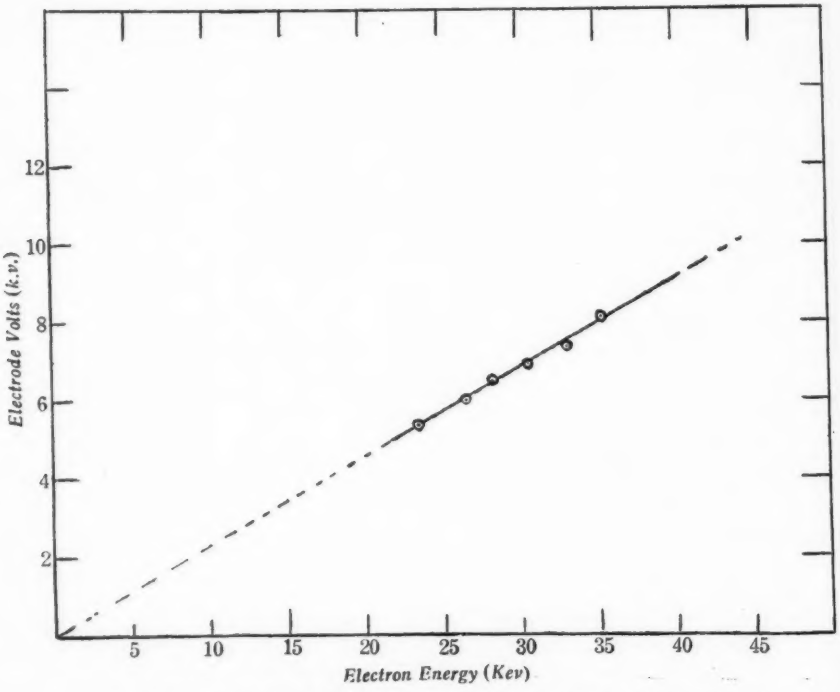

FIG. 2. Etectrode potential difference plotted against elebcron energy

line and that it passes through the origin, as required by the theory. The instrument constant K in the relation $E = K.V.$, comes out to be 4·37.

(2) To obtain a measure of the resolving power of the device, for the particular slit system used, a slight modification in the resistance chain and meter across the high voltage applied to the electrodes was made so that the electrode volts could be varied and read more accurately in smaller steps. The plot of the counting rate against electrode volts for the gun voltage of 26·5 K.V. is reproduced in Fig. 3. To obtain the spread dE of energy

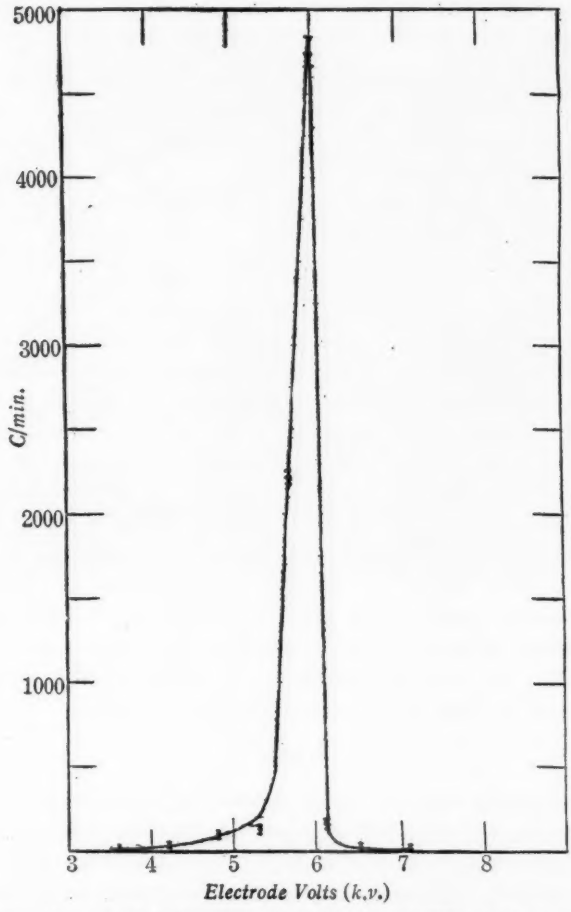

FIG. 3. Counting rate plotted against electrode potential difference for mono-energetic electrons of energy 26·5 KeV.

when electrons of energy E are being focussed, the width of the peak halfway between the base and the maximum has to be measured. It is seen that the two wings of the curve show a little asymmetry, the low energy side showing the effect of straggling of electron energies. This must be due to the scattering of the particles at the electrode walls. This effect will not be shown on the high energy wing of the peak, which is steeper. Obtaining the value of dE from the steeper side of the maximum alone, the resolving power dE/E comes out to be 1·66%, while the use of the overall width gives the value at about 3%. Also, the theory as worked out for a point source is not strictly applicable as the electrons issue out of a circular aperture of diameter 3/16″.

(3) The luminosity is determined by the solid angle over which the beam of electrons is admitted into the focussing space between the spheres. The angle of divergence of the beam in any central section of the spheres is, as already mentioned, $2 \times 3° 36'$ while the useful section of the sphere used is 130°. This gives the solid angle of acceptance as 1/44 of a sphere or 2·4%.

DISCUSSION

The instrument as described above is capable of further improvements in many respects. First, the electrodes should be spun metal spheres giving much greater mechanical accuracy as regards the spacing between them. Also to reduce the effect of scattering from these surfaces, they should preferably be of aluminium. The performance of the spectrometer can be improved by a more accurate voltage supply and voltage measuring device. The main characteristic of the instrument is large luminosity for a given resolving power so that comparatively weak sources may be studied. The upper limit to the electron energy that can be studied is set by the high voltage that can be steadily maintained on the electrodes, without spurious discharges taking place. Also there is the effect of defocussing due to relativity change of mass at higher energies, which has been referred to by Purcell (1938). At very low energies, the effect of the earth's magnetic field on the orbits may have to be taken into account.

SUMMARY

An electrostatic beta-ray spectrometer using a spherical condenser has been constructed for study of weak sources, and its performance has been tested with accelerated electron beams. The device, which is intended for low energy range of electrons, has, for the slit system employed, the resolving power of 1·6% with transmission 1/44 of a sphere which compares

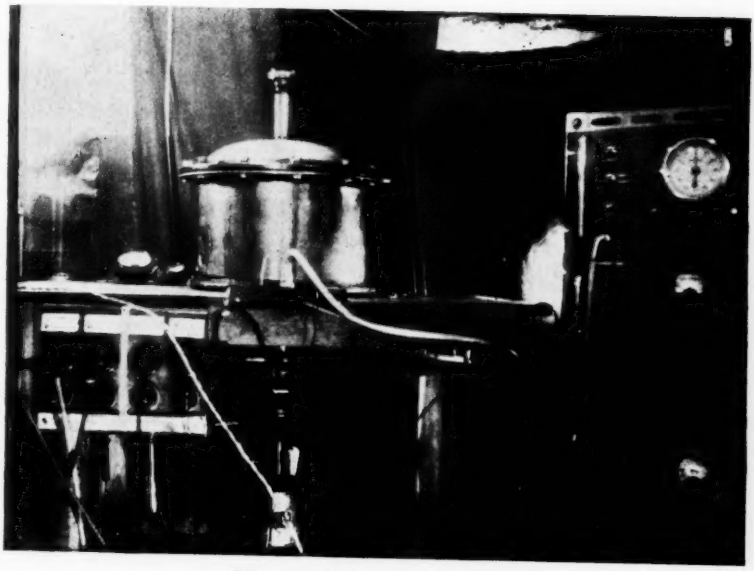

Electro-static Beta-ray Spectrometer

favourably with that in other types of spectrometer. The electron energy E (in KeV) focussed is 4·37 times the voltage V. in K.V. on the electrodes.

The authors wish to express their grateful thanks to Dr. H. J. Bhabha for encouragement and advice.

References

Hughes and Rojansky	..	*Phys. Rev.*, 1929, **34**, 284.
E. M. Purcell	..	*Ibid.*, 1938, **54**, 818.
Backus	..	*Ibid.*, 1945, **68**, 59,
B. V. Thosar	..	*Thesis, Birmingham*, 1949.
————	..	*Proc. Phys. Soc.*, 1949, **62 A**, 739.
Browne, Craig and Williamson		*Rev. Sci. Inst.*, 1951, **22**, 952.

Note added in proof:—Yoshiyuki and Kobayashi have recently published a letter, describing a similar instrument, in *Journ. Phys. Soc.*, Japan, 1953, **8**, No. 1, January–February.

APPLICATION OF THE Rb-Sr METHOD TO THE AGE DETERMINATION OF PHLOGOPITES

By V. S. Venkatasubramanian

(*Department of Physics, Indian Institute of Science, Bangalore-3*)

Received September 9, 1953

(Communicated by Prof. R. S. Krishnan, F.A.SC.)

1. Introduction

This paper describes the determination of the "uncorrected" ages of two phlogopite specimens belonging to the Archæan area by the "Rubidium-Strontium" method. The procedure adopted is similar to the one employed by Ahrens and co-workers (1946, 1949). The salient features of the method will be dealt with in brief.

The method depends on the natural β-decay of rubidium

$$Rb^{87} \rightarrow Sr^{87} + e^{-}$$

The amount of radiogenic strontium accumulated during a geological time t, is given by

$$N_{Sr} = N_{Rb}\,[1 - e^{-\lambda t}] \simeq N_{Rb} \cdot \lambda \cdot t$$

N_{Rb} = Initial concentration of Rb^{87}

since the decay constant λ is so small, $\lambda t \ll 1$ over the geological times considered, and the approximation holds; for the same reason, the decay of the parent is negligible.

Now, Rb^{87} forms 27% of the total Rb content (mass spectroscopic measurements), while the uncorrected ages are computed on the basis that the total measured strontium is radiogenic. The value obtained thereby provides an upper limit for the age.

For the uncorrected ages to be reliable, the radiogenic isotope Sr^{87} should predominate over the magmatic Sr^{87}. This fortunately happens to be the case in many minerals formed in the pegmatitic-pneumatolytic stage of crystallization. The tendency of Rb^{+} to follow K^{+} in potassium minerals and of Sr^{++} to follow Ca^{++} in calcium minerals cause a shift in association of Rb and Sr. Thus a progressive enrichment of Rb and impoverishment of Sr take place in hydrothermal potash minerals, especially the micas crystallizing out of pegmatites in the later stages.

Lepidolite is the most useful mineral. It contains the highest concentration of Rb, while mass-spectroscopic data show the concentration of Sr^{87} to be greater than 99%. Available data in the literature on phlogopite (Ahrens, 1950) indicate that a fair amount of Rb is present, and that the concentration of magmatic Sr is low. Of the two specimens of phlogopite investigated here, one is from Vizag District and the other from Travancore.

2. Spectrochemical Determination of Rubidium

The carbon arc with anode excitation was employed as the source. A Hilger E 1 spectrograph with glass train having a dispersion of 4 A.U./mm. in the 4000–4200 A.U. region was used to photograph the spectrum. The addition-plot method with a suitable internal standard was employed. The use of an internal standard and the factors governing its choice have been discussed in several publications (Ahrens, 1950 and Nachtrieb, 1950). In the addition-plot method the unknown itself is used as the base material and standards are prepared by adding known amounts of a compound of the element to be sought. The intensity ratio of the analysis pair (for the chosen internal standard) is plotted as a function of the percentage of element added. Then if I_a and I_s denote the intensities and C_a and C_s the concentrations of the analysis and internal standard elements,

$$\text{Log } \frac{I_a}{I_s} = \text{Log } \frac{K_a}{K_s} + \text{Log} \frac{C_a{}^{na}}{C_s{}^{ns}}$$

K_a and K_s are constants and n_a and n_s the emission factors.

Now, $C_s = \text{constant}$ and $C_a = (C_{a0} + C_{a'})$;

in the absence of self-absorption $n_a = n_s = 1$

C_{a0} initial and C'_a added concentrations.

$$\therefore \quad \frac{I_a}{I_s} = K\,(C_{a_0} + C_{a'});\ K = \text{constant}.$$

A plot of I_a/I_s *versus* $C_{a'}$ should be linear and should yield C_{a0} on extrapolation back to the abscissa.

The addition method avoids the use of purely external standards. It is based on the assumption that self-absorption is absent and errors due to compositional difference are negligible. These factors have to be verified in all cases.

3. Determination of Rb

The procedure adopted by Ahrens for lepidolite (Ahrens and Gorfinkle, 1951) is followed. The phlogopite is incorporated in an albite matrix.

First, the amount of rubidium in albite was found to be very small (just at the limit of detection) and was neglected. Next, the potassium content of the albite was determined using the addition-plot method. RbCl was added as the internal standard. The analysis pair was K — 4047 : Rb — 4202. In this way, by drawing the linear plot, the K-content of the albite was found to be **0·6%**. The primary standard is now prepared by dilution —10% RbCl + 90% Albite. Next, the phlogopite powder was diluted with 7 parts of albite. Finally, standards containing 0·1%, 0·25%, 0·5% and 1%, RbCl were prepared by the addition of the albite diluted RbCl standard to the albite diluted phlogopite. In such a case, the net concentration of K_2O in the mixture is of the order of 1·8%.

"Specpure" carbon electrodes were used. The electrodes were tested for purity by arcing after moistening by pure hydrochloric acid (Webb, 1937) and found to contain only traces of Ca and Ti impurities. (This was tested by finding the faint raies ultimes in the Hilger medium ultraviolet instrument.) D.C. arc excitation at 3 amps. was employed. The period of arcing was 2½ minutes, and a sector was employed transmitting half the intensity. Ilford Selochrome plates were used.

For calibration of the plates in the ragion 4100 A.U. the rotating stepped sector method was initially employed. However, after testing for the absence of self-absorption for the K-lines, K 4044 and 4047 A.U., internal calibration was employed. The theoretical ratio (I 4044/I 4047), (= 2·0) (obtained by the Lande rule for the doublet) was checked up and the plate curves were drawn by making use of this intensity relation.

Interference due to the cyanogen band with bandhead at 4216 A.U. was absent because of the high concentration of the alkali metal (Na—in Albite) during the whole period of arcing at low amperage.

As is well known, the analysis pair —K 4047—Rb 4202 is an ideal one. This is mainly because of the similarity in the volatilization rates of the alkali metals Rb and K, and the proximity of the excitation potentials (3·05 V for K—4044—4047 and 2·94 V for Rb 4202). The linear plot was very good and the line of best fit for the addition points passed through the point for the test specimen (*i.e.*, zero added percentage), thus revealing the absence of compositional errors.

To verify the absence of self-absorption the ratio Rb 4202/K 4047 was measured for larger dilutions with albite (9 times and 11 times) and the intensity ratio found to remain unchanged. (The rotating sector was employed for plate calibration in this experiment.)

The standard deviation was found to be equal to ± 3%.

4. Determination of Strontium

The most sensitive line of strontium is, of course, the atom line Sr 4607; but the fairly rapid variation of plate gamma with wavelength in this range is one difficulty for quantitative measurements. It is also impossible to use Sr 4215 because of interference with Rb 4215 and the cyanogen band-head. Hence the choice falls on Sr 4077.

Formerly, the main difficulty attending the use of this line was cyanogen band interference. This is because in the silicate specimen, the Sr-line is emitted with peak intensity not during the initial period of arcing, but during the later period when the alkalies have boiled off and cyanogen emission is most intense. The problem was solved by Ahrens, who converted the silicates into the low-boiling point fluorides. In this case CN-emission is quenched during the whole period of arcing and Sr 4077 can be used.

Ahrens has made use of the intensity ratio Sr 4077 : Rb 4202 for determining the Sr to Rb ratio, the latter line being effectively used as the internal standard. The same choice has been made in the present experiment. The choice is not quite good as Sr is an ion line, and the total excitation potentials differ considerably. However, the errors are not too great, possibly because the conversion to fluorides has reduced selective volatilization, and compositional differences were considerably reduced by the use of the addition-plot method, and the lines were comparable in intensity.

A primary $SrCl_2$ standard of 1% with phlogopite powder itself was prepared and by successive dilution, standards 0·05, 0·01, 0·005% $SrCl_2$ were obtained. All the standards were converted into fluorides and arced at 3·5 amps. (A second method of preparation of standards was also used involving addition of small volumes of dilute solutions before the hydrofluoric acid attack, and the results were very satisfactory.) An addition plot was made for % Sr added *versus* the intensity ratio of the analysis pair and the amount of total Sr was determined.

The standard deviation is rather high, $\pm$ **12%**.

5. Calculation of the Age

The most recent counter-measurements (Curran, 1951; Lewis, 1952; and MacGregor and Wiedenbeck, 1952) have not only established that the Rb $\rightarrow$ Sr radioactive process is one of simple β-decay, but also have given quite convergent values for the half life. The mean value of the half life of rubidium is taken as $6{\cdot}1 \times 10^{10}$ years. The geological age has been calculated as indicated below.

TABLE I

Specimen	(% Total Rb)	(% Total Sr.)	Age (10^6 years)
Phlogopite—Vizag	$(3{\cdot}5 \pm 0{\cdot}1) \times 10^{-1}$	$(1{\cdot}6 \pm 0{\cdot}2) \times 10^{-3}$	$[1490 \pm 200]$
Phlogopite—Travancore	$(2 \pm 0{\cdot}1) \times 10^{-1}$	$(1{\cdot}0 \pm 0{\cdot}15) \times 10^{-3}$	$[1630 \pm 200]$

As Ahrens has remarked, better reproducibility could be obtained by the use of barium as the internal standard.

I thank Prof. R. S. Krishnan for suggesting the problem and for his guidance and the Council of Scientific and Industrial Research for financial assistance.

SUMMARY

The geological ages of two Phlogopite Specimens have been determined by the Rubidium-Strontium method. The " addition-plot " is utilized with proper choice of internal standards.

REFERENCES

1. L. H. Ahrens .. *Report of the Committee for the Measurement of Geologic Time*, 1946-47, **47**.
2. ———— .. *Ibid.*, 1949–50, **29**.
3. K. Rankama and G. Sahama .. *Geochemistry*, University of Chicago Press, 1950.
4. L. H. Ahrens .. *Mineralogical Magazine*, 1948, **28**, 277.
5. ———— .. *Spectrochemical Analysis*, Addison-Wesley, 1950.
6. N. H. Nachtrieb .. *Ibid.*, McGraw Hill, 1950.
7. L. H. Ahrens and L. G. Gorfinkle *Am. J. Sci.*, 1951, **249**, 451.
8. D. A. Webb .. *Nature*, 1937, **139**, 248.
9. S. S. Curran *et al.* .. *Phys. Rev.*, 1951, **84**, 151.
10. M. H. Mac Gregor and M. L. Wiedenbeck *Ibid.*, 1952, **86**, 420.
11. G. M. Lewis .. *Phil. Mag.*, 1952, **43**, 1070.

SYNTHETIC EXPERIMENTS IN THE BENZOPYRONE SERIES

Part XXXIX. A Note on the Synthesis of Isogenistein and 8-Methyl Isogenistein

By A. C. Mehta, T. R. Seshadri, F.A.Sc.
and S. Varadarajan
(*From the Department of Chemistry, Delhi University*)

Received September 14, 1953

In an earlier paper on the Synthesis of Isogenistein, Seshadri and Varadarajan[1] observed that the condensation of 2-hydroxy-4:6:2′-trimethoxy phenyl benzyl ketone (I *b*) with ethyl formate gave rise to a product having a melting point of 180–81°. The analytical results agreed with the molecular formula $C_{18}H_{18}O_6$ and there was no loss on drying *in vacuo* at 110° for 6 hours. Since it did not give a green or blue colour with nitric acid (a reaction considered to be characteristic of isoflavanone derivatives), it was reported to be a hydrate of 5:7:2′-trimethoxy isoflavone, the molecule

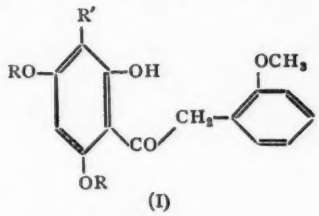

(I)

(*a*) R=R′=H
(*b*) R=CH₃; R′=H
(*c*) R=H ; R′=CH₃
(*d*) R=R =CH₃

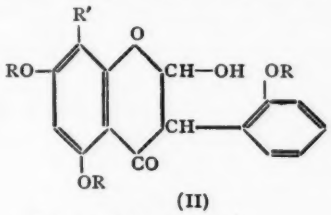

(II)

(*a*) R=CH₃; R′=H
(*b*) R=R′CH₃

of water being unusuallly strongly held. Prof. W. Baker in a private communication, however, suggested that this compound may be 2-hydroxy-5:7:2′-trimethoxy isoflavanone (II *a*), since 5:7:2′-trimethoxy-isoflavone (III *a*) obtained by him by the exthoxalyl chloride method[2] had a melting point 138–39°. Later Karmarkar *et al.*[3] reported that by the ethyl formate sodium method itself they obtained the above trimethoxy isoflavone (III *a*) melting at 138°. The condensation has now therefore been repeated a number of times; the product has invariably been found to melt at 180–81°. The same compound is also obtained by using methyl-formate in the place of ethyl formate. Whalley[4] has also reported a higher melting compound, m.p. 196° (decomp.), using methyl formate for the condensation. Since

Narasimhachari *et al.*[5] have found that with methyl formate 2-hydroxy isoflavanones are generally formed, it should be concluded that in this particular case ethyl formate has also behaved similarly and yielded 2-hydroxy-5:7:2′-trimethoxy-isoflavanone (II *a*). Dehydration of (II *a*) could be effected by using sodium acetate and acetic anhydride and also by 16% alcoholic sulphuric acid.[5] The dehydrated product is found to melt at 140–41° and the analytical values agree with the requirements of the anhydrous trimethoxy isoflavone (III *a*), $C_{18}H_{16}O_5$. When the above 2-hydroxy isoflavanone (II *a*) was boiled with animal charcoal in alcoholic solution, the dehydration was only partial; the resulting mixture could however be easily separated by fractional crystallisation. Whalley[4] has carried out the dehydration of (II *a*) using hot acetic acid and has reported 140° as the melting point of the dehydrated product.

Seshadri and Varadarajan[1] carried out the demethylation of 2-hydroxy-5:7:2′-trimethoxy isoflavanone (II *a*) using aluminium chloride in benzene and also hydriodic acid in acetic anhydride and reported that the isogenistein obtained thereby melted at 222–23° with sintering at 183°. Baker *et al.*[2] in their earlier note recorded 187° as the melting point for the Isogenistein (III *b*). Subsequently Karmarkar *et al.*[3] who used aluminium bromide in benzene for the demethylation of (III *a*) gave the same melting point (187°) for (III *b*). We have now demethylated our new sample of trimethoxy isoflavone (III *a*) (melting point 140–41°) using anhydrous aluminium chloride in benzene. After the first crystallisation from dilute alcohol the product melts at 187° but further crystallisation yields a sample which sinters at 183° and melts at 222–23°. More recently Baker *et al.*[6] have suggested that the isoflavone (III *b*) is dimorphic corresponding to the two melting points.

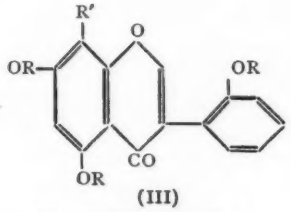

(III)

(*a*) R=CH_3; R′=H
(*b*) R=R′=H
(*c*) R=R=CH_3
(*d*) R=H; R′=CH_3

In connection with the above work another difference in the findings of different workers may be mentioned. Samples of 2:4:6-trihydroxy-2′-methoxy phenyl benzyl ketone (I *a*) obtained by Seshadri and Varadarajan[1]

and by Whalley[4] are monohydrates whereas Baker *et al.*[6] and Karmarkar *et al.*[3] have obtained it in the anhydrous form.

Investigations similar to above have now been made on the condensation of ethyl formate with 2-hydroxy-3-methyl-4 : 6 : 2′-trimethoxy phenyl bnzyl ketone (I *d*), reported earlier.[7] The product has been found definitely to be 2-hydroxy-5 : 7 : 2′-trimethoxy-8-methyl isoflavanone (II *b*); it undergoes dehydration when boiled with sodium acetate and acetic anhydride yielding 5 : 7 : 2′-trimethoxy 8-methyl isoflavone (III *c*). Whalley[4] has also reported similar results. However, Karmarkar *et al.*[3] under the same conditions have obtained 5 : 7 : 2′-trimethoxy-8-methyl isoflavone (III *c*) directly.

In the present work the above ketone (I *d*) has been made from C-methyl phloroglucinol[8] and *ortho* methoxy benzyl cyanide[1] and subsequent partial methylation of the trihydroxy ketone intermediate. Its condensation with methyl formate gave the same 2-hydroxy-isoflavanone (II *b*) as obtained from ethyl formate.[7] (II *b*) was dehydrated using sodium acetate and acetic anhydride and the dehydrated product (III *c*) was demethylated to 8-methyl isogenistein (III *d*) using anhydrous aluminium chloride in benzene following the method of Seshadri and Varadarajan.[7] However, Whalley[9] has reported that the demethylation of 8-methyl isogenistein trimethyl ether (III *c*) using aluminium chloride and benzene produces a mixture of 6 and 8-methyl isogenistein. But the exact conditions under which the change was brought about are not yet available. It has been conclusively established in several cases that anhydrous aluminium chloride in benzene does not cause any isomerisation of pyrone derivatives during demethylation (see Mukerji *et al.*[10]; Seshadri and Varadarajan[11]). In the present work also a single product was obtained and no isomeric change has been detected.

A careful research of the past literature has revealed that in the synthesis of a few complex isoflavones using sodium and ethyl formate the corresponding 2-hydroxy isoflavanones have been met with as intermediate stages. Wolfrom *et al.*[12] using osajetin and tetrahydro osajetin dimethyl ether and Harper[13] using derritol and elliptol methyl ethers have recorded this observation. However, the synthesis of isogenistein and 8-methyl isogenistein are the first two instances of the simple type of isoflavones wherein the exclusive formation of stable-2-hydroxy isoflavanones has been observed.

Experimental

2-Hydroxy-5 : 7 : 2′-trimethoxy isoflavanone (II a)

(i) *Preparation using methyl formate.*—A suspension of 2-hydroxy-4 : 6 : 2′-trimethoxy phenyl benzyl ketone[1] (I *b*) (1 g.) in freshly distilled methyl

formate (20 c.c.) was treated with powdered sodium (0·7 g.) at 0° and the mixture left in the refrigerator for 48 hours. Ice and hydrochloric acid were then added and the excess of methyl formate was allowed to evaporate slowly by gently warming the mixture in a hot water-bath. The precipitate was collected and crystallised from alcohol when 2-hydroxy-5: 7: 2′-trimethoxy isoflavanone came out as colourless rectangular rods melting at 180–81°. Yield 0·8 g. A mixed melting point with the product obtained by the ethyl formate condensation[1] was undepressed.

(ii) *Dehydration of (II a) to 5: 7: 2′-trimethoxy isoflavone (III a).*—(*a*) The above 2-hydroxy isoflavanone (II *a*) (1 g.) was refluxed with acetic anhydride (15 c.c.) and sodium acetate (5 g.) at 140–50° for 2 hours. The mixture was poured into ice and the solid product crystallised from dilute alcohol when 5: 7: 2′-trimethoxy isoflavone separated as colourless needles melting at 140–41°. Yield 0·4 g. (Found: C, 69·2; H, 5·2. $C_{18}H_{16}O_5$ requires C, 69·2; H, 5·1%).

(*b*) The above 2-hydroxy isoflavanone (II *a*) (0·5 g.) was dehydrated using 16% alcoholic sulphuric acid.[5] The product crystallised from dilute alcohol as colourless needles melting at 140–41°. Yield 0·35 g. A mixed melting point with the sample obtained in (*a*) was undepressed.

(*c*) 2-Hydroxy isoflavanone (II *a*) (0·5 g.) was taken in boiling alcohol (50 c.c.) and refluxed with animal charcoal (1 g.) for 30 minutes. The hot solution was filtered and allowed to cool. The crystalline mass, which separated out was filtered and was found to be the original 2-hydroxy isoflavanone (II *a*) (m.p. 180–81°). The mother liquor on concentration gave another crystalline solid which was identical in every respect with 5: 7: 2′-trimethoxy isoflavone obtained by methods (*a*) and (*b*).

5: 7: 2′-Trihydroxy isoflavone (Isogenistein) (III b)

Demethylation of 5: 7: 2′-trimethoxy isoflavone (III *a*) was carried out using anhydrous aluminium chloride in benzene in the same way as reported by Seshadri and Varadarajan.[1] But unlike the 2-hydroxy isoflavanone, 5: 7: 2′-trimethoxy isoflavone was easily soluble in benzene. The demethylated product crystallised from dilute alcohol as short yellow needles melting at 187°. On further crystallisation the substance sintered at 183° and melted completely at 222–23°.

5: 7: 2′-Triacetoxy isoflavone

The above trihydroxy isoflavone (III *b*) (0·15 g.) was acetylated by boiling with acetic anhydride and pyridine. The triacetate crystallised from alcohol as thin colourless plates melting at 135–37°. Baker *et al.*[6] have

reported 132–34° as the melting point of the acetate whereas Karmarkar *et al.*[3] have recorded 154°. (Found in a sample dried at 110° *in vacuo* for 5 hours: C, 63·6; H, 4·5. $C_{21}H_{16}O_8$ requires C, 63·6; H, 4·1%).

2:4:6-*Trihydroxy*-3-*methyl*-2′-*methoxy phenyl benzyl ketone* (*I c*)

To a solution of C-methyl phloroglucinol (7 g.) and *o*-methoxy phenyl acetonitrile[1] (9 g.) in dry ether (200 c.c.) was added powdered fused zinc chloride (2 g.). The mixture was cooled in an ice-bath and dry hydrogen chloride was passed in for 5 hours. The mixture was then left in the ice-chest for 12 hours, when the ketimine hydrochloride separated as a dark red oil. The ethereal layer was decanted and the residue washed with dry ether. Water (150 c.c.) was added to the residue and the mixture heated on a boiling water-bath under reflux for 2 hours. On cooling in the refrigerator a pale yellow solid separated. It was filtered and crystallised first from water, twice from ethyl acetate and finally from petroleum-ether when small yellowish white needles melting at 198–200° were obtained. Yield 5 g. (Found: C, 66·4; H, 5·5. $C_{16}H_{16}O_5$ requires C, 66·7; H, 5·6%).

2-*Hydroxy*-3-*methyl*-4:6:2′-*trimethoxy-phenyl-benzyl ketone* (*I d*)

The above ketone (I *c*) (2 g.) in dry acetone (150 c.c.) was refluxed with dimethyl sulphate (1·3 c.c.; 2 moles) and freshly ignited potassium carbonate (3 g.) for 4 hours. The potassium salts were filtered off and washed with acetone. The residue left after distilling off acetone crystallised from alcohol as thick colourless rectangular rods melting at 146–48°. Yield 1·8 g. A mixed melting point with an authentic sample of 2-hydroxy-3-methyl-4:6:2′-trimethoxy-phenyl-benzyl ketone described earlier[7] was not depressed.

2-*Hydroxy*-5:7:2′-*trimethoxy*-8-*methyl isoflavanone* (*II b*)

The above ketone (I *d*) (1 g.) was condensed with sodium (1 g.) and methyl formate (25 c.c.) at 0°. After keeping for 48 hours at the same temperature, ice and hydrochloric acid were added and the excess of methyl formate was removed under reduced pressure. The precipitate was collected and crystallised from alcohol when thick colourless prisms separated out and melted at 178–79°. A mixed melting point with the product obtained by the ethyl formate condensation[7] was undepressed.

5:7:2′-*Trimethoxy*-8-*methyl isoflavone* (*III c*)

The above 2-hydroxy isoflavanone (II *b*) (1 g.) was refluxed with fused sodium acetate (4 g.) and acetic anhydride (15 c.c.) for 2 hours at 140–50°. The mixture was treated with ice and the solid product filtered. It crystallised from dilute alcohol as colourless needles (m.p. 184–86°). Admixture

of this substance with the corresponding 2-hydroxy isoflavanone (II *b*) depressed the melting point to 160° (Found: C, 69·7; H, 5·3; $C_{19}H_{18}O_5$ requires C, 69·9; H, 5·5%).

5:7:2′-*Trihydroxy*-8-*methyl isoflavone* (8-*Methyl isogenistein*) (*III d*)

The above trimethyl ether (III *c*) (0·5 g.) was demethylated using anhydrous aluminium chloride in benzene following the procedure described earlier.[7] The demethylated product when crystallised from dilute alcohol twice, separated as colourless tablets melting at 230–32°. A mixed melting point with the sample described earlier[7] was not depressed.

SUMMARY

It is established that the condensation of 2-hydroxy-4:6:2′-trimethoxy phenyl benzyl ketone and its 3-methyl derivative with ethyl formate as well as with methyl formate produces the corresponding 2-hydroxy isoflavanones. These undergo dehydration to the trimethyl ether of isogenistein and 8-methyl isogenistein respectively. Demethylation of the above ethers can be conveniently effected by aluminium chloride in benzene solution. The 2-hydroxy isoflavanones also yield the same products by undergoing dehydration along with demethylation.

REFERENCES

1. Seshadri and Varadarajan .. *Proc. Ind. Acad. Sci.*, 1953, **37A**, 514.
2. Baker *et al.* .. *Chem. & Ind.*, 1952, 1058.
3. Karmarkar *et al.* .. *Proc. Ind. Acad. Sci.*, 1952, 552.
4. W. B. Whalley .. *J.A.C.S.*, 1953, **75**, 1059.
5. Narasimhachari *et al.* .. *J.S.I.R.*, 1953, **12B**, 287.
6. Baker *et al.* .. *J.C.S.*, 1953, 1860.
7. Seshadri and Varadarajan .. *Proc. Ind. Acad, Sci.*, 1953, **37A**, 526.
8. Shriner and Hull .. *J. Org. Chem.*, 1945, 228.
9. W. B. Whalley .. *Chem. & Ind.*, 1953, 277.
10. Mukerjee *et al.* .. *Proc. Ind. Acad. Sci.*, 1953, **37A**, 132.
11. Seshadri and Varadarajan .. *Ibid.*, 1953, **37A**, 149.
12. Wolfrom *et al.* .. *J.A.C.S.*, 1941, 1248.
13. Harper .. *J.C.S.*, 1942, 595.

STUDIES IN COLLOID OPTICS

Part IV. Sol-Gel Transition of Some Lyophilic Gels

By P. K. Katti

(*Lecturer in Physics, Delhi Polytechnic)

Received August 7, 1953

(Communicated by Dr. L. A. Ramdas, F.A.SC.)

1. Introduction

In an earlier paper[1] the results of our investigations on some lyophobic gels, obtained by the R. S. Krishnan[2] technique, have been discussed. In this paper we shall discuss very briefly the results on three lyophilic gels, *viz.*, agar-agar and gelatin in water and cellulose acetate in benzyl alcohol. Due to the great affinity of the solid to the liquid phase, these lyophilic gels show properties which widely differ from those of the lyophobic gels. These gels have been earlier investigated by Arisz,[3] Mardles[4] and Krishnamurthi[5] by using light scattering methods. Their results, based on the light scattering technique with only one beam of unpolarised light, is rather inadequate to investigate the size and shape of the colloid particles of the gels. The results of the present investigation will, therefore, be of interest.

2. Preparation of the Sols

Cellulose acetate sols of different concentration were prepared by mixing weighed quantities of pure cellulose acetate with benzyl alcohol which was previously dried over calcium chloride in a desiccator for several days. The mixtures of cellulose acetate and benzyl alcohol were allowed to stand in tightly corked test-tubes for a day. Clear sols of cellulose acetate in benzyl alcohol were then obtained by keeping the test-tubes containing the mixtures in a hot water-bath at 90° C. sufficiently long. As the removal of air bubbles from sols at high concentrations is difficult, the sols were maintained at 90° C. for a long time to keep their viscosity as low as possible and tapped several times to facilitate the upward movement of the air bubbles. At concentrations above 10% this process had to be continued for several days before the sols showed the absence of specks of light due to small air bubbles. The sols finally ready for investigation showed only faint Tyndall cones in a convergent beam of sunlight.

* These investigations were made when the author was working for his Doctorate under Dr. L. A. Ramdas, at the Meteorological Office, Poona.

Gelatine and agar sols of low concentration were obtained by the method of Krishnamurthi.[5] Sols of higher concentration, however, cannot be obtained by this method as it is impracticable to filter the viscous turbid sols in order to obtain clear sols suitable for investigation. Therefore clear sols of the highest concentration of agar-agar 1·5% and gelatine 3·0% respectively (obtainable by Krishnamurthi's method) were poured in shallow dishes and maintained at suitable high temperatures in order to remove sufficient water from them by evaporation. The shallow dishes containing the sol were covered with filter-paper which served the double purpose of protecting the sol from outside dust as well as of absorbing the moisture evaporated from the sol. The filter-paper was changed at intervals. By slow evaporation continued for sufficient time, dust-free sols of gelatin up to 12% and of agar-agar up to 8·0% concentration could be obtained.

3. THE SOL STATE

The lyophilic sols prepared at high temperatures remain unchanged when the temperature is reduced until the sols attain certain minimum values of temperature depending upon the type of the gel. We refer to these temperatures as optimum temperatures of sol-gel transition. The optimum temperatures for cellulose acetate, agar-agar and gelatin are 20° C., 39° C. and 25° C. respectively. Table I shows the intensity and depolarisation of

TABLE I

Intensity and Depolarisation Values of Cellulose Acetate Sols

Concentration %	1	2	3	4	5	7	10	15	20	25	30	40
ρ_h %	95	95	95	95	95	95	95	95	95	95	95	95
ρ_v %	1·3	1·3	1·5	1·8	1·8	1·8	1·8	1·5	1·5	1·3	1·3	1·3
$I_{4\pi/C} \times 10^3$	0·40	0·40	0·46	0·50	0·80	0·54	0·50	0·25	0·19	0·14	0·10	0·07

cellulose acetate of various concentrations. The values of ρ_h in the first row indicate that the size of the particles remains almost the same in all the sols. ρ_v increases slightly indicating an increase in the anisotropy of the sol particles in sols of concentration 4% to 10%. Variation of $I_{4\pi/C}$ [*i.e.*, the ratio of $I_{4\pi}$, the fraction of incident light scattered in all directions by 1 cm. of the medium, to the concentration (C) with concentration C] is shown in the third row. The ratio $I_{4\pi/C}$ remains constant up to about 3·0% showing that the light scattered by the sols varies directly as concentration. This is in complete agreement with the indications of ρ_h and ρ_v which show that

the size and shape of the particles in the sols do not alter sensibly in this range of concentration. A slight increase in the ratio between 3% to 5% may be due to the increase in the anisotropy of the particles. The ratio falls off rapidly with further increase in the concentration, the intensity of light scattered by a 40% sol being only seven times that scattered by a 1% sol. The values of ρ_h and ρ_v, however, remain unaltered indicating that the average size and shape of the particles in the 4·0% sol is nearly the same as in the 1% sol. Sols of agar-agar and gelatin show similar behaviour.

4. Sol-Gel Transition

If the lyophilic sols are cooled below the optimum temperatures mentioned in para 3, the viscosity and depolarisation values change continuously with time till the sols set completely. The increase in the viscosity is very rapid during the initial stages of the sol-gel transition. Therefore, while studying the sol-gel transition at temperatures far below the optimum temperature, increase in the viscosity of the sol at intermediate temperatures, while the hot sol is being cooled to the particular temperature, cannot be avoided. Moreover, the final size and shape of the gel particles set at any temperature depends to a large extent upon the initial viscosity of the sol. Therefore, for studying the sol-gel transition more in detail, four methods of cooling the hot sol to the particular temperature at which the sol-gel transition is to be studied were adopted. This enabled the study of four different groups of gels as it were.

(i) In the first group the gels were allowed to set completely at the optimum temperature. The constant values of intensity and depolarisation were recorded and the set gels were cooled to a lower temperature. They were again allowed to stand for sufficient time till the intensity and depolarisation attained constant values. These values of intensity and depolarisation were recorded and the gels were cooled to the next lower temperature. The values of intensity and depolarisation for a typical gel, *viz.*, 3% cellulose acetate gel as it is cooled from the optimum temperature of 20° C. to 5° C. are given in the first half of Table II (i). It may be remembered that at temperatures below 20° C. the changes in the size and shape of the gel particles are taking place in a highly viscous medium, *viz.*, the set gel.

(ii) In the second group the hot sols were cooled to the particular temperature under study at a slow rate of cooling, *i.e.*, about 1° C. in every three minutes. Measurements for I_z and ρ_v were made from the instant the required temperature was reached. Final values of intensity and depolarisation for 3% cellulose acetate gels set at different temperatures are shown in Table II (ii).

TABLE II

Intensity and Depolarisation for 3% Cellulose Acetate Gels

Temp. in °C.	(i)			(ii)			(iii)			(iv)		
	ρ_h %	ρ_v %	$I_{4\pi}\times10^3$	ρ_h %	ρ_v %	$I_{4\pi}\times10$	ρ_h %	ρ_v %	$I_{4\pi}\times10$	ρ_h %	ρ_v %	$I_{4\pi}\times10^3$
50	95	1·5	1·4	95	1·5	1·4	95	1·5	1·4	95	1·5	1·4
23	95	1·5	1·4	95	1·5	1·4	95	1·5	1·4	95	1·5	1·4
20	95	1·5	1·4	95	1·5	1·4	95	1·5	1·4	85	3·5	1·5
17	95	1·5	1·4	95	1·5	1·4	90	1·2	1·6	70	3·6	1·8
15	90	1·3	1·8	90	1·3	1·8	80	1·4	2·9	60	3·6	3·0
12	85	1·0	3·5	85	1·0	2·5	60	1·8	3·4	50	3·7	5·0
10	80	1·0	8·3	80	1·3	4·0	50	1·9	19·0	45	3·7	20·0
7	70	1·0	15·2	60	1·9	12·8	45	2·3	24·0	35	3·7	25·0
5	60	1·0	20·0	55	2·0	20·0	40	2·3	24·0	25	3·7	30·0
10	60	1·0	20·0	55	2·0	20·0	40	2·3	24·0	25	3·7	30·0
15	60	1·0	20·0	55	2·0	20·0	40	2·3	24·0	25	3·7	30·0
20	70	1·0	15·2	60	1·8	13·0	50	1·9	19·0	30	3·6	30·0
25	80	1·0	8·3	70	1·8	8·3	60	1·6	10·3	50	1·9	20·0
30	85	1·0	3·5	85	1·0	3·5	80	1·6	4·2	80	1·8	7·0
35	90	1·3	1·8	90	1·5	1·8	90	1·5	2·5	95	1·8	4·0
40	95	1·5	1·4	90	1·5	1·5	90	1·5	1·7	95	1·8	3·0
45	95	1·5	1·4	90	1·5	1·5	95	1·5	1·5	95	1·8	1·4
50	95	1·5	1·4	95	1·5	1·5	95	1·5	1·5	95	1·5	1·4
70	95	1·5	1·4	95	1·5	1·4	95	1·5	1·4	95	1·5	1·4

(iii) In the third group the hot sol was cooled to the required temperature as quickly as possible by introducing the test-tube containing the hot sol directly into a water-bath maintained at about the desired temperature. Measurements for I_z and ρ_v were made from the instant the sol reached the desired temperature. It is evident that in the third group the sol reaches the desired temperature earlier than in the second group and hence the increase in viscosity taking place at the intermediate temperatures in the third group is much less than that in the second group.

(iv) Next an attempt was made to reduce the effect of increase in the viscosity of the sol, at intermediate temperatures still further by keeping the sol well stirred while it was cooling rapidly as described above, was also tried. The stirring of the sols, however, introduces great limitations on the range of concentrations and the temperatures at which the sol-gel transition

can be studied. Stirring introduces inhomogeneity in viscous sols and thus no observations could be made at higher concentrations. This method is suitable only when the viscosity changes are not rapid. Cellulose gels up to 3%, gelatin gels up to 1% and agar-agar gels up to 1·5% concentration could be studied by this method.

5. Discussion of the Results

As mentioned in the above paragraph, Tables II (i), II (ii), II (iii) and II (iv) show the variation of intensity and depolarisation with temperature for a typical gel, *viz.*, 3% cellulose acetate gel. ρ_h decreases continuously with decrease in temperature indicating that gels set at lower temperature contain particles of larger size. On comparing the corresponding values of ρ_h in Tables II (i), (ii), (iii) and (iv) we find that the size of the particles increases as we go from the first group to the fourth. Table III shows the

Table III

Intensity and Depolarisation of Cellulose Acetate Gels set at 5° C.

Concentration	1	2	3	4	5	7	10	15	20	25	30	40
ρ_h %	40	40	40	30	30	45	50	50	60	65	75	75
ρ_v %	0·9	1·0	2·3	3·0	3·0	3·7	3·5	2·8	2·5	1·3	0·9	0·9
$I_{4\pi} \times 10^3$	7·3	16·0	24	90·0	120	80·0	60	25	20	12	4·4	4·4

variation of intensity and depolarisation with concentration for cellulose acetate gels of the third group set at 5° C. The values of ρ_h decreases continuously with increase in the concentration from 1% to 5%, and later with further increase in concentration ρ_h increases again. The values of ρ_h at the highest concentration of 40% show very slight decrease from the sol value of 95% to 85% after the gels set completely at 5° C. This indicates that the increase in the size of the particles when a sol sets to a gel is more appreciable as the concentration increases from 1% to 5% while with further increase in the concentration the changes in the size of the particles when the sol sets to a gel becomes less appreciable. At concentrations of 30% and 40% the sols change over to the gel state without any appreciable change in the size of the particles.

Variation of ρ_v.—The second row of Table III shows the variation of ρ_v with concentration. It is seen that the anisotropy of the gel particles

increases as we go from 1% to 5% gels. With further increase in the concentration the gel particles become more and more symmetrical.

On comparing the values of ρ_v at different temperatures in Table II (i), (ii), (iii) and (iv), we find that as temperature decreases ρ_v in general shows three different types of variations. (1) ρ_v continuously decreases with decrease in temperature showing that the particles of the gels become more symmetrical as the temperature decreases. (2) ρ_v decreases continuously at first but later on increases again as the temperature is decreased further indicating that as the temperature is decreased the gel particles at first tend to become more symmetrical but later on grow more asymmetric again. (3) ρ_v increases right from the start with decrease in the temperature. Table IV summarises the variation of ρ_v with temperature throughout the whole range of investigation on the lyophilic gels. These results indicate that the concentration range where the colloid particles grow to form asymmetric aggregates increases rapidly as we go from the first group of gels to the fourth indicating that the low initial viscosity of the sols

TABLE IV

Type of variation	Group to which the gels belong	Concentration range in which the type of variation of ρ_v mentioned in Col. 1 is noticed		
		Cellulose Acetate	Gelatin	Agar-Agar
ρ_v decreases continuously with decrease in tempeture.	I Group	1%, 2%, 3%, 30% and 40%	0·2% to 1·5 and 7% to 12%	0·06% to 1·0%
	II Group	1%, 2% and 40%	0·2% to 1·5% and 8% to 12%	0·06% to 0·5%
	III Group	1% and 40%	0·2% to 0·5% and 8% to 12%	0·06% to 0·2%
	IV Group	1%	0·2%	0·06%
ρ_v first decreases and then increaes again as the temperature decreases	I Group	4%, 5% and 15%	2% and 7%	1·5%
	II Group	3%, 25% and 30%	1·5% and 7%	1·0%
	III Group	2%, 3%, 25% and 30%	1%, 1·5% and 7·0%	0·5%
	IV Group			
ρ_v increases right from the beginning as temperature increases	I Group	No where	0·5%	No where.
	II Group	6% and 12%	2·5 to 6·0	1·5%
	III Group	4% and 20%	2·6%	1·0%
	IV Group	4% and 20%	2% to 6%	0·5%
		2% to 6%	1% to 2·5%	0·2%

suppresses the growth of the spherically symmetrical particles and favours the formation of asymmetric aggregates.

Variation of Intensity during the Sol-Gel Transition.—I_δ as in earlier papers of this series stands for the density scattering computed from the observed value I_z from the relation:

$$I_\delta = I_z \cdot \frac{3 + 3\rho_v}{3 - 4\rho_v}.$$

The I_δ-time curves during the sol-gel transition taking place at any temperature show different characteristics which seem to be closely related to the corresponding variation of ρ_v. (1) The I_δ-time curves show very prominent points of maxima when the particles increase in size and anisotropy as shown by the decrease in ρ_h and increase in ρ_v. (2) The points of maxima are absent when the increase in the size is accompanied by the increase in the spherical symmetry of the particles during the sol-gel transition. In the first case the existence of a point of maximum value is evidently due to the predominant aggregation of the particles where the total number of the scattering centres decreases rapidly. The aggregation in this case produces greater asymmetry of the particles as shown by the increase in ρ_v. In the latter case, however, the absenec of the points of maxima shows that the increase in the size may not be mainly due to the aggregation of the particles but may be due to the swelling of the individual particles, a process in which the total number of scattering centres does not decrease.

6. Gel-Sol Transition

In order to study the changes in the size and shape of the gel particles during the gel-sol transition, gels prepared at the lowest temperature during the sol-gel transition studies (see para. 4) were used. The gels were raised to a higher temperature. The temperature was kept constant until no further change in the intensity and depolarisation occurred. The constant values of intensity and depolarisation were recorded and the gel was then raised to the next higher temperature for further observation. The lower halves of Tables II (i), (ii), (iii) and (iv) show the gel-sol values of intensity and depolarisation for a typical case of a 3% cellulose acetate gel.

Variation in intensity and depolarisation ρ_h and ρ_v, tend to change in a direction opposite to that of the sol-gel transition discussed in para. 5, as the gels are raised to higher temperatures until they reach the original sol values. However, the changes in intensity and depolarisation with increase in temperature do not exactly retrace the path of the sol-gel transition. Instead, the values remain constant even when the gels are raised to

higher temperatures and change over slowly back to sol values in a temperature range much higher than that for the sol-gel transition. Moreover, the three different types of changes in ρ_v taking place during the gel-sol transition for different types of gels occur precisely in the same concentration range as mentioned in Table IV.

7. Changes in the Viscosity during the Sol-Gel and Gel-Sol Transition (Qualitative Study)

From qualitative observations on the mobility of the medium, it is noticed that viscosity of the sols increases rapidly with increase in the concentration. During the sol-gel transition, increase in viscosity always precedes the changes taking place in the size and shape of the particles. Viscosity of the corresponding gels decreases as we go from the first group of gels to the fourth, indicating that if the size of the particles increases rapidly during the sol-gel transition, the resulting gels are looser.

8. Mechanism of the Sol-Gel and Gel-Sol Transition of Lyophilic Gels as Suggested by the Present Investigation

The lyophilic sols are also solid-liquid systems in which the solid phase remains suspended in the dispersion medium. The disperse phase is in the colloid state. The lyophilic sols are quite stable at high temperatures and the disperse phase in them does not precipitate even at higher concentrations. Due to the great affinity of the solid phase to the liquid phase, viscosity of the sols increases very rapidly with concentration. Size and shape of the colloid sol particles is not affected to any appreciable extent by increase in concentration. At low concentrations the collodial sol particles scatter light independently of each other while at higher concentrations the intensity of scattered light varies much less rapidly than the increase in concentration. The changes taking place in the sol state when we go from sols of low concentration to sols of high concentration seem to be somewhat analogous to the change taking place when a vapour, in which molecules scatter light independently of each other changes over to the liquid state when the molecules are too closely packed to scatter light independently of each other.

The change from the sol to the gel state can be divided into three distinct stages:

(1) The clouding of the dispersion medium over the disperse colloid particles. During this stage which is very prominent in these gels, no change in the size and shape of the particles is yet evident and only the rapid increase in viscosity is noticed.

(2) Some of the disperse medium may actually enter the colloid particles by a sort of osmosis. It has been shown that during this process the individual particles swell and become spherically symmetrical.

(3) The swollen particles may then aggregate to form particles of larger size and greater asymmetry. The change in the size and shape of the particles actually observed during the sol-gel transition is in general due to the combined effects of swelling and aggregation. The relative parts played by the above two factors in bringing about the increase in the size and shape of the gel particles depends upon the concentration of the gel and the temperature at which the sol-gel transition is carried out. In gels of very low concentration the increase in the size is mostly due to swelling of the individual particles. With increase in concentration the aggregation tendency increases and we get gels consisting of highly anisotropic particles. At very high concentrations the sols are very viscous, and the aggregation of the particles during the sol-gel transition is again suppressed so that only the swelling of the particles is observed. Decrease in the temperature at which the sol-gel transition takes place has great influence in increasing the aggregation of the gel particles. At low concentrations where the probability of collision of the particles is very small, we notice mostly the particles swelling and the I_8-time curves show no points of maxima even at the lowest temperatures. At slightly higher concentrations, as one goes on lowering the temperature, swelling is noticed at first and aggregation becomes more predominant as the temperature is further decreased. For still higher concentrations aggregation starts right from the beginning. However, when the concentration becomes very high, the initial viscosity of the sol is so large that the decrease in temperature does not influence the aggregation of the particles in any way and swelling alone is noticed at very high concentrations.

The extreme stability of the lyophilic gels and the very wide range of concentrations over which the gels can be prepared is clearly due to the fact that in these gels the dispersion medium is bound in two different ways, *viz.*, by the clouding of the dispersion liquid over the colloid particles and also by some of the liquid actually entering inside the particles by a sort of osmosis. Unlike the lyophobic gels, increase in temperature does not bring about increase in the size of the particles by further coagulation. On the other hand, the size of the colloid particles and the viscosity of the medium rapidly decrease with the increase in the temperature. This is evidently due to the fact that with increase in temperature the thermal velocity of the molecules of the dispersion medium inside and outside the colloid particles increases rapidly. Due to the increase in the thermal velocity of the liquid molecules outside the colloid particles the clouding of the dispersion liquid

over the colloid particles is decreased, resulting in the decrease of viscosity in the gels. The increase in the thermal velocity of the liquid molecules inside the swollen particles causes the swollen particles perhaps to burst into fragments. The increase in the temperature thus causes the gels to go back to the sol state again.

9. Other Experimental Evidence of Swelling of the Gel Particles

In connection with the swelling of the individual particles observed in the present investigation, reference may be made to an interesting observation made by Krishnamurthi[6] on gelatin gels. He has shown that when a gelatin gel is kept in a desiccator, the shrinking of the gel is accompanied by a large decrease in the light scattered by the gel, suggesting that the shrinking of the gel as a whole may be due to the shrinking of the swollen colloid particles by the removal of the trapped water from them. However, Krishnamurthi has ruled out the possibility of the swelling of the individual particles and has pointed out the following features against the swelling theory: (1) Pieces of gelatin become opalescent when allowed to swell in water but the increase in the turbidity thus obtained is very small in comparison with the marked turbidity of the 2% gels. (2) Gelatin passes over from the sol to the gel state without any change in the intensity of scattered light. (3) Turbid gelatin which becomes clearer during the process of dehydration in a desiccator does not regain its original turbidity when kept again in water. We must remember, however, that the sol-gel transition is not due only to the swelling of the particles alone but is a much more complex phenomenon in which in addition to swelling, the aggregation of the different particles as well as the clouding of the dispersion medium over the disperse phase, are also taking place.

Diffusion of dilute hydrochloric acid into a gelatin gel and the resulting decrease in the light scattered by the gels observed by Krishnamurthi also follows directly from the fact that the hydrochloric acid outside the swollen particles will drag the water out again from the swollen particles causing them to shrink again by de-osmosis.

10. Acknowledgements

The author is indebted to Dr. L. A. Ramdas for suggesting the problem, guidance and facilities during the course of investigation.

Summary

Results of an extensive investigation on the changes in the size and shape of the colloid particles during the sol-gel transition of agar-agar,

gelatin and cellulose acetate gels, by the R. S. Krishnan colloid optical technique have been discussed. A possible mechanism of the sol-gel transition of lyophilic gels has been proposed.

References

1. Katti, P. K. .. *Proc. Ind. Acad. Sci.*, 1953, **38**, 148.
2. Krishnan, R. S. .. *Ibid.*, 1935, **1**, 717.
3. Arisz .. *Kolloidchemische Beihefte*, 1915, **7** 22.
4. Mardles .. *Trans. Farad. Soc.*, 1923, **18**, 318.
5. Krishnamurthi .. *Proc. Roy. Soc. A.*, 1929, **122**, 76; 1930, **129**, 490.
6. ———— .. *Nature*, 1929, **123**, 243.

OBSERVATIONS ON τ-MESONS AND ON K-MESONS GIVING RISE TO CAPTURE STARS

By D. Lal, Yash Pal and B. Peters

(*Tata Institute of Fundamental Research, Bombay* 1)

Received October 3, 1953

(Communicated by Prof. H. J. Bhabha, F.R.S., F.A.SC.)

Abstract

In an emulsion block detector[1] exposed in the stratosphere three cases of the production of τ-mesons in nuclear disintegrations have been observed and 5 cases of negative K-mesons which when brought to rest are captured by nuclei. In one case the production of a τ-meson is associated with the production of a charged hyperon in the same nuclear event. In another case the production of a negative K-meson is associated with the production of a slow positive K-meson. The production ratio of slow τ-mesons to slow positive π-mesons $\tau/\pi^+ = 1 \cdot 1^+ 0 \cdot 8\%$ and the ratio of slow negative K-mesons to slow negative π-mesons $K^-/\pi^- = 0 \cdot 95 \pm 0 \cdot 5\%$. The mass of the τ-meson is found to be

$$M\tau = 975 \cdot 9 \pm 2 \cdot 2\, m_e$$

and that of K^--mesons

$$M_{K^-} = 927 \pm 75\, m_e$$

Proof is given that all three of the decay products of the τ-mesons are π-mesons. It is suggested that all τ-mesons observed to decay in emulsions are positively charged and that the K^--mesons observed by us may be the negative counterpart of this particle. Possible relations between the various phenomenologically distinguished types of charged K-mesons are discussed.

I. Experimental Procedure

The work reported in this paper was carried out with an emulsion block detector whose construction has already been described in detail.[1] The block consisted of 24 sheets of 600 μ Ilford G-5 emulsions with lateral dimensions $4'' \times 6''$. It was exposed in a balloon flight at geomagnetic latitude 19° for $6\frac{1}{2}$ hours. The balloons spent $4\frac{3}{4}$ hours between 70,000 and 90,000 feet. Tracks of particles which traversed the detector during the balloon exposure could be traced from emulsion to emulsion. Tracks of particles which traversed the stack before the balloon flight (old tracks) could not in general be traced because the relative position of the emulsion sheets was

altered just before exposure in the stratosphere. A sample survey showed that a total of 4,800 positive and negative π-mesons came to rest in the stack of which 3,700 were produced in the stratosphere and 1,100 during the air transport of the emulsions from England to India.

We have selected for investigation a random sample consisting of 352 π-μ-e decays and 421 capture stars produced by slow mesons. Amongst the last mentioned events, we found four cases of heavy mesons coming to rest and producing nuclear distintegrations at the end of their range (K^--mesons). The remaining capture stars were produced by π^--mesons, while the π-μ-e events of the first group must be attributed to π^+-mesons.

The tracks of the π^+ and π^--mesons were traced from their end point backwards towards their origin. Some proved to be "old tracks" and could, therefore, not be traced, others were found to enter the stack from the outside and were presumably produced in the packing material. Some could not be traced completely due to faults in the emulsions or other reasons. Many were found to originate in some nuclear disintegration. A few originated in 2 prong stars some of which could be interpreted as the decay of neutral hyperons. Two positive mesons originated in the decay of τ-mesons.

The detailed information on the origin of the 773 slow π-mesons is given in Table I.

TABLE I

	π^+ – mesons	π^- – mesons
Old tracks ..	84	97
Not traced beyond 1–2 cm. of range ..	75	61
Entered from outside ..	109	109
Originated in stars > 2 prongs ..	80	146
Originated in 2 prong stars ..	2	8
From τ – mesons ..	2	0
Total ..	352	421

The two τ-mesons as well as a third τ-meson discovered at random could in turn be traced to their origin in nuclear events. All of their decay products could also be traced for appreciable distances into the emulsion block, some of them to the end of their range.

Of the four K^--mesons found by the investigation of capture stars one was produced before balloon exposure and could, therefore, not be traced

to its origin. Two were found to originate in nuclear explosions and one entered the block from the outside. A fifth K^--meson was found by tracing the grey and black prongs of a star which was already known to emit a positive K-meson.

II. MEASUREMENTS ON THE τ-MESONS AND THEIR DECAY PRODUCTS

Brown, Camerini, Fowler, Muirhead, Powell and Ritson[2] who discovered the first τ-meson suggested the decay scheme $\tau \rightarrow 3\pi$. Recently Amaldi *et al.*[3] reviewed the evidence for the nature of the decay particles based on a total of 11 τ-decays which had been observed until then. Although only three of their 33 decay products came to the end of their range in the emulsion and could definitely be identified as π-mesons, the evidence from grain density *versus* scattering on the tracks of the other decay products and the consistency of the Q-values obtained for the reaction assuming the proposed decay scheme, made it highly probable that as originally suggested all these decay products are π rather than μ-mesons and no additional neutral particles are involved.

The much more favourable observational conditions which exist in an emulsion block detector compared to single emulsions permit in our case to exclude the presence of neutral particles in the decay by a more rigorous test on the coplanarity of the charged decay particles. One can also show that in one of our cases in which two of the decay products come to rest in the block and can be identified as π-mesons, the evidence is very strong that also the third decay particle is a π rather than a μ-meson. The originally proposed decay scheme seems, therefore, very firmly established.

Apart from measurements on the track of the τ-meson itself (which will, however, give a mass and Q-value of very limited precision) one can measure the three momenta of the decay particles and the three angles between their tracks. Once the decay scheme is assumed, a Q-value can be calculated from one of the momentum values and any two of the remaining five measurable quantities. It is, therefore, possible to obtain for a given τ-decay a series of Q-values obtained from different sets of the measurable quantities and to obtain a check on the accuracy of measurement from the internal consistency of the results.

From such internal consistency checks it became soon apparent, that in order to measure the Q-value to an accuracy of the order of 1 MeV, the customary procedure for measuring angles and particle ranges in emulsions had to be greatly refined, by taking into account the variation in thickness of individual emulsion sheets and the effect of distortion on the angle between steeply dipping tracks. It seemed also desirable to determine

directly the stopping power of the particular emulsions used in order to avoid errors due to the variable moisture content of emulsions.

These refinements will eventually also play a role in determining accurate Q-values for the decay of other *K*-mesons and Hyperons, and, are therefore, described in some detail.

(*a*) *The Measurement of Particle Ranges*

The determination of particle range depends on an accurate knowledge of the shrinkage factor, and, therefore, on the emulsion thickness before processing for all emulsion sheets traversed by the track. The conversion of particale range into energy requires an accurate knowledge of the stopping power of the emulsion.

(1) *Stopping Power of the Emulsion Sheets.*—Since unbacked emulsion sheets are free to expand and contract laterally after manufacture it is possible that their stopping power at exposure slightly differs from that normally observed for glass backed emulsions. We found in fact, that the density of two control sheets is about 2% higher than that given by the manufacturer for G-5 plates.

We have, therefore, determined the range of μ-mesons emitted from π-mesons in a direction nearly parallel to the emulsion surface. Our mean value on 18 tracks is $R_\mu = 589\,\mu$. Since according to Fry and White[4] the μ-mesons have a 5% straggling in range our value should be accurate to about 1%. We have normalised the range-energy curves for emulsions as given by Beiser[12] to agree with the observed range for μ-mesons.

(2) *Variations in Emulsion Thickness.*—It is apparent from the manufacturing process used by Ilford Limited, where liquid emulsion is poured on a thick, carefully levelled sheet of plate glass, that individual emulsion sheets must be extremely uniform in thickness. Thus it is not necessary to consider thickness variation in a particular emulsion, but variations between different emulsion sheets must be taken into account.

The determination of the unprocessed emulsion thickness can, therefore, be divided into two parts:

(α) Determination of relative thickness of different emulsions.

(β) Determination of the average thickness of the emulsions forming the emulsion block detector.

(α) We select a number of tracks due to energetic heavy primary nuclei which traverse the block in different areas of the plates and with different

orientations. We measure for each track in each emulsion (i) the projected track length L_i and determine the average projected track length in the n emulsions:

$$\bar{L} = \frac{\Sigma L_i}{n}$$

The fractional variation of projected track length $\frac{\bar{L} - L_i}{\bar{L}} = \frac{\delta L_i}{\bar{L}}$ varies from emulsion to emulsion. The average variation is 4·6% but occasional values up to 10% do occur.

For the track of a high energy particle whose scattering is negligible, the projected length in two emulsions can differ either because the emulsions had unequal thickness or because of distortion (which moves the exit point on the air surface from its proper position) or because there were small air gaps between emulsions which permitted buckling such that the sheets at exposure were not exactly parallel.

Experimentally we found that except for tracks near the edge of the plates the quantity $\frac{\delta L_i}{\bar{L}}$ was for a given i (*i.e.*, for the same emulsion) nearly equal for all tracks. The main fluctuation of projected length was, therefore, due to variation in emulsion thickness, since buckling should have different effects on tracks in different areas of the plate and the effect of distortion on its projected length should depend both on the location of the track in the plate and on its orientation. From these measurements we obtained for each emulsion sheet its thickness (within 1%) in terms of the average thickness of the sheets.

(β) In order to determine the average thickness of the emulsion before exposure we measured the range of steeply dipping μ-mesons ejected from π-mesons. Taking into account the percentage variation in the thickness of individual emulsion sheets, this average range is nearly proportional to the average emulsion thickness. We find that the emulsion thickness at exposure is very nearly equal to 600 μ as specified by the manufacturer.

With this information on the thickness of individual emulsion sheets we can determine the range of stopping particles to about 1% accuracy corresponding to an uncertainty in energy of about 0·5%. Further uncertainty in the energy arises from possible errors in the deduced stopping power (0·5%) and from straggling which for π-mesons in the energy interval 15–35 MeV amounts to about 2%.

(*b*) *Measurement of Angles between Trajectories*

The angle measured between two tracks in a processed emulsion can differ from the angle between the trajectories responsible for the tracks for the following reasons:

(α) The emulsion has shrunk during processing in the direction perpendicular to the emulsion surface (Z-direction).

(β) The emulsion layers may during processing have moved with respect to each other (distortion). Unless the intersecting tracks are parallel to the emulsion surface, distortion will change the angle between tracks.

(γ) Coulomb scattering introduces an uncertainty in the true angle of intersection. Fortunately this does not affect the Q-values appreciably because if the track is due to a particle of high momentum the scattering is small and if it is due to a particle of low momentum the Q-value is insensitive to the angle between this track and those of the other decay products.

In order to measure the angle between two *tracks*, we have to measure the difference of x, y and z co-ordinates between the intersection of the tracks and another point P on each of the two tracks. This point must be chosen sufficiently far from the intersection to permit the accurate alignment of a hairline with the intervening grains of the track. If we want to measure, however, the angle between the *trajectories* of the particles producing the tracks, we must first correct the z co-ordinates of the points P for shrinkage and their x and y co-ordinates for the displacements caused by distortion.

Since we have determined the thickness of each emulsion sheet before exposure, the shrinkage factor involves simply a measurement of thickness of the processed emulsion sheet. This thickness, however, changes with the moisture content of the atmosphere and should, therefore, be redetermined for each angular measurement.*

We now consider the distortion correction to be made for the x and y co-ordinates of P. Let us assume that during the development stage and before the emulsion has hardened a uniform pressure is exerted on a surface perpendicular to the plane of the emulsion (y, z-plane) and let us assume that in this state the emulsion represents a homogenous and elastic solid. The emulsion material will then suffer a displacement S in the x-direction which (because one surface of the emulsion is firmly attached to a rigid glass plate)

* A. J. Oliver Radiation Laboratory Report U.C.R.L. 2176. April 1953.

will vary along the Z-direction. It is then easily shown that $\frac{\partial^2 S}{\partial Z^2}$ is equal to a constant ($= -K$), and for the boundary condition where one emulsion surface is rigidly fixed while the other is free to move.

$$S = \left(-\frac{K}{2}Z^2 + KZ_0 Z\right)$$

$$= S_0\left[2\frac{Z}{Z_0} - \left(\frac{Z}{Z_0}\right)^2\right] \qquad (1)$$

where Z_0 is the emulsion thikness and S_0 is the maximum value of S which occurs on the air surface. Thus, the various grains along a track will be displaced in the x, y plane by an amount which increases first rapidly then slower as one goes from the glass surface ($Z = 0$) to the air surface ($Z = Z_0$). The result is a C-shaped distortion of tracks, the curvature being largest near the glass surface. This is in fact the shape which is generally observed for tracks of fast particles traversing distorted emulsions. The projected shape of the track does not change when the thickness of the emulsion shrinks. The distortion in a certain region of the developed emulsion is defined by the magnitude of the displacement on the air surface $S_0 = \frac{K}{2} Z_0^2$ and the quantity $C = \frac{K}{2} = \frac{S_0}{Z_0^2}$ is a measure of distortion in covans if the surface displacement S_0 is expressed in microns and the emulsion thickness Z_0 in millimeters. Since in this type of distortion $\left(\frac{\delta S}{\delta Z}\right)_{Z=Z_0} = 0$ the projected track retains its true direction near the air surface. Consequently the component of the displacement vector $\vec{S}$ perpendicular to the projection of a given track can be obtained by measuring the distance of the point where the track enters the glass surface to the line which is tangent to the projected track at the air surface. The true vector $\vec{S}$ is determined by making such measurements in the same region of the emulsion on tracks of different orientation.

The x and y co-ordinates of the points P_1 and P_2 on the tracks 1 and 2 whose angle of intersection is to be measured must, therefore, be corrected for distortion in the following way:

(α) The vector $\vec{S}$ is determined from the apparent curvature of high energy tracks in the same region of the plate.

(β) The Z co-ordinate (Z_1) of point P and of the intersection point (Z') are measured and expressed as fractions of the emulsion thickness Z_0. The point P_1' which is to be used for the angular measurement is found by moving from P_1 in the direction of the displacement vector $\vec{S}$ by an amount obtained from equation 1:

$$S(Z_1) - S(Z') = S_0\left[\frac{2(Z_1 - Z')}{Z_0} - \frac{(Z_1^2 - Z'^2)}{Z_0^2}\right].$$

In our emulsions where the maximum displacement vector $\vec{S}_0$ is sometimes as large as 40 μ (corresponding to 110 covans) the distortion correction may amount to several degrees for steep tracks both when measuring the projected angle between tracks and when measuring dip angles.

If the decay occurs near one of the emulsion surfaces and one of the fragments is steep and leaves the surface giving a segment of very short length, the measurement of the dip and projected angles can sometimes be carried out more accurately in the adjacent emulsion which is completely traversed by the fragment.

It should be remarked that distortion in the emulsion does not in first order affect the coplanarity of the tracks made by the three decay products of the τ-mesons. The fact that the measured angles between the three tracks add up to 360° is, therefore, no indication that distortion corrections can be neglected.

(*c*) *Mass Measurements on τ-Mesons*

The result on the measurements of the 3 τ-mesons are given in Table V. In each case unfortunately, the plane of decay makes a large angle with the plane of the emulsion. The manner by which the Q-values were obtained and the errors were estimated is given below:

(α) τ No. 1. The momenta p_1 and p_2 of the stopping π-mesons were obtained from their range. In addition the dip angle of each track and the projected angle between tracks were measured. The decay occurred in a plane which made an angle of 77° with the emulsion surface. The measured deviation from coplanarity was 0·35°.

By using various sets of the measured angles and momenta we can calculate the remaining momenta, the energy of each decay product and the Q-value. Table II shows the results obtained; the measured quantities are indicated at the top of each column. (γ designates the angle between

p_1 and p_2, etc.). Energies and momenta in Table II are expressed in units of the π-meson rest mass ($c = 1$).

TABLE II

τ No. 1

	$p_1p_2\ \alpha$	$p_1p_2\ \beta$	$p_1p_2\ \gamma$	$p_1\ \alpha\beta$	$p_2\ \alpha\beta$
p_1	·641	·641	·641	·641	·625
p_2	·500	·500	·500	·513	·500
p_3	·7445	·715	·735	·7410	·722
E_1	·188	·188	·188	·188	·179
E_2	·118	·118	·118	·124	·118
E_3	·2465	·2295	·241	·245	·233
Q	·5525	·5355	·547	·557	·530

The variation in Q-values is partly due to uncertainty in angular measurements, but primarily it reflects errors due to straggling since we have used in its calculation the energy derived from the range of particles 1 and 2 and of each one separately. That straggling is the largest contribution to the uncertainty of the Q-values is indicated by the fact that both in case of τ No. 1 and τ No. 2 (Table III) the extreme Q-value occur if we rely in the calculation on the range of only one or the other of the two stopping π-mesons.

We, therefore, take the average of the various Q-values and assign as probable error a value covering the entire spread of values obtained:

$$Q_1 = \cdot 543 \pm \cdot 014\, m_\pi c^2$$

The track of the third meson which escapes, has near the decay point a grain density of $53 \cdot 5 \pm 2 \cdot 5/100\,\mu$ while the grain density expected for a π-meson of momentum calculated in Table III should be $53 \cdot 7 \pm 0 \cdot 7/100\,\mu$. If on the other hand the excaping particle were a μ-meson its grain density should be $39 \cdot 0/100\,\mu$ in disagreement with the observed value. Thus, it seems certain that all three decay products are π-mesons.

τ No. 2. One positive and one negative π-meson come to rest in the block. The plane of decay makes an angle of 85° with the plane of the emulsion. The measured deviation from coplanarity is 0·3°. The Q-values determined by using various sets of measured quantities are given in Table III.

TABLE III

τ No. 2

	p_1p_2 α	p_1p_2 β	p_1p_2 γ	p_1 αβ	p_2 αβ
p_1	·581	·581	·581	·581	·566
p_2	·482	·482	·482	·491	·482
p_3	·790	·773	·784	·789	·770
E_1	·1565	·1565	·1565	·1565	·149
E_2	·110	·110	·110	·114	·110
E_3	·274	·264	·270	·274	·262
Q	·5405	·5305	·5365	·5445	·521

$$Q_2 = 0{\cdot}533 \pm {\cdot}012\, m_\pi c^2$$

τ No. 3. The plane of decay makes an angle of 75° with the emulsion surface. The measured deviation from coplanarity is 1·6°. In this case only one (positive) π-meson comes to rest in the block, the others escape. The stopping π-meson (π_1) carries only 9% of the available energy. This makes it difficult to obtain good measurements:

(1) The strong scattering of π_1 introduces an uncertainty in the angle between π_1 and π_2 and between π_1 and π_3. This probably accounts for the measured lack of coplanarity.

(2) The Q-value becomes extremely sensitive to the angle between the energetic mesons π_2 and π_3 which travel very steeply in nearly opposite direction.

The most accurate Q-values are obtained in this case by determining the momentum of π_2 from grain density *versus* range in the 16 emulsions which this particle traverses before escaping and using p_1, p_2 and either of the angles between π_1 and the other mesons.

The results are given in Table IV. In addition to the error due to the angular measurements which is responsible for the difference in Q-values in the two columns, we have to make allowance for an additional 2% error arising from the uncertainty in the energy determination of π_2.

TABLE IV

τ No. 3

	p_1p_2 β	p_1p_2 γ
p_1	·310	·310
p_2	·7905	·7905
p_3	·672	·6965
E_1	·047	·047
E_2	·275	·275
E_3	·2045	·219
Q	·5265	·541

$$Q_3 = \cdot 534 \pm \cdot 017\, m_\pi c^2$$

The weighted average for these three τ-mesons ($m_\pi c^2 = 141 \cdot 1$ (MeV) is

$$Q_\tau = 75 \cdot 6 \pm 1 \cdot 1 \text{ MeV}$$

$$M_\tau = (3 \cdot 536 \pm 0 \cdot 008)\, m_\pi c^2 = 975 \cdot 9 \pm 2 \cdot 2\, m_e{}^*$$

TABLE V

Parent Particle					Decay Products			
No.	Origin	Range (cm.)	Energy MeV	Q-value (MeV.)	No.	Sign of Charge	Energy MeV	Angles
1	$21+2\alpha$	0·0367	6·4	76·7±2·0	1	+	26·2	$\sphericalangle$ 2·3 = α = 121·85°
					2	+	16·8	$\sphericalangle$ 3·1 = β = 137·2°
					3	(−)	33·7	$\sphericalangle$ 1·2 = γ = 100·8°
2	$6+0\rho$	0·665	31·7	75·3±1·7	1	+	21·8	α = 132·9°
					2	−	15·6	β = 141·6°
					3	(?)	37·9	γ = 85·5°
3	$13+10\alpha$	0·747	33·6	75·3±2·4	1	+	6·6	α = 161·8°
					2	?	38·8	β = 79·3°
					3	?	29·9	γ = 118·8°

* Recent determinations by Smith *et al.* [11] show that the mass of the π-meson should be reduced to $m_\pi c^2 = 139 \cdot 5$ Mev. Using this mass would reduce the Q value by ½% and lead to a mass $M^\tau = 966 \pm 2 \cdot 2\, m_e$.

In addition to the statistical error, this Q-value may be in error by somewhat less than 1 MeV due to uncertainty in the range energy relation.

Our value is in good agreement with the value $Q_\tau = 76{\cdot}3 \pm 1{\cdot}7$ derived by Amaldi, *et al.*[3] based on the average of 11 τ-mesons observed in emulsions by various laboratories. It is somewhat higher than the value reported by one of us at the Cosmic Ray Conference at Bagnéres de Bigorre in July 1953, a value which had been obtained without corrections for distortions and for variations in emulsion thickness.

III. The Charge of τ-Mesons

τ No. 1 can be definitely identified as positive because two of its decay products undergo π-μ-e decay. A similar event was recently observed at Bristol.† Among the 15 τ-mesons observed so far in emulsions there are, therefore, 3 cases, where the charge of two of the decay products was identified ($5\,\pi^+$ and $1\,\pi^-$) and 4 cases in which the charge of one decay product was identified ($3\,\pi^+$ and $1\,\pi^-$). The probability of obtaining 8 or more positive π-mesons among 10 identified decay products under these conditions is $3{\cdot}5\%$ if they are obtained from a sample which consist of equal numbers of positive and negative τ-mesons. The probability is, however, 7 times as high if the sample consists of positive τ-mesons only. While it cannot as yet be ruled out, therefore, that some of the τ-mesons observed to decay in emulsions are negatively charged it is more likely that all are positive.

On the other hand from the report of Leighton at the Cosmic Ray Conference in Bagnéres it appears that at least one of the three τ-mesons whose decay in the gas of the cloud chamber was observed by him was negatively charged. It seems, therefore, reasonable to assume that both positive and negative τ-mesons are produced but that in the dense material of the emulsion the negative ones are absorbed by nuclei before decay.

IV. K^--Mesons

We have already mentioned that among 421 capture stars investigated in our emulsion block we found 4 examples where the incident slow meson was heavier than a π-meson. A fifth example of this type of event was found by following tracks from a star among whose fragments was a previously identified positive K-meson (emitting a relativistic singly charged decay particle at the end of its range.) The particles producing these capture stars are certainly negatively charged and have a mass intermediate between π-mesons and protons. They are, therefore, designated as K^-particles.

† D. H. Perkins (Priv. Comm.)

The relevant data on these events are given in Table VI, most of these data have already been given in our preliminary report.[5] Details on the

TABLE VI

Negative K-Mesons

No.	Origin	Range	Mass (m^e)	Range total (t) or observed (o)	Mass (m_e)	Energy (MeV)	Remarks	Energy Release excluding Neutral Fragments
1	$14+2n$	308 μ	1000^{+720}_{-400}	15·8 μ (t)		1·0	Probably proton	
				5·7 μ (t)		0·5	Probably proton	185 MeV
				0·39 cm.(o)	290^{+80}_{-50}	28·1 ± ·8	π-meson	
2	$25+5n$	92 μ	?	48 μ (t)		2·2	Probably proton	
				5·5 μ (t)		0·5	Probably proton	
				139 μ (t)		4·2	Probably proton	
				0·354 cm. (o)	200^{+60}_{-30}	29·2±0·9	This particle is a π-meson since it produces a nuclear interaction in flight after traversing 3·5 mm. of path	199 MeV
3	$4+6n$	2·5 cm.	1015±120	385 μ (t)		7·8	Probably proton	
				46 μ (t)		2·1	Probably proton	
				140 μ (t)		4·1	Probably proton	>246 MeV
				0·14 cm. (o)		> 17 MeV	Proton or deuteron	
				1·76 cm. (o)	1836	>180 MeV	Proton	
4	Outside of block	2·926 cm.	850±95	407 μ (t)		8·1	Probably proton	
				456 μ (t)		9·0	Probably proton	31 MeV
	Old Track 5	1·2mm.	540^{+290}_{-170}	282 μ (t)		6·5	Probably proton	
				295 μ (o)		>120 MeV	Probably proton	>140 MeV

mass measurements for those K^--mesons for which sufficient track length is available have been given in an earlier paper.[6] Our best mass value is

$$M_{K^-} = 927 \pm 75\, m_e$$

Event No. 1 can be attributed to the capture of a K^--meson because a L-meson (presumably a 28 MeV π-meson) is emitted from the capture star and the particle which produces the star can be identified as singly charged with a mass which is probably lower than that of a proton but higher than that of a π-meson.

Event No. 2 is very similar to event No. 1, but here the track of the particle responsible for the capture star is so short ($92\,\mu$) that the only information on the particle producing the capture star is that it has a mass larger than the π-meson and carries a charge Z less than 3. An Alternative interpretation along the line of Danysz and Pniewski[7] is, therefore, possible in this case: the event may be the emission of a helium fragment incorporating a hyperon which subsequently decays and breaks up the nucleus. The measured energy of the emitted π-meson would not be inconsistent with such an interpretation.

In Event No. 3 the K^--meson is identified both by direct mass measurement and by the fact that the observable energy release in the capture star exceeds the rest energy of a π-meson.

In Event No. 4 the identification of the K^--mesons rests only on measurements of its mass.

Event No. 5. This is an "old event" in which the track of the K^--mesons cannot be traced. The mass value is, therefore, rather inaccurate because the available track length is small. The mass seems to lie higher than the π-meson mass. The observable energy release in the capture star lies close to but does not clearly exceed the rest energy of a π-meson. It is, therefore, highly probable but not quite conclusive that this event should be attributed to a capture of a K^-meson at rest.

V. The Frequency of Production of Slow τ and K^-Mesons

Although our statistics are still very poor, we can at least make a rough estimate of the frequency of production of τ and K^--mesons.

Excluding "old tracks" we have in a particular area located and traced towards their origin 268 positive and 324 negative π-mesons (see Table I). 56% and 42% respectively originated outside the emulsion block. If we apply the same percentages to the tracks which have been followed only through part of their range in the block we find 117 out of 268 π^+-mesons and 189 out of 324 π^--mesons are created in the block, and give rise to decays

or capture stars after coming to rest. If n designates the number of particles satisfying these criteria we have in a given area

$$\frac{n_{\pi^+}}{n_{\pi^-}} = \frac{117}{189} = \cdot 62$$

We now assume that all τ-mesons decaying in emulsion are positive and, therefore, give rise to $2\pi^+$ and $1\pi^-$-mesons. In our 3 cases we found that 5 of the 9 decay products came to rest in the block ($1 \cdot 7\,\pi$-mesons per τ-meson). In view of the dimensions of our block and the most probable range of 1 cm. for the decay products it seems reasonable to accept this number as the average number of stopping π's per τ-decay.

Let n_τ be the number of τ-mesons created and decaying in the block. They will give rise to $\frac{2}{3} \times 1 \cdot 7\, n_\tau$ positive and to $\frac{1}{3} \times 1 \cdot 7\, n$ negative π-mesons stopping in the block. The fraction of stopping π^+ which have their origin in τ-decays is, therefore, $1 \cdot 13\, \frac{n_\tau}{n_{\pi^+}}$.

The ratio of π^--mesons which have their origin in τ decays and which come to rest *and produce capture stars* to the total number of such mesons is $\frac{1}{3} \times 1 \cdot 7 \times 0 \cdot 73 \times \frac{n_\tau}{n_{\pi^-}} = \cdot 256\, \frac{n_\tau}{n_{\pi^+}}$. (The factor $0 \cdot 73$ arises from the fact that 27% of π^- mesons fail to produce visible capture stars).

Since we have found 2 τ mesons by tracing $117\,\pi^+$ from their decay and $189\pi^-$ from their capture stars towards their origin we find

$$\frac{n_\tau}{n_{\pi^+}} = \frac{2}{1 \cdot 13 \times 117 + 0 \cdot 256 \times 189} = (1 \cdot 1 \pm 0 \cdot 8)\%$$

For the ratio of κ^--mesons to π^--mesons which come to rest in the block and produce capture stars we obtain

$$\frac{n_{K^-}}{n_{\pi^-}} = \frac{4}{421} = (0 \cdot 95 \pm 0 \cdot 50)\% \quad \text{if we include all observations,}$$

$$\frac{n_{K^-}}{n_{\pi^-}} = \frac{3}{324} = (0 \cdot 93 \pm 0 \cdot 55)\% \quad \text{if we omit "old tracks",}$$

and $$\frac{n_{K^-}}{n_{\pi^-}} = \frac{2}{189} = (1 \cdot 05 \pm 0 \cdot 75)\%$$ if we confine ourselves to particles originating inside the emulsion block detector.

VI. On the Nature of Charged *K*-Mesons

The relations which exist among the various phenomena which involve the disintegration or nuclear capture of charged *K*-mesons are still far from clear and the remarks in this section which owe a great deal to the discussions at the Cosmic Ray Conference at Bagnéres in July 1953 are, therefore, largely speculative.

In the Cloud Chamber observations we have three types of events:

(1) Particles which are either positive or negative and disintegrate in flight into 3 L-mesons.

(2) Particles which are either positive or negative and decay in flight into a single charged L-meson (V-events).

(3) Particles which when brought to rest in an absorber inside the cloud chamber disintegrate and give rise to a single L-meson (and sometimes a γ-ray going in the opposite direction). The sign of charge of these particle (giving rise to the so-called S-events) is known only in the four cases observed by the Pic du Midi group of the Ecole Polytechnique and was positive in each of the four cases.

The type No. 2 is about 20 times as frequent as type No. 1.

In nuclear emulsions one has also observed three types of events.

(4) Particles which disintegrate at rest into 3 π-mesons.

(5) Particles which give rise to capture stars when brought to rest.

(6) Particles which decay at rest into a single charged L-meson. In at least two cases the L-meson is not relativistic and can be identified as a μ-meson. In the other cases the L-mesons are relativistic though not monoenergetic and cannot definitely be identified as π or μ.

(The possible division of this group into Kappa-mesons giving rise to μ-mesons of varying energies and χ-mesons giving rise to π-mesons of a unique energy cannot as yet be considered to be established beyond doubt).

Types No. 4 and No. 5 seem to occur with about equal frequency as we have shown in the preceeding section. In scanning emulsions in various laboratories type No. 6 has been found about 9 times as frequently as type No. 4. Since decay event No. 4 is much easier to observe than the event No. 6 it seems that type No. 6 is at least 10 times, possibly as much as 20 times more frequent than type No. 4.

It seems quite certain that events No. 1 observed in cloud chambers are related to the τ-meson (event No. 4) observed in emulsions. In a previous section we have shown that very probably all τ-mesons observed in emulsion are positive. Therefore, we may identify the *positively* charged particles decaying into 3 L-mesons in the gas of the cloud chamber with the τ-meson. We believe that the *negatively* charged particles decaying into 3 L-mesons in the gas of the cloud chamber should be identified with event No. 5, *i.e.*, the negative K-mesons giving rise to capture stars at rest. The arguments in favour of this identification are:

(α) τ^+-mesons and K^--mesons have within rather narrow limits the same rest mass.

(β) τ^+-mesons and K^-mesons have lifetime sufficiently long to be brought to rest in solid matter.

(γ) τ^+-mesons and K^--mesons of low energy are produced with comparable frequency.

It seems fairly certain that the S-events in cloud chambers (event No. 3) should be identified with the S-events in emulsions (event No. 6) and that the particles giving rise to these events are included among those giving rise to the V-events (group No. 2). The evidence of the Paris group on the charge of S-particles would indicate that the S-events in cloud chambers and emulsions should be identified only with the *positively* charged particles giving rise to the V-events although this evidence rests on only four charge determinations.

If we admit all these suggested identifications it follows that the *negatively* charged particles which give rise to V-events have not been observed when at rest either in cloud chambers or in photographic emulsions. It is hard to believe that they could have escaped detection in photographic emulsions unless they simply come to rest without producing any capture star. We must then assume that this particle is captured by a nucleus, but that in spite of the resultant release of half a BeV of energy no visible prongs are emitted in at least 80% of the cases. Or we may assume that the negative particle giving rise to V-events has a much shorter lifetime than its positive counterpart and hardly ever comes to rest in emulsions. (Cloud Chamber evidence on the lifetime of charged V's does not however, support this conclusion.)

If in order to escape from the conclusion that this negative particle is captured without producing a capture star, we discount the as yet incomplete evidence of the Paris group in favour of the exclusively positive charge

of particles giving rise to S-events, we must assume alternatively that at least 80% of these particles do not interact with nuclei when at rest, but decay even in the presence of fairly heavy nuclei.

These conclusions are not appreciably modified if we assume that part or even all of the observed capture stars produced by negative K-mesons should be attributed not to negative τ-mesons but to the negative primaries of V-events brought to rest. The frequency of occurrence of such capture stars as measured by us is too low, being comparable to the frequency of τ-decays rather than to the 20 times more abundant number of S-events in emulsions. This is supported by the evidence of Harris and Friedlander[8] who failed to find any clear cases of K^--capture in a large sample of stars induced by slow particles (σ-stars).

Nevertheless this alternative is worth considering because it offers the possibility for a certain simplification. In a recent paper[6] we have pointed out that the masses of τ-mesons, K^--mesons giving rise to capture stars and at least the majority of particles giving rise to S-events are equal within rather narrow limits. The approximate equality of the relative frequency of S-events to τ-decays in emulsions and of V-events to τ-decays in cloud chambers indicates that also the lifetimes of these particles are similar. The available observations are, therefore, consistent with the view that there exists only one type of charged K-particle which can decay either into a single L-meson plus some neutral particles or into 3 π-mesons, the former mode of decay being more probable by a factor of the order of 20. We have then to assume that the negative particle when brought to rest in heavy material gives rise to capture stars in about 5% of the cases and gives no visible star in the remaining cases. The observed equality in the number of τ-decays and of capture stars produced by K-mesons must then be considered to be accidental. If we make this assumption then it follows that the negative particles which fail to produce visible capture stars are nevertheless captured by nuclei and do not decay; otherwise we could not account for the preponderance of positive π-mesons among the disintegration products of the τ-decay occurring at rest.

Thus if we are dealing with only one type of charged K-mesons, the negative particle when brought to rest in emulsion is captured but rarely produces a visible capture star. If we consider the τ-particle to be of different nature and we are dealing, therefore, with more than one type of charged K-particle then the negative particle responsible for V-events in cloud chambers either is captured when at rest in nuclear emulsions without normally

producing visible capture stars or it is a non-interacting particle which decays into one L-meson even if brought to rest.

A decision between the last mentioned alternatives could in principle be derived from observations of the interaction mean free path of shower particles in high energy jets, which according to Daniel, *et al.*[9] contain $23 \pm 10\%$ of *K*-mesons. In view of the existing cloud chamber evidence only a small percentage should be τ-mesons. The mean-free path for nuclear interaction in emulsion of shower particles from jets of more than 50 BeV energy has been studied in Bristol and in our laboratory. We have observed so far 22 interactions‡ in an integrated path length of 532 cm. while the Bristol group[9, 10] has reported 9 interactions in 239 cm. path in emulsion. This gives a mean free path for shower particles from high energy jets of $24{\cdot}9 \pm 4{\cdot}5$ cm. compared to the geometric mean free path of $24{\cdot}2$ cm. This result seems to indicate geometric interaction cross-section also for *K*-mesons but is within statistical error still consistent with a mixture consisting of π-mesons and about 10% protons with geometric cross-section and not more than $17{\cdot}5\%$ *K*-mesons with zero cross-section. This latter alternative also implies that the ratio of neutral π-mesons to shower particles in high energy jets should be larger than $0{\cdot}35$, if we assume that the production ratio $\pi^{\circ}/(\pi^{+} + \pi^{-})$ is always equal to one half. Neither the mean-free path of shower particles nor the ratio of π°-mesons to shower particles is as yet known with sufficient accuracy to decide whether the majority of *K*-mesons are interacting or non-interacting particles.

We believe then that this evidence and that of the Paris group on the charge of S-particles, while not conclusive, favours the view that negative particles of mass $\sim 1000\, m_e$ which when decaying in flight emit a single charged L-meson, are captured by nuclei when brought to rest in emulsions but do not in the majority of cases give rise to visible capture stars.

If subsequent cloud chamber experiments should confirm that S-events are always produced by positively charged particles or if mass measurements on particles coming to rest in emulsion selected without bias as to their possible decay should prove the existence of *K*-particles which neither decay nor give capture stars, these conclusions would be greatly strengthened. If on the other hand cloud chamber experiments gave positive and negative S-particles in comparable number or in emulsion work particles of mass $\sim 1000\, m_e$ selected without bias were found to decay in the large majority of cases, the particle responsible for charged V-events are very probably

‡ We are indebted to Mr. Rama of this laboratory for permission to quote some of his unpublished results.

non-interacting. The observed mean free-path of shower particles would then give an upper limit to their production frequency. Furthermore, in this case the K^--particles observed by us must be of a different type and their identification with negative τ-mesons would seem more compelling.

In conclusion we would like to emphasize again two observations which may or may not be relevant to the question of the production of K-particles:

Among 9 nuclear events which give rise to charged K-mesons we found:

One event in which a τ-meson is emitted together with a charged hyperon which decays in flight into a L-meson and one or more neutral particles. (If there is only one neutral particle its rest mass must exceed 1570 m_e) and one event in which a K^--meson is emitted which gives rise to a capture star together with a K-meson which gives rise to an S-event.

ACKNOWLEDGEMENTS

In various phases of this work we have been assisted by Dr. R. R. Daniel, Mr. G. Friedmann, Miss P. A. Irani, Mr. P. N. Krishnamurthy, Mrs. S. Mitra and Mr. Rama to whom, we wish to express our gratitude.

REFERENCES

1. Lal, D., Yash Pal and Peters, B. — *Proc. Ind. Acad. Sci.*, 1953, **38**, 277.
2. Brown, R., Camerini, U., Fowler, P. H. Muirhead, H. Powell, C. F. and Ritson, D. M. — *Nature*, 1949, **163**, 82.
3. Amaldi, E., Baroni, G., Castagnoli, C., Cortini, G. and Manfredini, A. — *Nuovo Cimento*, 1953, **10**, 937.
4. Fry, W. F. and White, G. R. .. — *Phys. Rev.*, 1953, **90**, 207.
5. Lal, D., Yash Pal and Peters, B. — "Properties of Heavy Unstable Particles," *Ibid.*, (In press).
6. Biswas, S., George, E. C. and Peters, B. — "An Improved Method for Determining the Mass of Particles from Scattering *versus* Range and its Application to the Mass of K-mesons," *Proc. Ind. Acad. Sci.*, 1953, **38**, 418.
7. Danysz, M. and Pniewski, J. .. — *Phil. Mag.*, 1953, **44**, 348.
8. Harris, G. G. and Friedlander, M. — Reported at Bagnéres de Bigorre Conference, 1953.
9. Daniel, R. R., Davies, J. H., Mulvey, J. H. and Perkins, D. H. — *Phil. Mag.*, 1952, **43**, 753.
10. Mulvey, J. H. .. — Reported at Bagnéres de Bigorre Conference, 1953.
11. Smith, F. M., Birnbaum, W. and Barkas, W. H. — *Phy. Rev.*, 1953, **91**, 765.
12. Beiser, A. .. — *Rev. Mod. Phys.*, 1952, **24**, 282.

AN IMPROVED METHOD FOR DETERMINING THE MASS OF PARTICLES FROM SCATTERING *VERSUS* RANGE AND ITS APPLICATION TO THE MASS OF *K*-MESONS

By S. Biswas, E. C. George and B. Peters

(*Tata Institute of Fundamental Research, Bombay-1*)

Received September 26, 1953

(Communicated by Prof. H. J. Bhabha, F.R.S. F.A.SC.)

Abstract

A new method is developed for determining the mass of particles coming to rest in nuclear emulsions. Multiple coulomb scattering is measured with cells whose lengths vary along the trajectory in such a manner as to compensate for the momentum loss of the particle and keep the mean deviation between adjacent cells constant over the entire track. It is shown that this procedure is more convenient and inherently more accurate than that based on scattering measurements with constant cellsize. The method has been applied to *K*-mesons which at the end of their range either decay into a single charged relativistic particle (K^+-mesons) or into 3π-mesons (τ-mesons) or give rise to capture stars (K^--mesons). The results are within experimental error consistent with the assumption that the mass of these three classes of particles are identical and equal to the well established mass of the τ-mesons. The average mass of a group of 9 long *K*-mesons determined with our scattering procedure is $M_K = 974 \pm 42 m_e$.

I. Introduction

The mass of particles which come to rest in photographic emulsions can be obtained by measuring as a function of residual range, either the variation of ionization or the variation of multiple scattering along their track. The choice of the method which will give highest accuracy in a particular case depends on the mass of the particle, the orientation and length of the track available for measurement and the sensitivity of the emulsion.

A measurement of ionization can be obtained from the photometric density of the track, from the number of developed grains per unit track length (grain density) or from the proportion of the track length which is free of developed silver grains (integrated gap length). Of these three methods for comparing ionization, the measurement of grain density is by

far the most accurate when applicable and has been used in most of the earlier work to determine the mass of particles stopping in emulsions. The reason why mass determination from grain density *versus* range is no longer used extensively is two fold:

(*a*) With the development of more sensitive emulsions it has become possible and, for most experiments, desirable to employ emulsions which are sensitive to particles of minimum ionization. In such emulsions the grain density begins to saturate when the velocity of a singly charged particle falls below $v = \cdot 4\,c$. Accurate grain density measurements require, therefore, that the track of the particle is observable over an appreciable length such that in at least part of the trajectory the particle's velocity exceeds $v = 0 \cdot 4\,c$.

(*b*) Interest has shifted to particles of rest mass considerably larger than that of π-mesons. The saturation effect extends, therefore, over a large part of the residual range. For instance, accurate grain density measurements on particles of mass 1,000 electron masses or larger require observable residual ranges of more than $1 \cdot 6$ cm. while the available track length is usually much shorter. Even if sufficient track length is available, there is the danger that some inelastic scattering which is unobservable in the long saturated portion of the track, introduces a large error in the mass value obtained from grain density *versus* residual range.

Comparative ionization measurements by photometric density or integrated gap length on the other hand are applicable in sensitive emulsions to tracks of particles with small residual range and large rest mass. These methods promise to gain in importance in the near future, since recent technical improvements have increased their accuracy.[1, 2, 3]

However, the method which is most frequently used at present for obtaining the mass of stopping particles consists of measuring multiple coulomb scattering of tracks and residual range. A serious difficulty in this method as used in the past arises from the fact that the rapid energy loss of slow particles produces a rapid variation of the scattering values with range. The available track length must therefore be sub-divided into sections for which the scattering value is determined separately and these results of necessarily low statistical accuracy have to be fitted by trial and error to the best fitting of a series of scattering *versus* range curves representing various mass values. A modification of this procedure has been adopted by Menon and Rochat[4] who relate the scattering value obtained for half of the available track length to an empirically determined function of the particle mass and range.

All methods so far employed have however in common the use of a constant cell length to determine scattering in limited sections of the track.

Apart from the inaccuracy involved in relating scattering values of comparatively low statistical accuracy obtained from various sections of the track to the particle mass, there are other disadvantages, arising from the necessity of sub-dividing the available track length.

(*a*) Correction for large angle single scattering is usually made by omitting from the averaging process all deflections which exceed the average deflection by a certain factor (usually all readings larger than four times average are rejected). This cut-off value varies with residual range and must be determined separately on the basis of the limited number of measurements available in each of the sections into which the track was divided. Such a procedure for large angle scattering correction introduces therefore appreciable fluctuations.

(*b*) The optimum cell length is obtained by the compromise that the cell must be small enough to permit a large number of individual measurements yet large enough so that the scattering between cells is sufficiently high above the noise level. When the scattering increases due to the particle's slowing down, this optimum cell size decreases. A cell size which is optimum at the high energy end of a section of track is larger than optimum at the low energy end, resulting in a waste of information.

These disadvantages can be overcome if instead of using cells of constant size along parts of the track one uses a set of cell sizes which vary continuously in such a way as to keep the mean deflection per cell constant along the trajectory.* The mean deflection obtained with such a set of cell sizes is therefore independent of particle energy and only a function of mass. The set of cell sizes can be chosen such as to yield for a given noise level, optimum statistical accuracy for all parts of the track and the cut-off value for the single scattering correction can now be determined on the basis of deflections averaged over the entire available track length.

In Section II this method is described in detail. In Section III it is shown that once a set of cell lengths has been calculated which make the mean deviation independent of range for tracks produced by particles of a given mass, the same set of cells will give a mean deflection independent of range when applied to tracks produced by a particle of different mass. Similarly it can

* A very similar scattering method has been worked out simultaneously and independently by C. Dilworth, S. Goldsack and L. Hirschberg at Bruxelles. An outline of the method was presented by Mrs. Dilworth-Occhialini as a joint paper of the Bruxelles and the Bombay groups at the Cosmic Ray Conference at Bagnères de Bigorre, July 1953.

be applied to the projection into the plane of the emulsion of a steeply dipping track. A simple relation is derived giving the mass of the particle as a function of the mean deviation and the dip angle of its track.

In Section IV, we discuss noise corrections and also the choice of the schemes which will give optimum statistical accuracy. We also estimate the error in mass values obtained by this method.

In Section V, we apply the method to tracks of known particles and determine their mass. Here it appears that within statistical accuracy correct mass values are obtained and in agreement with our calculations the experimental mass values are independent of the particular scheme which is used.

Finally in Section VI, we apply our method to *K*-mesons coming to rest in an emulsion block detector and compare the results with mass values obtained by other methods and in other laboratories.

II. Outline of a Scattering Measurement Using Variable Cell Length

We have modified Fowler's[5] "co-ordinate method of scattering determination" in the following way.

Based on the semi-theoretical relation between range in emulsion and energy and the relation between scattering, velocity and cell length, we have calculated for particles of a given mass the cell length required such that at a given residual range the average absolute value of the second difference† $\bar{D}$ has a certain predetermined value Δ. We then obtain a relation between cell length and range and can use this relation to find along the track a set of points (whose separation increases in the direction away from the stopping point), which when used as the end points of successive cell intervals give an average second difference whose value is constant along the track and equal to Δ.

Such a set of increasing cell lengths calculated for a given value of Δ and for a given particle mass M we shall call a "scattering scheme" and designate it as "M_Δ scheme". We shall show in Section III, that if such a scattering scheme is applied to the projection into the plane of the emulsion of a track produced by a particle of mass $M' \neq M$, traversing the emulsion

† The second difference D and the cell length t are defined as follows: Let P_i, P_{i+1}, P_{i+2}, etc., represent individual points on a track and let y_i be the perpendicular distance between point P_i and an arbitrary line which is approximately parallel to the track, then the second difference D_i is defined by $D_i = y_i - 2y_{i+1} + 2y_{i+2}$ and the cell length t_i by the distance between P_i and P_{i+1}.

making an angle θ with the emulsion surface, the resulting average second difference Δ' (M, Δ, M′, θ) is to a high degree of accuracy independent of residual range and can be represented by a simple function of the variables. The mass M′ can, therefore, be easily determined by applying an arbitrary scattering scheme to any track ending in the emulsion.

The measured quantity Δ' must be interpreted as the average absolute value of the second differences (obtained from measurements on the projected track) after correction has been made for noise and for large angle single scattering. The noise correction is treated in Section IV. The large angle scattering correction is made by omitting from the averaging process all those second differences which exceed four times the average value of all the remaining second differences measured along the track.

III. Calculation of Scattering Schemes and the Relation Between Scattering Values and Particle Mass

In order to calculate the cell length required such that when measuring scattering on the track of a particle of mass M and residual range R, one obtains on the average a value for the second difference whose absolute magnitude is Δ, one needs a relation between energy and residual range in emulsion as well as a relation connecting the multiple scattering with particle mass and velocity and with the cell length employed.

(*a*) *The Range-Energy Relation.*—For protons of energy up to 35 Mcv we have used the available experimental information on ranges in photographic emulsions as quoted by Beiser[6] (we have decreased all his ranges by 1% to take into account the slightly greater stopping power of Ilford G-5 emulsions). The experimental values were plotted on the graph giving the range-energy relation for protons in Air, Aluminium and Lead which was published by the Princeton group and is based on the calculations of Smith.[7] When plotted in such a way it becomes apparent that the ratio $r = \dfrac{R^2_{emulsion}}{R_{alum} \times R_{lead}}$ approaches a constant value as the proton energy increases. We have made the assumption that "r" remains constant for proton energies higher than those for which emulsion data are available and have used this extrapolation up to residual ranges of 10 cm. in emulsion.

The range-energy curve for singly charged particles of mass M different from the proton mass M_p is then easily obtained from the relation

$$R_M(v) = \frac{M}{M_p} R_p(v) \qquad (1)$$

where v is the particle velocity and R its range.

(*b*) *The Scattering Formula.*—For the relation between the mean absolute value of the second difference Δ, the particle mass M and velocity βc and the cell length t we have used a formula based on the theory of Williams[8] and calculated for emulsions by Voyvodic and Pickup.[9] This formula may be written

$$\frac{M\Delta}{m_e} = 0{\cdot}96 \sqrt{\frac{2}{3}} \frac{1{\cdot}006\, t^{3/2} \sqrt{1-\beta^2}}{0{\cdot}511 \times 57{\cdot}3\, \beta^2} \left[1{\cdot}45 + 0{\cdot}8 \left\{ ln \frac{0{\cdot}94\, t}{\beta^2 + 0{\cdot}3} \right\} \right] \quad (2)$$

(here the factor 0·96 represents the effect of smoothing out scattering since the position of the track is measured by observing the position of a small number of grains rather than that of a single grain. The factor $\sqrt{\frac{2}{3}}$ arises because the second difference is determined using successive sagittas rather than tangents. The factor 0·511 converts the rest energy of the electron $m_e c^2$ into *M*eV. Δ and t are measured in microns.)

The numerical factor 1·006 represents the "scattering constant" derived theoretically for the case that no correction is made for large angle single scattering when measuring Δ. It can be shown that for the particular choice of cell lengths as a function of range which keep Δ constant, the introduction of a large angle cut-off corresponds simply to a reduction in the scattering constant. Although we employ the customary cut-off procedure, we have calculated our schemes with the theoretical constant 1·006 and later introduced a correction to the scattering constant on the basis of the calibration measurements on the masses of known particles (see Section V).

(*c*) *Relation Between Cell Length* t *and Residual Range R for Constant M and* Δ.—Using the range energy relation for protons in elmusion, together with equations 1 and 2, we can now for any value of M and Δ calculate the required cell length t as a function of residual range. The corresponding graphs for $\Delta = 1\,\mu$ and $\Delta = 1{\cdot}6\,\mu$ are shown in Fig. 1 using for M the mass of the proton and of the π-meson respectively. From these graphs one can now easily construct the scattering schemes $P_{1\cdot0}$ and $\pi_{1\cdot6}$. Starting at a small but arbitrary residual range R_0 one finds from Fig. 1, the corresponding value t_0, next one finds the value of t_1 corresponding to the residual range $R_0 + t_0$ and the value t_2 corresponding to the residual range $R_0 + t_0 + t_1$, etc. The scattering schemes $P_{1\cdot0}$ and $\pi_{1\cdot6}$ obtained in this manner for protons and π-mesons are given in the Appendix. When for instance the cell lengths t listed in the $P_{1\cdot0}$ scheme are used for measuring scattering on flat proton tracks we expect to find for any of the tracks and for any part of the tracks the same mean absolute value for the second difference, namely 1·0 microns.

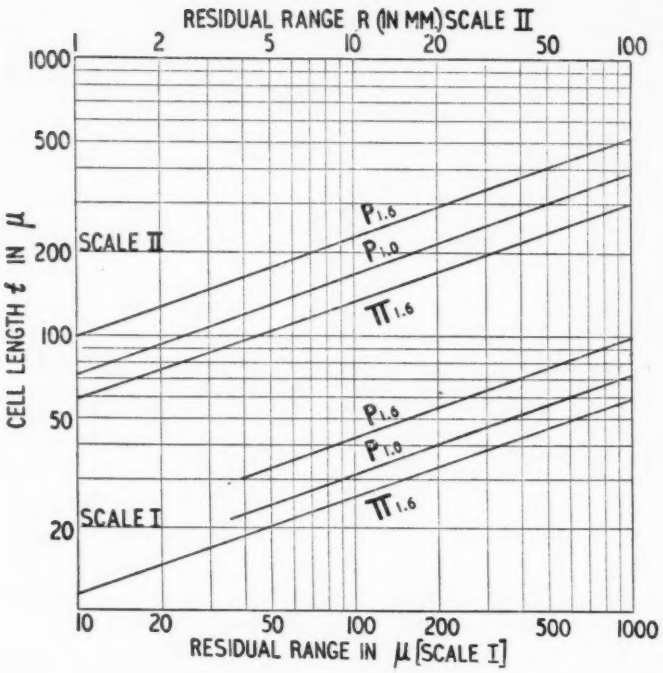

FIG. 1. The variation of the cell-length, t with Residual Range R for constant value of the mean absolute second difference, $\triangle$. The curves correspond to $\triangle = 1{\cdot}6\ \mu$ for protons and π-mesons and to $\triangle = 1{\cdot}0\ \mu$ for protons.

(*d*) *The Application of a Scattering Scheme to Dipping Tracks.*—In ordinary nuclear plates no reliable mass measurements can be made on tracks which make an appreciable angle with the plane of the emulsion, because the available track length is always short. If one employs, however, an emulsion block detector[10] tracks with appreciable dip when traced through many contiguous emulsion sheets often provide sufficient track length for mass determinations. For this reason the usefulness of the scattering method proposed here will be greatly extended if it can be applied to mass determinations on dipping tracks.

Consider for instance a proton track which in the undeveloped emulsion makes an angle θ with the plane of the emulsion and let us calculate from the range-energy relation and equations (1) and (2), the mean second difference $\bar{D}(\theta, R)$ which we should obtain by using at a residual range $R_i = R^{proj} \sec\theta$ not the cell length t_i obtainable from the graph in Fig. 1, but the

increased value $t_i' = t_i \sec\theta$. The value $\bar{D}(\theta, R)$ so calculated represents then the mean second difference which we should measure if we simply applied our scattering scheme to the projection into the plane of the emulsion of a uniformly dipping track. [The measured value of $\bar{D}(\theta, R)$ is not affected by a subsequent uniform shrinkage of the emulsion thickness.] In Table I the ratio, $\bar{D}(\theta, R)/\Delta$ is shown for various values of R and θ using the $\pi_{1\cdot6}$ scheme on a π-meson track. One sees that $D(\theta, R)$ is very nearly independent of R and this independence also holds for other scattering schemes. Its dependence on θ can in the range $0 < \theta < 60°$ be represented by the empirical formula.

$$\bar{D}(\theta) = \Delta (\sec\theta)^{0\cdot975} \tag{3}$$

Equation 3 permits then to obtain the mean absolute value of the second difference for a flat track from measurements carried out on the projection of a uniformly dipping track. (If the dip angle is different in different sections of the track, the sections must be treated separately.)

TABLE I

$D(\theta, R)/\Delta$ as a Function of Range for Various Values of the Dip Angle θ and for the $\pi_{1\cdot6}$ Scattering Scheme

Dip Angle θ \ Range	1 mm.	2 mm.	5 mm.	1 cm.	2 cm.	5 cm.	10 cm.
0°	1·000	1·000	1·000	1·000	1·000	1·000	1·000
15°	1·035	1·030	1·030	1·030	1·030	1·035	1·035
30°	1·150	1·150	1·145	1·145	1·145	1·150	1·150
45°	1·405	1·405	1·405	1·405	1·400	1·405	1·405

(e) *Application of Scattering Schemes to Particles of Unkown Mass.*— Using again the range-energy relation and equations (1) and (2), we calculate now as a function of residual range the mean absolute second difference $\bar{D}(M', R)$ which we should obtain if a certain scattering scheme M_Δ is applied to a flat track produced by a particle of mass $M' \neq M$. We find that in the range interval of ·1 to 10 cm., if the particle's mass M′ is nearly equal to the scheme mass M, the variation of $\bar{D}(M', R)$ with range is less than 1%. As M′ becomes much smaller than M, the variation of $\bar{D}(M', R)$ with range increases, but even when $M' \sim \frac{1}{6} M$ as in the case of

a π-meson measured with the proton scheme, the variation of $\bar{D}(M', R)$ with range does not exceed 3% of the mean value‡. We can, therefore, neglect this slight dependence on range and plot for any scheme M_Δ the mean absolute second difference $\bar{D}(M')$ as a function of particle mass (M'). This graph is shown in Fig. 2. The curves can be represented by the relation

$$\bar{D}(M') = \Delta\left(\frac{M}{M'}\right)^{0.439} \tag{4}$$

If we designate by Δ' the mean absolute second difference obtained on a track of dip angle θ using the scattering scheme M_Δ we obtain by combining

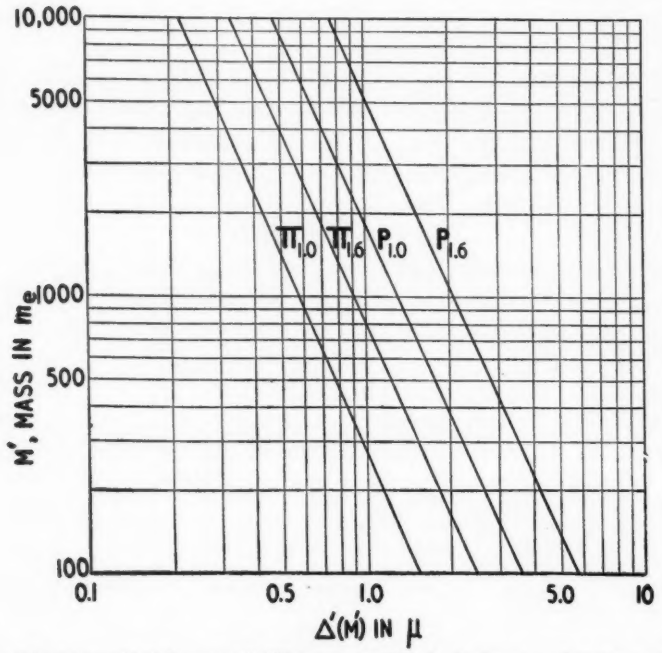

FIG. 2. The mean absolute second difference $\Delta'(M')$ is shown as a function of particle mass M' when measured with $P_{1\cdot6}$, $\pi_{1\cdot6}$, $P_{1\cdot0}$ and $\pi_{1\cdot0}$ scattering schemes.

the results of paragraphs (*d*) and (*e*) the mass M' of the particle responsible for the track

$$M' = M\left(\frac{\Delta}{\Delta'}\right)^{2.276}(\sec\theta)^{2.221} \tag{5'}$$

‡ If the range-energy curve is approximated by a single power law the variation is much larger and reaches about 10% for π-mesons scattered according to a proton scheme. The deviation from a power law in the range-energy relation tends to decrease the variation of $\bar{D}(M', R)$ with range.

IV. Noise Correction and Errors in the Mass Determination

The statistical accuracy of the measured scattering value and therefore of the particle's mass depends for a track of given length on the number of available cells and, therefore, on the choice of the scattering scheme. The choice is essentially limited by the condition that the measured scattering value must be significantly larger than the noise level. The noise arises from the fact that the centres of individual grains are not located exactly on the trajectory and that the determination of the exact location of these centres involves a small reading error.

The former factor is the most important source of noise, which should, therefore, have a magnitude of order or half the diameter of the average grain. In the region where the method discussed here is useful (particle range < 10 cm.) the cell lengths will never get so large as to make the noise in the movement of the microscope stage a significant contribution to the noise level; the spurious scattering due to noise should, therefore, be independent of cell length. Since the position of the track is determined by fitting a hairline in the eyepiece through a short section of track, the spurious scattering may be expected to increase slightly with decreasing grain density. We shall show, however, in this section that it is advantageous to chose the scattering scheme in such a way that the noise correction becomes very small and, therefore, the small variations of noise along the track can be neglected.

When measuring the spurious scattering on tracks of singly and doubly charged particles which, because they produce very energetic nuclear interactions, are known to have very high energy, we find that the noise has a value of $0{\cdot}16\,\mu$ and varies only slightly with cell length and track density. We shall assume that the noise has a gaussian distribution and a mean absolute value of $0{\cdot}16\,\mu$ for all our scattering measurements. We shall also assume that the *true* second differences due to multiple coulomb scattering and therefore also the *measured* second differences (which include noise) have a gaussian distribution. On these assumptions one can show that if Δ, D, ϵ represent the mean absolute values of the true second differences, the measured second differences and the noise respectively, Δ is given by

$$\Delta = (\mathrm{D}^2 - \epsilon^2)^{\frac{1}{2}}. \qquad (6)$$

For a track of finite length the contribution of the noise to the scattering value is not the noise measured on infinitely long tracks but will fluctuate around this value. If n readings are taken the standard deviation in the

mean absolute values D and ϵ are $\frac{0\cdot76}{\sqrt{n}}$ D and $\frac{0\cdot76}{\sqrt{n}}\epsilon$* respectively (Kendall[11]).

The standard deviation for Δ becomes, therefore,

$$\delta\Delta = \frac{0\cdot76}{\sqrt{n}}\left(\frac{D^4+\epsilon^4}{D^2-\epsilon^2}\right)^{\frac{1}{2}}. \tag{7}$$

Since n is inversely proportional to the cell length, and, therefore, proportional to Δ^{-1} we can write equation (7) as

$$\frac{\delta\Delta}{\Delta} = \sigma\left[\frac{D^4+\epsilon^4}{(D^2-\epsilon^2)^{5/3}}\right]^{\frac{1}{2}} \tag{7a}$$

where σ is a constant.

The quantity $\frac{\delta\Delta}{\Delta}$ has a flat minimum at $\Delta = 2\cdot40\,\epsilon$ and this minimum value is

$$\left(\frac{\delta\Delta}{\Delta}\right)_{min} = \frac{0\cdot90**}{\sqrt{n_0}}. \tag{8}$$

The optimum scattering scheme is, therefore, one in which the second difference is 2·40 times the average noise and the corresponding error in the mass determination (from equations 5′ and 8) is

$$\left(\frac{\delta M}{M}\right)_{min} = \frac{2\cdot05}{\sqrt{n_0}} \tag{9}$$

n_0 being the number of independent cells available for this scheme and track length. If, however, we decide to use a scheme in which the second difference has two and a half times its value at optimum, the percentage error in the mass value increases only slightly because the increase due to reduction in the number of available cells by the factor $(2\cdot5)^{\frac{1}{2}}$ is partly compensated

* This is not strictly true because the noise due to the displacement of the centre of a small group of grains from the true trajectory will affect three successive readings of second differences. We believe, however, that the simplified relations which we use here are sufficiently accurate for our purpose.

** An estimate of the standard deviation lying between $\frac{\cdot8}{\sqrt{n}}$ and $\frac{\cdot9}{\sqrt{n}}$ has been in use in most laboratories. They have however, been applied even in such cases where the second difference Δ was much smaller than its optimum value of 2·4 ϵ. For instance if the cell lengths are chosen so small as to give $\Delta \approx \epsilon$ the error according to equation 7 becomes $\frac{\delta\Delta}{\Delta} = \frac{1\cdot7}{\sqrt{n}}$ or twice as large as the estimate based on the usual convention. We believe, therefore, that our estimates of error are more conservative than those which have been in use until now.

by the reduced effect of noise fluctuations on the final value. One obtains for $\Delta = 6\,\epsilon$ a percentage error in the mass

$$\frac{\delta M}{M} = \frac{1\cdot 78}{\sqrt{n}} = \frac{2\cdot 41}{\sqrt{n_0}} = 1\cdot 17\left(\frac{\delta M}{M}\right)_{min}. \qquad (10)$$

Thus the error is only increased by 17% over its lowest possible value if we use a scattering scheme in which the second difference is six times the noise level. With such a scheme the noise correction to the measured second difference D amounts to only 1·4%. If we use such a scheme the small variations of noise along the track and small differences between the values obtained by different observers become unimportant. Therefore, we believe that in practice the most reliable and accurate mass values are obtained by choosing a scattering scheme in which the second differences are from four to six times larger than the noise level ($0\cdot 6\,\mu \lesssim \Delta \lesssim 1\,\mu$).

V. Application of Scattering Schemes to Particles of Known Mass

We have applied the $\pi_{1\cdot 6}$ scheme to long tracks of known π-mesons and obtained about 900 values of the second difference D. The distribution of the D values is shown in Fig. 3, together with the Gaussian curve

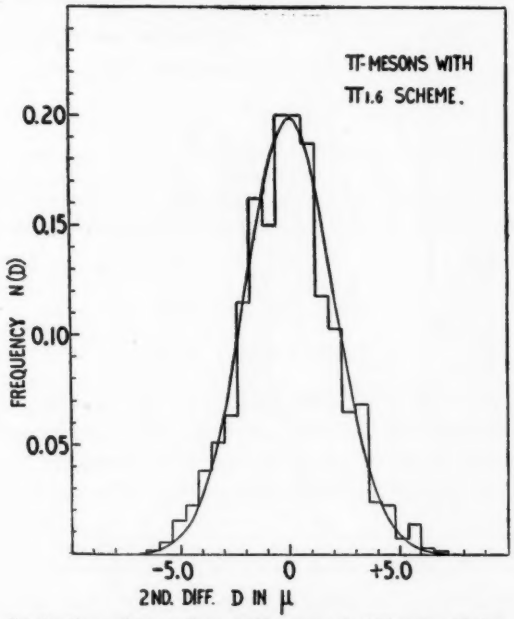

Fig. 3. The distribution of the values of the second difference D for π-mesons measured with $\pi_{1\cdot 6}$, scheme is shown in the histogram together with the Gaussian curve normalised to the same area and corresponding to the theoretically predicted mean absolute deviation of 1·6μ.

normalized to the same area and corresponding to the theoretically predicted mean absolute deviation of 1·6 microns. The average of the 900 experimental D values (after correction for the noise $\epsilon = 0{\cdot}16\,\mu$ and a small correction for dip) is

$$\frac{\Sigma \mid D_i \mid}{n} = \Delta = 1{\cdot}630 \pm {\cdot}0415\,\mu$$

and the corresponding value of the mass is

$$m_\pi = 264 \pm 17\, m_e \text{ (electron masses)}$$

In order to exhibit the fact that the experimental D value distribution is independent of range as predicted by theory we show in Figs. 4*a* and 4*b* separately the distribution of D values from the last 2·7 mm. of track length and from those parts of the tracks where the residual range exceeded 2·7 mm. The curves shown in Figs. 4*a* and 4*b* are again the expected Gaussian distribution curves.

We have also applied the $P_{1\cdot 6}$ scheme to long proton tracks and obtained about 800 D values.

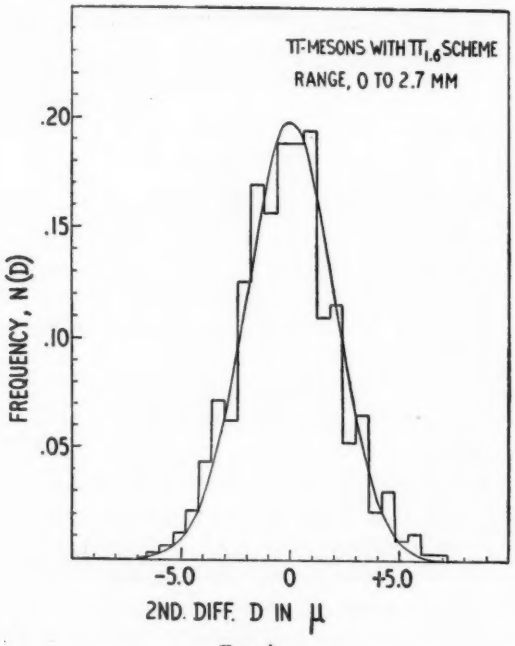

FIG. 4*a*

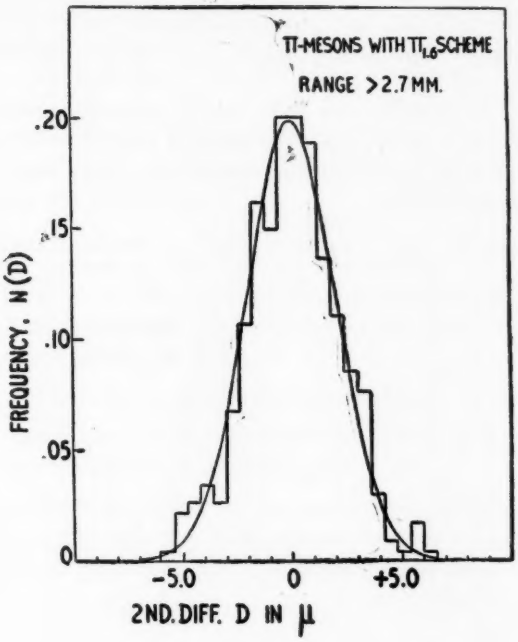

FIG. 4*b*

FIGS. 4 (*a*) and (*b*). The distribution of the values of the second difference D for π-mesons measured with $\pi_{1\cdot6}$ scheme is shown in the histogram 4(*a*) for ranges of 0 to 2·7mm. and n 4 (*b*) for ranges > 2·7 mm., together with the Gaussian curve normalised to the same area and corresponding to the theoretically predicted mean absolute deviation of 1·6μ.

Their average is

$$\Delta = 1\cdot602 \pm \cdot046\,\mu$$

$$m_p = 1831 \pm 120\,m_e.$$

In order to test our conclusion derived in Section III that the mass of a particle may be obtained from equation 5′ by inserting the average second difference Δ' obtained by applying an arbitrary scattering scheme we have determined Δ' by using the $P_{1\cdot0}$ scheme on π-meson tracks and the $\pi_{1\cdot6}$ schemes on proton tracks.

The application of the $P_{1\cdot0}$ scheme to π-mesons gave $\Delta' = 2\cdot339 \pm \cdot061\,\mu$

$$m_\pi = m_p \left(\frac{1\cdot0}{2\cdot339}\right)^{2\cdot276} = 266 \pm 16\,m_e.$$

The application of the $\pi_{1\cdot6}$ scheme to protons gave $\Delta' = 0\cdot706 \pm 0\cdot019\,\mu$

$$m_p = m_\pi \left(\frac{1\cdot6}{\cdot706}\right)^{2\cdot276} = 1780 \pm 110\, m_e.$$

In Fig. 5 the distribution of D values of protons measured with $\pi_{1\cdot6}$ scheme is shown, together with the Gaussian curve normalised to the same area and corresponding to the theoretically predicted mean absolute value of Δ', from equation (5′).

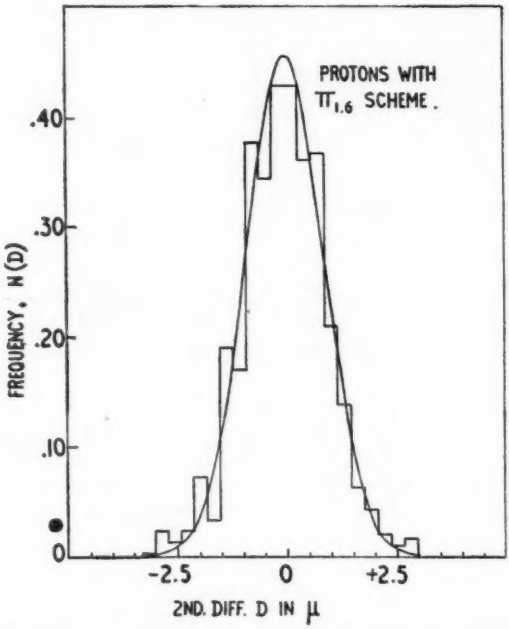

FIG. 5. The distribution of the values of the second difference D′ for protons measured with $\pi_{1\cdot6}$ scheme is shown in the histogram together with the Gaussian curve normalised to the same area and corresponding to the theoretically predicted mean absolute value of $\Delta' = .696\mu$ (from equation 5′).

These results then, verify the conclusions derived in the previous section that Δ' is independent of range and that formula 5′ is valid. They also establish that the stopping power of G-5 emulsions and the scattering constant for emulsions which we have used implicitly in our scattering schemes are approximately correct. A slightly better fit with the known masses of our calibration particles is obtained if we change the scattering

constant (equation 2) from $K = 1{\cdot}006$ to $K = 1{\cdot}020 \pm {\cdot}013$. Correspondingly equation 5′ must be changed to

$$M' = (1{\cdot}03 \pm {\cdot}03)\, M \left(\frac{\Delta}{\Delta'}\right)^{2.276} (\sec\theta)^{2.221}. \qquad (5)$$

This implies that in addition to the statistical errors our mass values derived with these schemes may be subject to a 3% systematic error until more accurate calibration data are available.

VI. Determinations on the Mass of Slow *K*-Mesons

The method of variable cell length has been applied to mass determinations on 9 long *K*-mesons which come to rest in an emulsion block. Of these 9 particles,

2 decay into 3 π-mesons and are therefore designated as τ-mesons.

5 decay and emit a single charged relativistic particle at the end of their range and are designated as K^+-mesons.

2 produce stars when they come to rest and are designated as K^--mesons (it is, however, possible that they are the negative counterpart of the τ-mesons rather than that of the particles designated as K^+-mesons).

The data on these particles are summarized in Table II.

Column 1 describes the nature of the particle.

Column 2 describes the nuclear event in which the particle originates (The notation is that introduced by Brown *et al.*[12]).

Column 3 gives the observed range and

Column 4 gives the mean dip angle.

Columns 5, 6 and 7 give the mass values obtained by our method and with three different scattering schemes. ($K_{1\cdot 0}$ denotes a scheme calculated for particles of mass $M = 1000\, m_e$).

Column 8 gives the mean mass value from different schemes.

Column 9 the mass value obtained from grain density *versus* range.

In each case the mass value derived from the track of a given particle by applying different scattering schemes are consistent with each other. If we assume that the 9 particles listed in Table II form a homogeneous group as far as their masses are concerned we obtain as a weighted average from scattering *versus* residual range.

$$M_K = 974 \pm 42\, m_e.$$

TABLE II

Data on K-mesons

Particle	Origin	Range (cm.)	Dip	Mass from Scattering Schemes (m_e)				Mass from G. d vs. R
				$^{\pi}(1\cdot6)$	$^{P}(1\cdot0)$	$^{K}(1\cdot0)$	Mean	
1 K^+ ..	$20+5n$	1·37	0°	875±140	1100±190	930±145	955±140	950±100
2 K^+ ..	$14+2n$	1·13	·5°	885±115	1020±195	1040±175	980±155	1120±100
3 K^+ ..	Outside of Block	5·41	9·5°	930±95	1085±125	1060±115	1025±95	1115±100
4 K^+ ..	$1+2n$	3·20	1° to 9°	700±85	850±115	690±85	740±85	980±100
5 K^+ ..	$8+?\alpha$	1·33	4°	1070±170	1075±190	875±145	1005±170	865±100
3 K^- ..	$4+6n$	2·49	2°	980±120	1065±150	..	1015±120	975±100
4 K^- ..	Outside of Block	2·85	3°	770±95	960±140	..	850±95	1320±100
1 τ^+ ..	$6+0p$	0·665	12°	1175±230	1225±280	..	1195±230	970±100
3 τ^+ ..	$13+10\alpha$	0·745	29–43°	1485±315	1535±375	..	1505±315	..
Mean ..							974±42	1035±35

The mass values obtained for 7 of the 9 particles agree with the mean value within one standard deviation and the remaining two mass values lie within two standard deviations.***

We shall now compare our results with those obtained in other laboratories. Upto the time of the Cosmic Ray Conference at Bagnéres de Bigorre in July 1953 a total of 41 scattering measurements on K^+-mesons have been reported by various other laboratories; 25 of these measurements were carried out on tracks of length greater than 2 mm. and will be compared with our results.

The average obtained on three tracks each, by the groups at Brussels, Milan, Paris and Rochester are in agreement with each other. The weighted mean mass of these 12 particles is

$$M_{K^+} = 974 \pm 29\, m_e$$

in excellent agreement with our own value.

The 13 particles measured by the Bristol group give a weighted average mass of

$$M_{K^+} = 1120 \pm 43\, m_e$$

which lies higher by about four standard deviations. The discrepancy could be either due to a slight systematic difference in the measuring procedures, but probably it should be considered as an indication that there exists another type of K^+-meson with somewhat greater mass.

It seems, in any case, very likely that at least a large fraction of K^+-mesons have a mass close to $975\, m_e$.

The mass of the τ-mesons can be determined from an analysis of its decay products more accurately than from direct measurements. The weighted mean mass for 11 τ-mesons reported by various laboratories upto July 1953 is given by Amaldi *et al.*[13] as

$$M_\tau = 980 \pm 4{\cdot}4\, m_e$$

While similar mass determinations on 3 τ-mesons in our own laboratory[14] gave

$$M_\tau = 976 \pm 2{\cdot}0\, m_e.$$

*** We have no explanation for the high mass value obtained for particle 3 τ (the mass derived from the energy of its decay products is 975 m_e). Its track is very steep and traverses. 8 emulsions such that only ~ 900 μ of track length is available for scattering in each emulsions On the other hand scattering measurements on an equally steep proton track gave no anomalous results.

We conclude that within experimental error the masses of K^+, -K^- -and τ-mesons are identical and close to about 975 m_e, although the existence of some K-mesons with somewhat higher mass cannot be ruled out.

We are indebted to Mrs. S. Mitra and to Dr. R. Daniel for assistance in some of the measurements reported here.

REFERENCES

1. Kayes, G. and Morellet, D. .. *J. Physique Rad.*, 1953, **14**, 353.
2. Van Rossum, L. .. *Comptes Rendus*, 1953, **236**, 2234.
3. Ritson, D. M. .. "Some *K*-particle Mass Measurements." To be published in *Phys. Rev.*
4. Menon, M.G.K. and Rochat, O. *Phil. Mag.*, 1951, **42**, 1232.
5. Fowler, P. H. .. *Ibid.*, 1950, **41**, 169.
6. Beiser, A. .. *Rev. Mod. Phys.*, 1952, **24**, 282.
7. Smith, J. H. .. *Phys. Rev.*, 1947, **71**, 32.
8. Willams, E. J. .. *Proc. Roy. Soc.*, London, 1939, **A 169**, 531 and *Phys. Rev.*, 1940, **58**, 292.
9. Voyvodic, L. and Pickup, E. .. *Phys. Rev.*, 1952, **85**, 91.
10. Lal, D. Yash Pal and Peters, B. *Proc. Ind. Acad. Sci.*, 1953, **38 A**, 277.
11. Kendall, M. G. .. *The Advanced Theory of Statistics*, Vol. I (Charles Griffin and Co., Ltd.), 1945, p. 215.
12. Brown, R. H., Camerini, U. Fowler, P. H., Heitler, H., King, D. T. and Powell, C. F. *Phil. Mag.*, 1949, **40**, 862.
13. Amaldi, E., Baroni, G., Castagnoli, C., Cortini, G. and Manfredini, A. *Nuovo Cimo*, 1953, **10**, 937.
14. Lal, D., Yash Pal and Peters, B. *Proc. Ind. Acad. Sci.*, 1953, **38A**, 398.

APPENDIX I

(A) $\pi_{1\cdot 6}$ SCATTERING SCHEME

No.	Range R (μ)	Cell length t (μ)	No.	Range R (μ)	Cell length t (μ)
1	10	11	36	1597	70
	21	15		1667	71
	36	18		1738	72
	54	21		1810	73
	75	24		1883	74
6	99	26	41	1957	75
	125	28		2032	76
	153	30		2108	77
	183	33		2185	78
	216	35		2263	79
11	251	36	46	2342	80
	287	38		2422	81
	325	40		2503	82
	365	41		2585	83
	406	43		2668	84
16	449	45	51	2752	85
	494	46		2837	86
	540	48		2923	86
	588	49		3009	87
	637	50		3096	88
21	687	52	56	3184	89
	739	53		3273	90
	792	54		3363	91
	846	56		3454	92
	902	57		3546	93
26	959	58	61	3636	94
	1017	60		3730	94
	1077	61		3824	95
	1138	62		3919	96
	1200	63		4015	97
31	1263	64	66	4112	98
	1327	66		4210	98
	1393	67		4308	99
	1460	68		4407	100
	1528	69		4507	100

No.	Range R (μ)	Cell No. t (μ)	No.	Range R (μ)	Cell length t (μ)
71	4607	101	96	7343	119
	4708	101		7462	120
	4809	102		7582	120
	4911	102		7702	121
	5013	103		7823	121
76	5116	104	101	7944	122
	5220	104		8066	122
	5324	105		8188	123
	5429	106		8311	124
	5535	107		8435	125
81	5642	109	106	8560	126
	5751	110		8686	127
	5861	110		8813	127
	5971	111		8940	128
	6082	112		9068	129
86	6194	112	111	9197	130
	6306	112		9327	130
	6418	113		9457	130
	6531	113		9587	131
	6644	114		9718	131
91	6758	115	116	9849	132
	6873	116		9981	132
	6989	117		10113	133
	7106	118			
	7224	119			
	(B) $P_{1\cdot0}$ SCATTERING SCHEME				
1	40	22	11	418	53
	62	27		471	55
	89	30		526	57
	119	34		583	60
	153	37		643	62
6	190	40	16	705	64
	230	43		769	66
	273	46		835	68
	319	48		903	70
	367	51		973	72

No.	Range R (μ)	Cell length t μ)	No.	Range R (μ)	Cell length t (μ)
21	1045	74	61	5216	132
	1119	76		5348	133
	1195	78		5481	134
	1273	80		5615	136
	1353	81		5751	138
26	1434	83	66	5889	139
	1517	85		6028	140
	1602	86		6168	141
	1688	88		6309	142
	1776	90		6451	142
31	1866	91	71	6593	143
	1957	93		6736	145
	2050	95		6881	146
	2145	96		7027	148
	2241	98		7175	150
36	2339	100	76	7325	150
	2439	100		7475	151
	2539	101		7626	152
	2640	102		7778	153
	2742	104		7931	154
41	2846	105	81	8085	155
	2951	106		8240	156
	3057	108		8396	157
	3165	110		8553	159
	3275	112		8712	160
46	3387	113	86	8872	161
	3500	114		9033	162
	3614	115		9195	162
	3729	116		9357	163
	3845	118		9520	164
51	3963	120	91	9684	165
	4083	121		9849	167
	4204	122		10016	168
	4326	123			
	4449	124			
56	4573	126			
	4699	127			
	4826	129			
	4955	130			
	5085	131			

1481-53 Printed at The Bangalore Press, Bangalore City, by C. Vasudeva Rao, Superintendent and Published by the Indian Academy of Sciences, Bangalore.

NOTICE TO AUTHORS

Scientific papers intended for publication in the *Proceedings of the Indian Academy of Sciences* can be accepted only when they are communicated by a Fellow of the Academy whose duty shall be to satisfy himself that such communications are fit to be read at the Meeting of the Academy and published in its *Proceedings*.

Papers should not ordinarily exceed fifty pages of foolscap. MSS. should be either typewritten or written in legible hand on one side of the paper. All papers should be carefully revised by the authors and should be absolutely in final form for printing. Position for text-figures should be indicated. Each paper shall conclude with a critical summary not exceeding 350 words.

Drawings, diagrams or other illustrations should be made on larger scale (preferably) twice the size than the ones in which they are intended to appear. They should be done in Indian ink on bristol board with lettering in pencil. Scale of magnification of camera lucida tracings should be indicated by the side of drawings. In certain special cases arrangements will also be made for monochrome lithographic and other colour plates. Reduction of illustrations desired should be indicated in pencil. Appropriate legends should accompany all drawings. Names of authors are to be marked in pencil on the left-hand corner of drawing sheets. Photomicrographs should be securely mounted with colourless paste.

All tables, quotations and footnotes which will be set hereafter (beginning from Vol. I, No. 2) in types smaller than the text, should be typewritten on separate sheets and placed with the text in proper sequence. Footnotes should be numbered in Arabic numerals.

References to literature in the text should be given, whenever possible, in chronological order, only the names of authors and years of publication, in brackets, being given. They should be cited in full after the summary, the authors' names following in alphabetical order. Thus,

Name or Names of author; Name of Journal (abbreviation) with a single underline; Year of publication; Number of Volume with a double underline, and lastly page. The following would be a useful illustration:—

Bergmann and Stather . . . . . Z. Physiol. Chem., 1926, 152, 189.

Two copies of slip-proof and wherever possible, a page proof for final revision will be sent to authors. All corrections are best made on the slip-proof which should be transmitted to the Office of the Academy. All proof corrections involve heavy expenses which would be negligible if the papers are carefully revised by the authors before submission.

Authors will be supplied with reprints of their papers at cost price, if intimation is given at the time of returning the slip-proof.

Blocks appearing in the *Proceedings* will be available for purchase by their respective authors. Orders for the same should be sent along with the corrected proofs and in any case not later than one month after the date of publication of the paper. The price charged would be 25% of the actual cost of the blocks *plus* freight and despatching charges. If the blocks are reproduced in other journals or publications, due acknowledgment should be made in them to the *Proceedings*.

The original drawings and plates of blocks appearing in the *Proceedings* will be returned to such of the authors as may require them provided the cost of despatching such originals is borne by them.

CONTENTS

PAGE

The Structure and Optical Behaviour of Iridescent Opal . . . . . Sir C. V. Raman and A. Jayaraman 343

Anthraquinone and Anthrone Series. Part XII. The Benzanthrone Condensation on 2-Chloroanthraquinone . . . . . P. N. Pandit, B. D. Tilak and K. Venkataraman 355

Anthraquinone and Anthrone Series. Part XIII. Synthesis of 5-Substituted Benzanthrones . . S. S. Malhotra, B. D. Tilak and K. Venkataraman 361

An Electro-static Beta-Ray Spectrometer, Using a Spherical Condenser . . . . . M. C. Joshi and B. V. Thosar 367

Application of the Rb-Sr Method to the Age Determination of Phlogopites . . . . . V. S. Venkatasubramanian 376

Synthetic Experiments in the Benzopyrone Series. Part XXXIX. A Note on the Synthesis of Isogenistein and 8-Methyl Isogenistein . . . . . A. C. Mehta, T. R. Seshadri and S. Varadarajan 381

Studies in Colloid Optics. Part IV. Sol-Gel Transition of Some Lyophilic Gels . . . . . P. K. Katti 387

Observations on τ-Mesons and on *K*-Mesons Giving Rise to Capture Stars . . . . . D. Lal, Yash Pal and B. Peters 398

An Improved Method for Determining the Mass of Particles from Scattering *Versus* Range and its Application to the Mass of *K*-Mesons . . . . . S. Biswas, E. C. George and B. Peters 418